UNIVERSITÉ DU QUÉBEC À TROIS-RIVIÈRES

RÉCUPÉRATION DES MÉTAUX PAR LIXIVIATION DE MATÉRIAUX DE CATHODE DE BATTERIES LITHIUM-ION DU TYPE NMC ET LFP : ANALYSE DE LEURS INTERACTIONS SYNERGIQUE

METAL RECOVERY BY LEACHING CATHODE MATERIALS FROM LITHIUM-ION (NMC AND LFP) BATTERIES: ANALYSIS OF SYNERGISTIC INTERACTIONS

THÈSE PRÉSENTÉE
COMME EXIGENCE PARTIELLE DU
DOCTORAT EN SCIENCES DE L'ÉNERGIE ET DES MATÉRIAUX

PAR

MOLOOD SAEEDI

Octobre 2025

UNIVERSITÉ DU QUÉBEC À TROIS-RIVIÈRES

DOCTORAT EN SCIENCES DE L'ÉNERGIE ET DES MATÉRIAUX (PH. D.)

Direction de recherche :

Jacques Huot	Directeur de recherche

Jury d'évaluation :

Jacques Huot	Directeur de recherche
Samaneh Shahgaldi	Président de jury
Jean-François Blais	Évaluateur externe
Bernard Tougas	Évaluateur externe

Thèse soutenue le 22 septembre 2025.

RÉSUMÉ

L'extraction de métaux par lixiviation acide des matériaux de cathode des batteries lithium-ion du type lithium nickel manganèse cobalt oxyde (NMC) et lithium fer phosphate (LFP) a été étudié. Le projet se concentre principalement sur l'extraction par lixiviation acide de NMC et LFP séparément et mélangés. L'étude comprend trois sections principales qui sont détaillées ci-dessous.

La première section se concentre sur le développement de méthodes de caractérisation des matériaux de cathode pour les batteries NMC et LFP et de méthodes d'extraction de métaux par lixiviation avec de l'acide sulfurique utilisant des matériaux de cathode individuels. L'effet de la concentration de l'acide sulfurique, du rapport solide-liquide (S/L) et de l'ajout de H_2O_2 sur l'efficacité de lixiviation des métaux a été étudié. Les résultats préliminaires ont démontré que la concentration d'acide sulfurique, dans une plage de 2 M à 6 M, a eu un effet plus négligeable sur l'efficacité de lixiviation de métaux pour les deux matériaux, soient le NMC et LFP. Tandis que l'efficacité de lixiviation a diminué avec l'augmentation du rapport solide-liquide (S/L) de 0,10 g/mL à 0,20 g/mL. L'ajout de H_2O_2 a eu un effet différent sur la dissolution du NMC que sur celle du LFP. Ainsi, une concentration en H_2O_2 de 0,68 M lors de la lixiviation a changé les conditions d'oxydo-réduction permettant ainsi de réduire les états d'oxydation des métaux de transition contenus dans le NMC, augmentant ainsi leur solubilité respective et améliorant du même coup l'efficacité de lixiviation du Mn, du Ni, du Co et du Li. Cependant, pour les métaux contenus dans le matériel LFP, l'ajout de H_2O_2 à la même concentration, a eu un effet négligeable sur la dissolution de Fe et P pour des rapports S/L inférieurs à 0,20 g/mL, tandis que leur efficacité de lixiviation a diminué, une lixiviation sélective a été observée pour 0,20 g/mL.

La deuxième section porte sur l'étude de l'extraction des métaux par lixiviation acide d'un mélange de matériaux NMC et LFP. L'effet du rapport S/L, de l'ajout de H_2O_2 et de sa concentration, du rapport molaire NMC/LFP et de la concentration de H_2SO_4 sur l'efficacité de lixiviation ont été étudiés. L'objectif principal de cette section est d'extraire sélectivement le Mn, le Ni, le Co et le Li tout en conservant intact la forme orthorhombique initiale du $FePO_4$. La lixiviation sélective d'un mélange de matériaux NMC et LFP améliore l'efficacité et la rentabilité du processus de lixiviation, prévient la contamination du lixiviat et réduit les coûts tout en permettant la récupération de $FePO_4$ orthorhombique, un sous-produit précieux ayant un potentiel de réutilisation dans la fabrication des LIBs. Les résultats ont démontré que que les rendements de lixiviation de Mn, Ni, Co et Li a été près de 100%. Cependant, pour le Fe et le P a été de 62,4% et 65,7% respectivement, sous des conditions de H_2SO_4 2M, H_2O_2 0,68M, rapport S/L 0,15 g/mL, rapport molaire NMC/LFP 1,36, 75°C et 51 minutes. La structure cristalline du sous-produit solide de la lixiviation a été analysée par diffraction des rayons X (DRX), et la morphologie et la distribution des éléments ont été

analysées par microscopie électronique à balayage (MEB) et spectroscopie de rayons X à dispersion d'énergie (EDS). Ces analyses ont montré la présence dans ces résidus de $FePO_4$ avec une structure orthorhombique.

La troisième section démontre l'effet des ions ferreux et ferriques sur la lixiviation de métaux du mélange NMC et LFP. L'étude a comme objectif d'analyser l'effet de l'ajout de $Fe(II)SO_4$ ou de $Fe(III)_2(SO_4)_3$ en solution comme agent d'oxydo-réduction sur l'efficacité d'extraction du Ni, du Co, du Mn et du Li et sur la préservation du $FePO_4$ (s) orthorhombique comme sous-produit lors de la lixiviation d'un mélange de LFP et de NMC. L'étude a démontré que la présence du $Fe(II)SO_4$ augmente la lixiviation du NMC supposément dû à son pouvoir réducteur sur les métaux de transition (Mn, Ni et Co), permettant d'obtenir des composés solubles. L'effet du rapport molaire Fe^{2+}/NMC et l'ajout postérieur ou simultané de LFP au mélange $Fe(II)SO_4$- NMC a été étudié. Pour un ajout postérieur du LFP, lorsque le rapport Fe^{2+}/NMC a augmenté de 0,27 à 0,74 la solubilisation de Mn, Ni et Co et la cinétique de réaction a augmenté pendant les 10 premières minutes de lixiviation, aboutissant finalement à leur dissolution complète à la fin de l'essai. De plus, cela a favorisé la formation d'une plus grande quantité de $FePO_4$ (s). Des tendances similaires ont été observées lorsque le LFP a été ajouté au $Fe(II)SO_4$ et au NMC simultanément dès le début de la réaction. De plus, cela a favorisé la conservation d'une plus grande quantité de $FePO_4$.

Dans l'ensemble, ce projet a contribué au développement d'une méthode d'extraction des métaux à partir d'un mélange des matériaux de cathode NMC et LFP en utilisant de l'acide sulfurique, en mettant en évidence le rôle crucial du LFP dans l'amélioration de l'efficacité de lixiviation. Contrairement aux études précédentes, qui se concentraient principalement sur des cathodes uniques ou ne prenaient pas en compte les interactions entre différentes chimies mixtes, ce travail aborde les effets synergiques des mélanges NMC et LFP lors du lixiviation acide. Des informations clés sur l'utilisation de $Fe(II)SO_4$ comme agent réducteur et sur l'amélioration de la lixiviation lors de l'utilisation de Fe^{2+} ont été produites, ouvrant la voie au développement d'une lixiviation sélective des matériaux de cathode mixtes. En conséquence, du $FePO_4$ orthorhombique, un sous-produit avec un potentiel de réutilisation dans la fabrication des batteries lithium-ion et irrécupérable dans les méthodes classiques de lixiviation des batteries Li-ion, a pu être récupéré.

ABSTRACT

The extraction of metals by acid leaching of cathode materials from lithium nickel manganese cobalt oxide (NMC) and lithium iron phosphate (LFP) lithium-ion batteries was studied. The project focused primarily on acid leaching of NMC and LFP individually and as a mixture. The dissertation is divided into three main sections, outlined below.

The first section describes the characterization methods for the cathode materials of NMC and LFP batteries and of metal extraction methods involving acid leaching of individual cathode materials. The effects on metal leaching efficiency of sulphuric acid concentration, solid-to-liquid (S/L) ratio and addition of H_2O_2 were studied. Preliminary results indicated that sulphuric acid concentrations in the range of 2 M to 6 M had negligible effects on metal leaching efficiency with NMC and LFP. However, leaching efficiency decreased when S/L ratio was increased from 0.10 g/mL to 0.20 g/mL. Furthermore, the addition of H_2O_2 at a concentration of 0.68 M changed the redox potential of the media, making it possible to reduce the oxidation states of NMC transition metals, increase their solubility and thus improve leaching efficiencies for Mn, Ni, Co and Li. However, for metals in the LFP material, the addition of H_2O_2 at the same concentration had a negligible effect on the dissolution of Fe and P at S/L ratios below 0.20 g/mL while leaching efficiencies decreased and selective leaching was observed at an S/L ratio of 0.20 g/mL.

The second section examines metal extraction by acid leaching of a mixture of NMC and LFP materials. The effects of S/L ratio, addition and concentration of H_2O_2, NMC/LFP molar ratio and sulphuric acid concentration on leaching efficiency were studied. The main objective was to selectively extract Mn, Ni, Co and Li while maintaining the initial structure of the orthorhombic $FePO_4$ as a solid by-product. Selective leaching of mixed NMC and LFP materials enhances the efficiency and profitability of the leaching process, prevents leachate contamination and reduces costs while allowing recovery of orthorhombic $FePO_4$, a valuable by-product with potential for reuse in the manufacture of LIBs. Results showed that leaching efficienciesy for Mn, Ni, Co and Li were nearly 100%, whereas Fe and P reached efficiencies of 62.4% and 65.7%, respectively, under conditions of 2 M H_2SO_4, 0.68 M H_2O_2, S/L ratio 0.15 g/mL, NMC/LFP molar ratio 1.36, 75°C and 51 minutes. The crystalline structure of the solid by-product was analyzed using X-ray diffraction (XRD), while morphology and elemental distribution were studied using scanning electron microscopy (SEM) and energy-dispersive X-ray spectroscopy (EDS). Analyses confirmed the presence of $FePO_4$ with an orthorhombic structure.

The third section of the dissertation examines the effect of ferrous and ferric ions on leaching of metals from the NMC and LFP mixture. The objective was to analyze the effect of adding $Fe(II)SO_4$ or $Fe(III)_2(SO_4)_3$ as a redox agent on Ni, Co, Mn and Li extraction efficiencies and on the preservation of

orthorhombic $FePO_4$ (s) as a by-product during the leaching of an LFP and NMC mixture. The study showed that the presence of $Fe(II)SO_4$ enhanced the leaching of NMC, presumably due to its reducing effect on transition metals (Mn, Ni and Co), leading to the formation of soluble compounds. The effect of Fe^{2+}/NMC molar ratio and of sequential or simultaneous addition of LFP to the $Fe(II)SO_4$-NMC mixture was investigated. With sequential LFP addition, when Fe^{2+}/NMC molar ratio was increased from 0.27 to 0.74, solubilization of Mn, Ni, and Co and reaction kinetics increased in the first 10 minutes of leaching and ultimately led to complete dissolution of these metals by the end of the experiment. Additionally, this promoted maintaining a greater amount of $FePO_4$(s). Similar trends were observed when LFP added to $Fe(II)SO_4$ and NMC simultaneously from the start of the reaction.

Overall, this project contributes to the development of a method for extracting metals from a mixture of NMC and LFP cathode materials using sulphuric acid and highlights the crucial role of LFP in boosting leaching efficiency. Unlike previous studies that primarily focused on single cathode or did not account for interactions between mixed chemistries, this work addresses the synergistic effects of NMC and LFP mixtures during acid leaching. Key insights were gained regarding the use of $Fe(II)SO_4$ as a reducing agent and the enhancement of leaching when Fe^{2+} is introduced, paving the way for development of selective leaching of mixed cathode materials. Additionally, orthorhombic $FePO_4$ could be recovered, a valuable by-product with a potential for reuse in the manufacture of LIBs that is not recovered by the traditional LIB hydrometallurgical recycling process.

ACKNOWLEDGEMENTS

I am deeply grateful to all who have contributed to the completion of my doctoral research. Their support, encouragement and insightful guidance have been invaluable throughout this journey. I sincerely appreciate their contributions and extend my heartfelt thanks to each and every one.

I would like to express my deepest gratitude to my supervisor, Professor Jacques Huot, for his trust and invaluable guidance throughout my academic journey. I also extend sincere thanks to my co-supervisor, Dr. Antonio Avalos Ramirez, for his guidance, contributions and continuous support. Additionally, I am profoundly thankful to Dr. Sakine Khajavi for her unwavering support and guidance, which have been a constant source of encouragement.

I would like to express my appreciation to Hydro-Québec's Center of Excellence in Transportation Electrification and Energy Storage, the MITACS Accelerate Fellowship, PRIMA Québec and the Natural Sciences and Engineering Research Council of Canada (NSERC) for their financial support. In particular, I am grateful to Dr. Kamyab Amouzegar and Dr. François Larouche at Hydro-Québec for their invaluable guidance and engagement in the project. Their expertise and contributions significantly enriched this work and helped in achieving its objectives.

Heartfelt thanks to the researchers and technicians at the National Center for Electrochemistry and Environmental Technologies (CNETE) for their technical support and their analysis of my laboratory samples, crucial to this research. I would also like to extend special thanks to Professor Alain Wilkin for his guidance and valuable assistance with the XRD analysis for this project.

Lastly, I want to express my gratitude to my beloved husband Rasoul, my parents, my family and friends for their unwavering support, patience and encouragement. Their presence and moral support have been a source of strength and motivation throughout my PhD journey, and I am deeply grateful for their encouragement every step of the way.

Table of Contents

RÉSUMÉ i
ABSTRACT iii
ACKNOWLEDGEMENTS v
LIST OF FIGURES ix
LIST OF TABLES xiii
LIST OF ABBREVIATIONS xvi
CHAPTER I 1
INTRODUCTION 1
1.1. Lithium-ion battery structure 1
1.1.1. Anode materials 4
1.1.2. Cathode materials 5
1.1.2.1. Lithium transition metal oxides 5
1.1.2.2. Polyanionic compounds 7
1.2. Management of spent LIBs 8
1.3. Recycling spent LIBs 9
1.3.1. Battery sorting 9
1.3.2. Pretreatment 10
1.3.3. Recycling 10
1.4. Hydrometallurgical recovery of valuable metals 11
1.4.1. NMC cathodes 12
1.4.2. LFP cathodes 14
1.4.3. Mixture of LIBs 17
1.5. Research hypothesis 20
1.6 Research goals 21
1.7. Dissertation structure 21
CHAPTER II 22
MATERIALS AND METHODS 22
2.1. Materials 22
2.2. Characterization methods 22
2.2.1. Crystallography 22
2.2.2. Morphology and element distribution on particle surface 24
2.2.3. Carbon-sulphur content 26
2.2.4. Metal content 26

2.2.5. Oxidation-reduction potential (ORP) 29
2.3. Leaching of NMC and LFP materials 29
2.3.1. Metal content of initial and final solids in leaching assays 30
2.3.2. Leaching efficiency 31
2.4. Errors and standard deviation 31
CHAPTER III 34
CHARACTERIZATION OF MATERIALS AND METAL EXTRACTION BY ACID LEACHING OF SINGLE NMC AND LFP CATHODE MATERIALS 34
3.1. Introduction 34
3.2. Methodology 34
3.3. Results 34
3.3.1. Characterization of NMC and LFP materials 34
3.3.2. Study of NMC acid leaching 38
3.3.2.1. Effect of sulphuric acid concentration on leaching efficiency 38
3.3.2.2 Effect of solid-liquid ratio on leaching efficiency 41
3.3.2.3 Effect of H_2O_2 addition on leaching efficiency 42
3.3.3. Study of LFP acid leaching 44
3.3.3.1. Effect of sulphuric acid concentration on leaching efficiency 44
3.3.3.2. Effect of solid-liquid ratio on leaching efficiency 47
3.3.3.3. Effect of H_2O_2 addition on leaching efficiency 48
3.4. Discussion 52
3.5. Conclusion 58
CHAPTER IV 60
STUDY OF METAL EXTRACTION EFFICIENCY OF SULPHURIC ACID LEACHING OF MIXED NMC AND LFP CATHODE MATERIALS 60
4.1. Introduction 60
4.3. Results 60
4.3.1. Effect of solid-liquid ratio on metal leaching efficiency 60
4.3.2. Effect of H_2O_2 addition on metal leaching efficiency 63
4.3.3. Effect of NMC/LFP molar ratio on metal leaching efficiency 69
4.3.4. Effect of sulphuric acid concentration on metal leaching efficiency 78
4.3.5. Effect of H_2O_2 concentration on metal leaching efficiency 80
4.4. Discussion 82
4.5. Conclusion 86
CHAPTER V 88

SYNERGISTIC ACTION OF FERROUS AND FERRIC IONS ON LEACHING OF MIXED NMC AND LFP MATERIALS 88
5.1. Introduction 88
5.2. Methodology 88
5.3. Results 89
5.3.1. Effect of $Fe(II)SO_4$ addition on metal leaching efficiency 89
5.3.2. Effect of LFP addition on NMC leaching in a ferrous sulfate solution 95
5.3.2.1. Addition of LFP to an initial mixture of $Fe(II)SO_4$ and NMC 95
5.3.2.2. Initial simultaneous addition of $Fe(II)SO_4$, NMC and LFP 100
5.3.3. Addition of NMC to an initial mixture of $Fe(III)_2(SO_4)_3$ and LFP 106
5.4. Discussion 109
5.5. Conclusion 116
CHAPTER VI: CONCLUSION AND RECOMMENDATIONS 117
REFERENCES 119
APPENDICES 126

LIST OF FIGURES

Figure 1.1 Main types of LIB cells: (a) cylindrical, (b) coin, (c) prismatic, and (d) pouch [5] 2

Figure 1.2 Schematic operational principle of LIB charging [7] 3

Figure 1.3 Schematic operational principle of LIB discharging [7] 4

Figure 1.4 Layered structure of $LiMO_2$ ($LiCoO_2$) [9] 6

Figure 1.5 Schematic drawing of different Ni layered oxides ($LiNixMnyCozO_2$) [17] 6

Figure 1.6 Spinel structure of $LiMn_2O_4$ [9] 7

Figure 1.7 Crystal structure of olivine $LiFePO_4$ for Li-ion batteries [21] 8

Figure 1.8 Five significant classes of cathode materials (875 million metric tons, 2025) [22] 8

Figure 2.1 Schematic diagram of Bragg diffraction [91] 23

Figure 2.2 Schematic of a scanning electron microscope [93] 25

Figure 2.3 Schematics of emissions SEM: secondary electron (SE), backscattered electron (BSE), and characteristic X-rays [94] 25

Figure 2.4 Schematic diagram of an ICP-OES system [95] 25

Figure 2.5 Plasma generation [96,97] 27

Figure 2.6 Schematic representation of leaching setup 30

Figure 3.1 XRD patterns of NMC sample and lattice parameters of NMC111 and NMC622 reported by Azhari et al. [98] 36

Figure 3.2 XRD patterns of LFP sample and $LiFePO_4$ with COD ID: 1101111 38

Figure 3.3 Effect of sulphuric acid concentration on leachate concentrations of Mn, Ni, Co, and Li (2 M and 6 M H_2SO_4, S/L 0.10 g/mL, 75°C) 39

Figure 3.4 Leaching efficiencies for Mn, Ni, Co, and Li: (a) 2 M H_2SO_4, S/L 0.10 g/mL, 75°C; (b) 6 M H_2SO_4, S/L 0.10 g/mL, 75°C 40

Figure 3.5 Solid leached residue XRD patterns (2 M and 6 M H_2SO_4, S/L 0.10 g/mL, 75°C) 41

Figure 3.6 Effect of H_2O_2 on Mn, Ni, Co, and Li leachate concentrations (0 M and 0.68 M H_2O_2, 2 M H_2SO_4, S/L 0.10 g/mL, 75°C, H_2O_2 added at 60 min) 43

Figure 3.7 Leaching efficiencies for Mn, Ni, Co, and Li (2 M H_2SO_4, S/L 0.10 g/mL, 75°C, 0.68 M H_2O_2 added at 60 min) 43

Figure 3.8 Effect of sulphuric acid concentration on leachate concentrations of Fe, P, and Li (2 M and 6 M H_2SO_4, S/L 0.10 g/mL, 75°C) 45

Figure 3.9 Leaching efficiency for LFP: (a) 2 M H_2SO_4, S/L 0.10 g/mL, 75°C; (b) 6 M H_2SO_4, S/L 0.10 g/mL, 75°C 46

Figure 3.10 XRD pattern of leach residue (6 M H_2SO_4, S/L 0.10 g/mL, 75°C) 47

Figure 3.11 Effect of H_2O_2 on leachate concentrations of Fe, P, and Li (0 and 0.68 M H_2O_2, 2 M H_2SO_4, S/L 0.10 g/mL, 75°C, H_2O_2 added at 60 min) 49

Figure 3.12 Leaching efficiencies for Fe, P, and Li (2 M H_2SO_4, S/L 0.10 g/mL, 75°C, 0.68 M H_2O_2 added at 60 min) 49

Figure 3.13 XRD patterns of leach residue (2 M H_2SO_4, 75°C, S/L 0.20 g/mL, 82 min) and of $Li_2SO_4 \cdot H_2O$, $FeSO_4 \cdot H_2O$, and $FePO_4 \cdot 2H_2O$ (orthorhombic) 51

Figure 3.14 XRD patterns of leach residue (2 M H_2SO_4, 0.68 M H_2O_2, 75°C, S/L 0.20 g/mL, 82 min) and of $FePO_4 \cdot 2H_2O$ (monoclinic and orthorhombic) 51

Figure 3.15 Assessed and experimental solubility data for the H_2O–$FeSO_4$–H_2SO_4 system at 80°C (Koblyn et al. [109]) 55

Figure 4.1 Leaching efficiencies for Mn, Ni, Co, Li, Fe, and P with S/L ratios 0.10–0.20 g/mL (2 M H_2SO_4, NMC/LFP molar ratio 1.67, 75°C, 82 min) 62

Figure 4.2 XRD patterns of leach residues with S/L ratios 0.10–0.20 g/mL and phases $Li_{0.115}MnO_2$, $FePO_4$, $LiNi_{0.6}Mn_{0.2}Co_{0.2}O_2$ 63

Figure 4.3 Concentrations of Mn, Ni, Co, Li, Fe, and P (2 M H_2SO_4, S/L 0.10 g/mL, 75°C, 0 and 0.68 M H_2O_2 added at 60 min) 65

Figure 4.4 Leaching efficiencies for Mn, Ni, Co, Li, Fe, and P (2 M H_2SO_4, S/L 0.10 g/mL, 75°C, 0.68 M H_2O_2 added at 60 min) 66

Figure 4.5 Effect of S/L ratio on leaching efficiencies (2 M H_2SO_4, 0.68 M H_2O_2, NMC/LFP molar ratio 1.67, 75°C, 82 min) 67

Figure 4.6 XRD patterns of leach residues (2 M H_2SO_4, 0.68 M H_2O_2, NMC/LFP molar ratio 1.67, 75°C, 82 min) 68

Figure 4.7 Leaching efficiencies as a function of time for Mn, Ni, Co, Li, Fe, and P (2 M H_2SO_4, 0.68 M H_2O_2, 75°C, H_2O_2 added at 30 min) 71

Figure 4.8 Effect of NMC/LFP molar ratio on leaching efficiencies (2 M H_2SO_4, 75°C, 30 min) 72

Figure 4.9 Effect of NMC/LFP molar ratio on leaching efficiencies (2 M H_2SO_4, 0.68 M H_2O_2, 75°C, 51 min) 72

Figure 4.10 XRD patterns of leach residues at NMC/LFP molar ratios 1.02 and 1.36 and $FePO_4$ phase pattern 73

Figure 4.11 SEM images of leach residue (a–f) obtained under conditions of (NMC/LFP molar ratio 1.02, 2 M H_2SO_4, 0.68 M H_2O_2, S/L 0.15 g/mL, 75°C, 51 min) 74

Figure 4.12 SEM and EDS mapping images of leach residue (same conditions as Fig. 4.11) 75

Figure 4.13 SEM images of leach residue (a–f) (NMC/LFP molar ratio 1.36, 2 M H_2SO_4, 0.68 M H_2O_2, S/L 0.15 g/mL, 75°C, 51 min) 76

Figure 4.14 SEM and EDS mapping images of leach residue (NMC/LFP molar ratio 1.36, 2 M H_2SO_4, 0.68 M H_2O_2, 75°C, 51 min) 77

Figure 4.15 Effect of H_2SO_4 concentration on leaching efficiencies for Mn, Ni, Co, Li, Fe, and P (0.25–2 M H_2SO_4, 0.68 M H_2O_2, 75°C, 51 min) 79

Figure 4.16 XRD patterns of leach residues with 0.25–2 M H_2SO_4 and phases $LiNi_{0.6}Mn_{0.2}Co_{0.2}O_2$, $FePO_4$, $Li_{0.115}MnO_2$, $LiFePO_4$ 80

Figure 4.17 Effect of H_2O_2 concentration on leaching efficiencies (0.10 and 0.68 M H_2O_2, 2 M H_2SO_4, 75°C, 51 min) 81

Figure 4.18 Comparison of leaching of separate and mixed NMC and LFP materials (2 M H_2SO_4, 75°C, 82 min) 83

Figure 5.1 Simplified flow sheet for study of the effect of adding $Fe(II)SO_4$ on metal leaching 90

Figure 5.2 Leaching efficiencies for Mn, Ni, Co, Li, Fe and P (2 M H_2SO_4, 0.095 M $Fe(II)SO_4$, NMC/LFP molar ratio 1.36, S/L ratio 0.15 g/mL, 75°C, $Fe(II)SO_4$ added at 30 minutes) 91

Figure 5.3 Leaching efficiencies for Mn, Ni, Co, Li, Fe and P (2 M H_2SO_4, 0.285 M $Fe(II)SO_4$, NMC/LFP molar ratio 1.36, S/L ratio 0.15 g/mL, 75°C) with 0.190 M $Fe(II)SO_4$ added at 30 minutes followed by incremental additions of 0.019 M $Fe(II)SO_4$ every 2 minutes 92

Figure 5.4 Eh-pH diagram of Fe-Li-P-H_2O system at 25℃ and one atmosphere of pressure [85] 93

Figure 5.5 XRD patterns of leach residues with 0.095 M and 0.285 M $Fe(II)SO_4$ (2 M H_2SO_4, NMC/LFP molar ratio 1.36, S/L ratio 0.15 g/mL, 75°C, 51 minutes) and of $LiNi_{0.6}Mn_{0.2}Co_{0.2}O_2$ and $FePO_4$ 95

Figure 5.6 Simplified flow sheet for addition of LFP to an initial mixture of $Fe(II)SO_4$ and NMC 96

Figure 5.7 Leaching efficiencies for Mn, Ni, Co, Li, Fe and P (2 M H_2SO_4, NMC/LFP molar ratio 1.36, Fe^{2+} /NMC molar ratio 0.27, S/L ratio 0.15 g/mL, 75°C) with addition of LFP to initial mixture of $Fe(II)SO_4$ and NMC at 10 minutes 97

Figure 5.8 Leaching efficiencies for Mn, Ni, Co, Li, Fe and P (2 M H_2SO_4, NMC/LFP molar ratio 1.36, Fe^{2+} /NMC molar ratio 0.74, S/L ratio 0.15 g/mL, 75°C) with addition of LFP to initial mixture of $Fe(II)SO_4$ and NMC at 10 minutes 98

Figure 5.9 XRD patterns of leach residues with Fe^{2+}/NMC molar ratios 0.27 and 0.74 (2 M H_2SO_4, NMC/LFP molar ratio 1.36, Fe^{2+} /NMC molar ratio 0.74, S/L ratio 0.15 g/mL, 75°C, LFP added to initial mixture of $Fe(II)SO_4$ and NMC at 10 minutes) and pattern of $FePO_4$ 100

Figure 5.10 Simplified flow sheet for initial simultaneous addition of $Fe(II)SO_4$, NMC, and LFP 101

Figure 5.11 Leaching efficiencies for Mn, Ni, Co, Li, Fe and P (2 M H_2SO_4, NMC/LFP molar ratio 1.36, Fe^{2+} /NMC molar ratio 0.27, S/L ratio 0.15 g/mL, 75°C) with initial simultaneous addition of $FeSO_4$, NMC, and LFP 102

Figure 5.12 Leaching efficiencies for Mn, Ni, Co, Li, Fe and P (2 M H_2SO_4, NMC/LFP molar ratio 1.36, Fe^{2+} /NMC molar ratio 0.74, S/L ratio 0.15 g/mL, 75°C) with initial simultaneous addition of $FeSO_4$, NMC, and LFP 103

Figure 5.13 XRD pattern of leach residue (2 M H_2SO_4, NMC/LFP molar ratio 1.36, Fe^{2+} /NMC molar ratio 0.27, S/L ratio 0.15 g/mL, 75°C) with initial simultaneous addition of $FeSO_4$, NMC, and LFP (XRD carried out with Co source) 105

Figure 5.14 XRD pattern of leach residue (2 M H_2SO_4, NMC/LFP molar ratio 1.36, Fe^{2+} /NMC molar ratio 0.74, S/L ratio 0.15 g/mL, 75°C) with initial simultaneous addition of $FeSO_4$, NMC, and LFP, and pattern of $FePO_4$ 105

Figure 5.15 Simplified flow sheet for addition of NMC to an initial mixture of $Fe(III)_2(SO_4)_3$ and LFP 106

Figure 5.16 Leaching efficiencies for Mn, Ni, Co, Li, Fe, and P (2 M H_2SO_4, NMC/LFP molar ratio 1.36, S/L ratio 0.15 g/mL, 75°C) with addition of NMC to initial mixture of $Fe_2(SO_4)_3$ and LFP at 10 minutes 107

Figure 5.17 XRD patterns of leach residue (2 M H_2SO_4, NMC/LFP molar ratio 1.36, S/L ratio 0.15 g/mL, 75°C) with addition of NMC to initial mixture of $Fe_2(SO_4)_3$ and LFP at 10 minutes and phases $Li_{0.84}Ni_{0.6}Mn_{0.2}Co_{0.2}O_2$, $Li_{0.115}MnO_2$ and $FePO_4$ 109

Figure 5.18 Effect of the timing of the addition of LFP on leaching efficiencies for Mn, Ni, Co, Li, Fe and P (2 M H_2SO_4, NMC/LFP molar ratio 1.36, Fe^{2+} /NMC molar ratio 0.27, S/L ratio 0.15 g/mL, 75°C) .

..... 114

LIST OF TABLES

Table 1.1 Advantages and disadvantages of anode materials [14] 5

Table 1.2 Advantages and disadvantages of spent battery recycling methods 11

Table 1.3 Use of organic acids for metal leaching from spent NMC 13

Table 1.4 Use of inorganic acids for metal leaching from spent NMC 14

Table 1.5 Use of organic acids for metal leaching from spent LFP 15

Table 1.6 Use of inorganic acids for metal leaching from spent LFP 16

Table 1.7 Use of inorganic/organic acids for metal leaching from spent mixtures 19

Table 2.1 Breakdown of analytical errors 31

Table 2.2 Leaching efficiencies (2 M H_2SO_4, NMC/LFP molar ratios 1.02, S/L ratio 0.15 g/mL, 0.68 M H_2O_2, 75 °C, 51 minutes) 32

Table 2.3. Calculation of Standard Deviation for each element (2 M H_2SO_4, NMC/LFP molar ratio 1.02, S/L ratio 0.15g/mL, 0.68 M H_2O_2, 75 °C, 51 minutes) 33

Table 3.1. Metal content of NMC (g/kg), error +/- 5% 35

Table 3.2. Calculated stoichiometry of NMC 35

Table 3.3. Metal content of LFP (mg/kg), error +/- 5% 37

Table 3.4. Calculated stoichiometry of LFP 37

Table 3.5. Metal content (mmol/g) of leach residue (2 M and 6 M H_2SO_4, S/L 0.10 g/mL, 75°C) 41

Table 3.6. NMC leaching efficiencies with S/L ratios of 0.10, 0.15 and 0.20 g/mL (2 M H_2SO_4 at 75°C for 82 min) 42

Table 3.7. Leaching efficiency for NMC with S/L ratios 0.10, 0.15 and 0.20 g/mL (2 M H_2SO_4, 0.68 M H_2O_2, 75°C, 82 minutes, H_2O_2 added at 60 minutes) 44

Table 3.8. Metal content (mmol/g) of leach residue (6 M H_2SO_4, S/L 0.10 g/mL, 75°C) 47

Table 3.9. Leaching efficiencies for LFP at S/L ratios of 0.10, 0.15 and 0.20 g/mL (2 M H_2SO_4, 75°C, 82 minutes) 48

Table 3.10. Leaching efficiency of LFP (S/L ratio 0.10, 0.15 and 0.20 g/mL, 2 M H_2SO_4, 0.68 H_2O_2, 75°C, 82 minutes) with H_2O_2 added at 60 minutes 50

Table 3.11. Metal content (mmol/g) of leach residue with and without 0.68 M H_2O_2 (2 M H_2SO_4, 75°C, S/L 0.2 g/mL, 82 minutes) 50

Table 3.12. Phase identification and lattice parameters of $FePO_4.2H_2O$ 52

Table 3.13. Calculation of stoichiometric acid requirement for NMC622 leaching 56

Table 3.14. Calculation of stoichiometric acid requirement for LFP leaching 57

Table 4.1. Experimental design for study of the effect of S/L ratio on metal leaching efficiency from mixed NMC and LFP 61

Table 4.2. Effect of S/L ratio on metal content (mmol/g) in leach residue (S/L ratios ranging from 0.05 to 0.20 g/mL, 2 M H_2SO_4, NMC/LFP mass ratio 1 (NMC/LFP molar ratio 1.67), 75°C, 82 minutes) 62

Table 4.3. Effect of S/L ratio on metal content (mmol/g) in leach residue (S/L ratios ranging from 0.10 to 0.20 g/mL, 2 M H_2SO_4, 0.68 M H2O2, NMC/LFP mass ratio 1 (NMC/LFP molar ratio 1.67), 75°C, 82 minutes) 68

Table 4.4. Experimental design for studying the effect of NMC/LFP molar ratio on metal leaching efficiency in mixed NMC and LFP materials 69

Table 4.5. Effect of NMC/LFP molar ratio on metal content (mmol/g) in leach residue (NMC/LFP molar ratios ranging from 0.5 to 4.1, 2 M H_2SO_4, 0.68 M H_2O_2, S/L ratio 0.15 g/mL, 75°C, 51 minutes) 73

Table 4.6. Elemental content determined by EDS analysis that corresponds to the SEM image (Figure 4.12) (NMC/LFP molar ratio 1.02, 2 M H_2SO_4, 0.68 M H_2O_2, S/L ratio 0.15 g/mL, 75°C, 51 minutes) 75

Table 4.7. Elemental content determined by EDS analysis that corresponds to the SEM image (Figure 4.14),) (NMC/FLP molar ratio 1.36, 2 M H_2SO_4, 0.68 M H_2O_2, S/L ratio 0.15 g/mL, 75°C, 51 minutes) 78

Table 4.8. Experimental design for studying the effect of H_2SO_4 concentration on metal leaching efficiency from mixed NMC and LFP materials 78

Table 4.9. Effect of H2SO4 concentration on metal content (mmol/g) in leach residue with 0.25 M, 0.50 M and 2 M H_2SO_4 (0.68 M H_2O_2, S/L ratio 0.15 g/mL, NMC/LFP molar ratio 1.36, 75°C, 51 minutes, H_2O_2 added at 30 minutes) 79

Table 4.10. Experimental design for studying the effect of H_2O_2 concentration on metal leaching efficiency from mixed NMC and LFP materials 81

Table 4.11. SO_4^{2-}/metal molar ratios of initial solid with 0.25 M, 0.50 M and 2 M H_2SO_4 (0.68 M H_2O_2, S/L ratio 0.15 g/mL, NMC/LFP molar ratio 1.36, 75°C, 51 minutes, H_2O_2 added at 30 minutes) 86

Table 5.1. Experimental design for study of the effect of adding $FeSO_4$ on metal leaching efficiencies.. 89

Table 5.2. Effect of $FeSO_4$ concentration on ORP (V) under conditions of 2 M H_2SO_4, 0.285 M Fe(II)SO_4, NMC/LFP molar ratio 1.36, S/L ratio 0.15 g/mL, 75°C, Fe(II)SO_4 added at 30 minutes and first sample taken at 35 minutes and followed by incremental additions of 0.019 M Fe(II)SO_4 every 2 minutes 93

Table 5.3. Effect of Fe(II)SO_4 concentration on metal content (mmol/g) in leach residues with 0.095 M and 0.285 M Fe(II)SO_4 (2 M H_2SO_4, NMC/LFP molar ratio 1.36, S/L ratio 0.15 g/mL, 75°C, 51 minutes) 94

Table 5.4. Experimental design for study of addition of LFP to an initial mixture of Fe(II)SO_4 and NMC 96

Table 5.5. Effect of Fe^{2+}/NMC molar ratio on ORP (v) with Fe^{2+}/NMC molar ratios 0.27 and 0.74 (2 M H_2SO_4, NMC/LFP molar ratio 1.36, S/L ratio 0.15 g/mL, 75°C, addition of LFP to initial mixture of Fe(II)SO_4 and NMC at 10 minutes) 98

Table 5.6. Effect of Fe^{2+}/NMC molar ratio on metal content (mmol/g) in the leach residues with Fe^{2+}/NMC molar ratios 0.27 and 0.74 (2 M H_2SO_4, NMC/LFP molar ratio 1.36, S/L ratio 0.15 g/mL, 75°C) and LFP added to the initial mixture of Fe(II)SO_4 and NMC at 10 minutes 99

Table 5.7. Experimental design for study of initial simultaneous addition of $FeSO_4$, NMC and LFP 101

Table 5.8. Effect of Fe^{2+}/NMC molar ratio on ORP (v) with Fe^{2+}/NMC molar ratios 0.27 and 0.74 (2 M H_2SO_4, NMC/LFP molar ratio 1.36, S/L ratio 0.15 g/mL, 75°C) and initial simultaneous addition of $FeSO_4$, NMC and LFP 103

Table 5.9. Effect of Fe^{2+}/NMC molar ratio on metal content (mmol/g) of leach residues with Fe^{2+}/NMC molar ratios 0.27 and 0.74 (2 M H_2SO_4, NMC/LFP molar ratio 1.36, S/L ratio 0.15 g/mL, 75°C) and initial simultaneous addition of $FeSO_4$, NMC and LFP 104

Table 5.10. Experimental design for study of addition of NMC to an initial mixture of $Fe_2(SO_4)_3$ and LFP 106

Table 5.11. Effect of Fe^{3+}/LFP molar ratio on ORP (V) (2 M H_2SO_4, NMC/LFP molar ratio 1.36, S/L ratio 0.15 g/mL, 75°C) with addition of NMC to initial mixture of $Fe_2(SO_4)_3$ and LFP at 10 minutes 108

Table 5.12. Effect of Fe^{3+}/LFP molar ratio on metal content (mmol/g) in leach residue (2 M H_2SO_4, NMC/LFP molar ratio 1.36, S/L ratio 0.15 g/mL, 75°C) with addition of NMC to initial mixture of $Fe_2(SO4)_3$ and LFP at 10 minutes 108

Table 5.13. Calculation of Fe(II)SO_4, NMC and LFP moles based on the experimental design..... 110

Table 5.14. Calculation of NMC, LFP and Fe(II)SO_4 moles based on the experimental design..... 112

Table 5.15. Calculation of NMC, LFP and Fe(II)SO_4 moles based on the experimental design..... 113

Table 5.16. Calculation of NMC, LFP and $Fe(III)_2(SO4)_3$ moles based on the experimental design 115

LIST OF ABBREVIATIONS

BM	Black Mass
Co	Cobalt
EDX	Energy Dispersive X-ray Spectroscopy
EV	Electric Vehicle
Fe	Iron
FP	Iron (III) Phosphate
ICP-OES	Inductively Coupled Plasma–Optical Emission Spectrometry
Li	Lithium
LCO	Lithium Cobalt Oxide
LFP	Lithium Iron Phosphate
LIB	Lithium-Ion Battery
LMO	Lithium Manganese Oxide
LNO	Lithium Nickel Oxide
Mn	Manganese
Ni	Nickel
NMC	Lithium Nickel Manganese Cobalt Oxide
NCA	Lithium Nickel Cobalt Aluminum Oxide
ORP	Oxidation–Reduction Potential
P	Phosphorus
PVDF	Polyvinylidene Fluoride
SEM	Scanning Electron Microscopy
S/L	Solid–Liquid Ratio
XRD	X-ray Diffraction

CHAPTER I

INTRODUCTION

Renewable energy is expected to supply 20-30% of global energy requirements by 2040, thanks to efforts to reduce greenhouse emissions [1]. Lithium-ion batteries (LIBs), today's transformative energy storage solution of choice, are key enablers of this transition and have significantly affected modern life. These batteries are commonly used in portable devices, electric vehicles (EVs) and renewable energy systems, changing how we store and use energy. The transition away from fossil fuels towards renewable energy sources is driving the demand for LIBs, particularly the use of cylindrical LIBs in electric vehicle (EV) applications. Annual LIB demand for new electric vehicles is projected to reach 5,910 GWh by 2040 [2]. This growing demand presents significant challenges for the supply of raw materials required for LIB production and means generation of substantial quantities of spent LIBs, creating complexities in resource management and environmental protection. Additionally, the anticipated demand for lithium (Li), cobalt (Co) and nickel (Ni) for LIBs for electric cars will exceed current production levels by 2040. For example, projected demand for Li and Co is as much as eight times the current production levels [3]. Recycling can be a good way of returning materials to the value chain, and it is also ecologically and economically significant. Accordingly, this chapter begins with a synthetic literature review that covers the structure of LIBs (types of anode and cathode materials, composition), the management of spent batteries and the most common recycling processes. Research goals and structure of the dissertation are also outlined in this chapter.

1.1. Lithium-ion battery structure

A typical LIB consists of several components: cathode, anode, polymeric separator, electrolyte, current collector and casing. These components are arranged in layers and are curled and wrapped in thin aluminium-stainless steel or aluminium-plastic covers [4]. LIBs come in different shapes, including cylindrical, coin, prismatic and pouch (see Figure 1.1) [5]. EVs and other devices mainly use cylindrical cell batteries, because they are cost effective and stable. Cylindrical cells offer consistent performance, reliability and durability across batches and over time. In 2008, Tesla's inaugural electric vehicle used cylindrical cells to store energy because these cells have a higher volumetric and gravimetric density than alternative cell types [6].

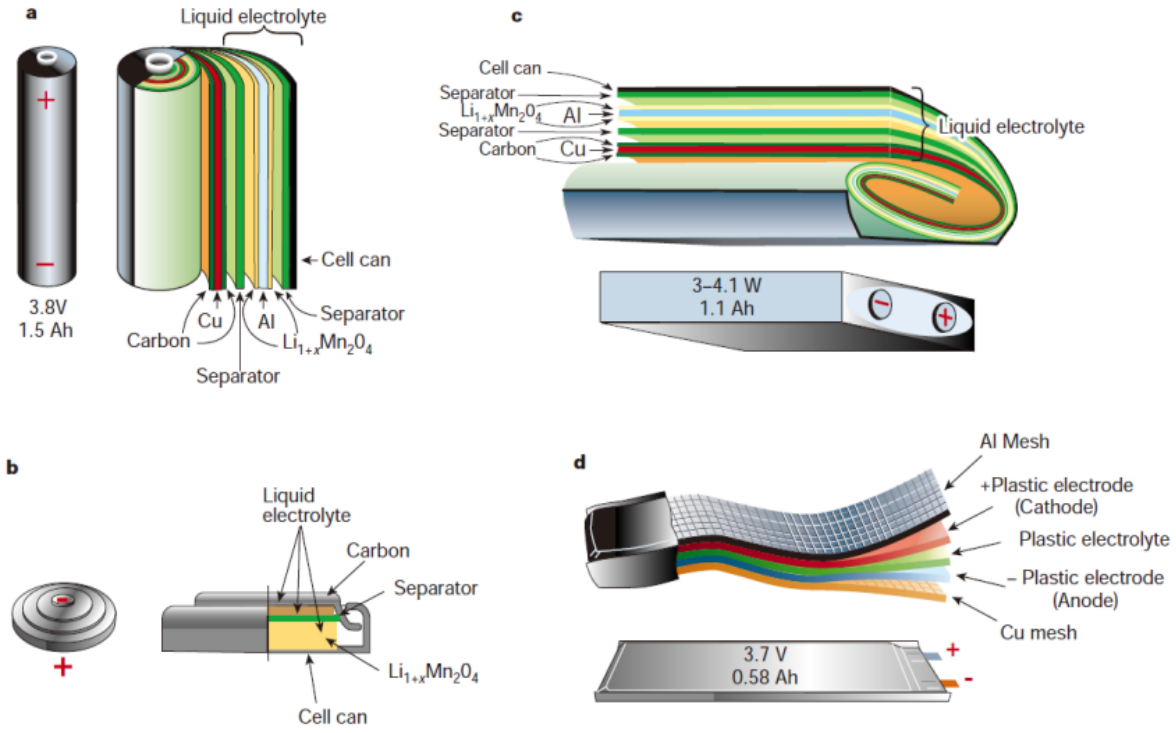

Figure 1.1. Main types of LIBs cells: a) cylindrical, b) coin, c) prismatic and d) pouch [5]. *Reproduced with permission from Springer Nature*

The components of an LIB are assembled to facilitate charging and discharging. During charging, lithium ions start moving from the cathode to the anode through the electrolyte, while electrons are released from the cathode and flow through the external circuit, providing electrical energy. The graphite anode accepts the Li^+ ions and undergo a process called intercalation whereby the Li^+ ions become embedded in the structure of the graphite anode as shown in Figure 1.2 [7].

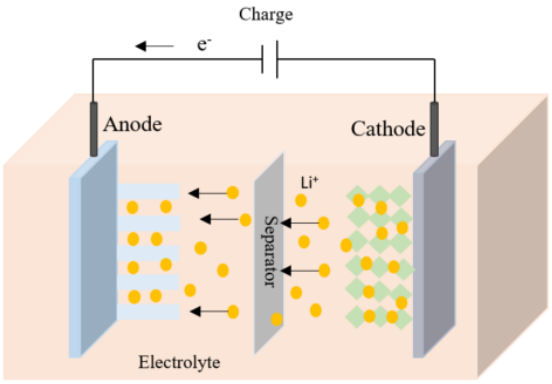

Figure 1.2. Schematic operational principle of LIB charging [7]

This movement reverses during discharge: the anode releases the embedded Li^+ ions, which then travel back to the cathode through the electrolyte. During discharge, electrons flow through the external circuit, creating an electric current that powers the device, as shown in Figure 1.3.

The chemical reactions in the two electrodes during charge and discharge can be expressed as follows:

Cathodic reaction:

$$6C + xLi^+ + xe^- \leftrightarrow Li_xC_6 \quad (1.1)$$

Anodic reaction:

$$LiM(III)O_2 \leftrightarrow Li_{(1-x)}M(IV)xM(III)(1-x)O_2 + xLi^+ + xe^- \quad (1.2)$$

The charge reaction occurs forward, while the discharge reaction occurs in reverse. The reversible electron transfer reaction and energy storage through the movement of Li^+ ions from the cathode to the anode during charge and discharge for a typical layered oxide cathode (M= transition metal) and carbon anode is expressed in Equation (1.3) [8] .

$$6C + LiMO_2 \leftrightarrow Li_xC_6 + Li_{(1-x)}MO_2 \quad (1.3)$$

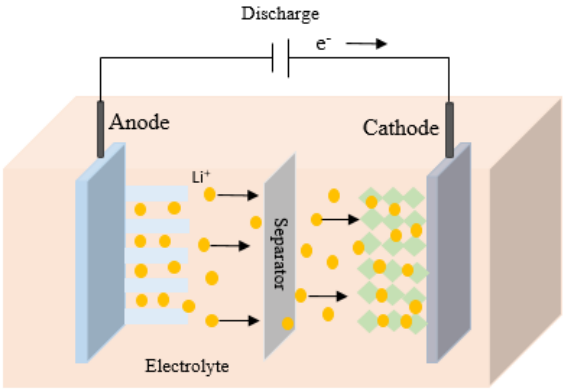

Figure 1.3. Schematic operational principle of LIB discharging [7]

Based on the principle of LIB charge and discharge, the electrode material should be both thermally stable and a good conductor for the ions and electrons, while the electrolyte should be less reactive to the electrodes and have good ionic conductivity [9]. The electrolyte most commonly used in LIBs is a solution of lithium hexafluorophosphate in an alkyl carbonate solvent such as ethyl carbonate or dimethyl carbonate [10]. Cathodes and anodes are composed of intercalation compounds bound together with organic binders like polyvinylidene fluoride (PVDF) and coated onto electronic conductors, ensuring optimal performance and functionality [10]. The current collector must maintain chemical and electrochemical stability in the electrolyte during cell operation. The current collector material, accordingly, must have outstanding mechanical qualities and adhere well to electrode slurries [11]. Aluminum foil is ideal for cathode collectors because of its characteristics and its ability to generate a passive coating that stabilizes the electrolyte/Al contact [12]. Copper foil is commonly used as an anode current collector given its low resistivity (1.68×10^{-8} Ω·m at 20°C) [13]. All components, including the cathode, anode and membrane layers, are consolidated by rolling or folding them together, after which they are enclosed within a casing made of plastic or metal.

1.1.1. Anode materials

The original negative electrode material was Li metal, the periodic table's lightest solid. Li metal electrodes and polar aprotic electrolyte solvents produce a dense surface coating, making passivation impossible [14]. Such an anode has a high specific capacity but is more sensitive to Li dendrite formation, which raises safety concerns and results in excessive Li consumption. Graphite is a typical anode material that is simple to manufacture, but it has a low specific capacity and is unsuitable for high-performance Li batteries. As a

result, researchers have been working hard to produce alternative anode materials, such as carbon nanomaterials, transition metal oxides and metal organic frameworks. Table 1.1 shows the advantages and disadvantages of each type of anode material.

Table 1.1. Advantages and disadvantages of anode materials [14]

Type of anode material	Advantages	Disadvantages
Lithium alloys	Light	Safety issues
Graphite carbon	Low cost Easy preparation Multiple forms	Low specific capacity Not high performance
Non-graphite carbon	Good stability	Disordered intrinsic crystallites High reversibility Capacity loss issues
Transition metal oxides	High theoretical specific capacity Adjustable operating voltage Excellent cycle performance	Inherent poor conductivity Continuous electrolyte decomposition
Metal organic frameworks	Good charge-carrying capacity Porous structure	Early phase of research

1.1.2. Cathode materials

Cathode materials generally fall into two major categories: Li transition metal oxides and polyanionic compounds.

1.1.2.1. Lithium transition metal oxides

Lithium transition metal oxides are key positive electrode materials in lithium batteries [15]. These oxides fall into two major categories: Li metal oxides ($LiMO_2$) with a layered structure, where M is a transition metal such as Co, Mn, Al or Ni or some combination thereof (Ni-Mn-Co, for example); and Li metal oxides with the formula LiM_2O_4, which exhibit a spinel structure [16]. In layered structures, the transition metal and oxygen are arranged in distinct parallel planes or layers within a crystal lattice, while the Li ions are located in the interstitial sites between the layers as shown in Figure 1.4 [9]. The most notable feature of these layered structures is the ability of Li ions to intercalate or insert themselves between the layers. As mentioned, Li ions move in and out of these interlayer spaces during charge and discharge, a crucial

mechanism for battery operation [16]. Basic layered transition metal oxides are Li-Co oxide ($LiCoO_2$ or LCO), Li-Ni oxide ($LiNiO_2$ or LNO) and Li-Mn oxide ($LiMnO_2$ or LMO). Ternary layered transition metal oxides are Ni-layered oxide ($LiNi_{0.333}Mn_{0.333}Co_{0.333}O_2$), Ni-rich layered transition metal oxides ($LiNi_xMn_yCo_zO_2$ or NMC) and Al substituted NMC ($LiNi_xCo_yAl_zO_2$ or NCA). The nickel-manganese-cobalt (NMC) battery is the most commonly used LIB thanks to the high energy density conferred by its components. As Figure 1.5 shows, there are different levels of Ni in NMC composition: for example, $LiNi_{0.333}Mn_{0.333}Co_{0.333}O_2$ (abbreviated NMC111 or NMC333) $LiNi_{0.5}Mn_{0.3}Co_{0.2}O_2$ (NMC532), $LiNi_{0.6}Mn_{0.2}Co_{0.2}O_2$ (NMC622) and $LiNi_{0.8}Mn_{0.1}Co_{0.1}O_2$ (NMC811). The NMC battery benefits from the best characteristics of $LiNiO_2$, $LiCoO_2$ and $LiMnO_2$: $LiNiO_2$'s high charge capacity; $LiCoO_2$'s excellent rate capability with respect to capacity and power output; and $LiMnO_2$'s thermal stability and low cost [17].

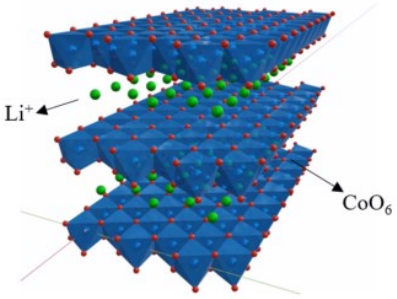

Figure 1.4. Layered structure of LiMO2 (LiCoO2) [9]

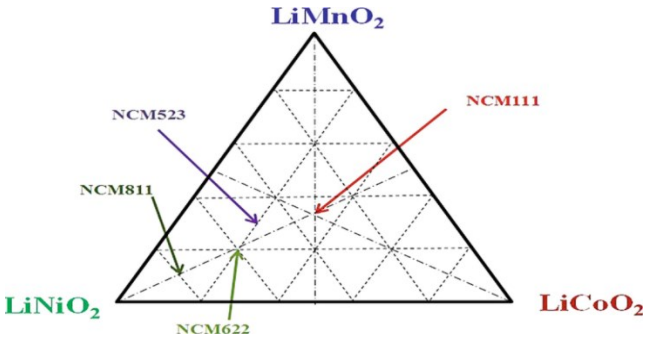

Figure 1.5. Schematic drawing of different Ni layered oxides ($LiNi_xMn_yCo_zO_2$) [17]

Spinel $LiMn_2O_4$ (Figure 1.6) is among the most attractive energy storage materials due to its low production cost, high thermal stability, high voltage and good safety profile [18]. However, it has limitations, including its lower energy density than cathode materials with Ni or Co. In sum, the choice between spinel and layered cathode materials depends on the specific requirements of the application. Spinels are known for their

safety, cost-effectiveness and excellent rate capability, making them suitable for high-power applications [19]. Layered structures achieve higher energy densities but come with higher costs and environmental issues. Cathode material selection often calls for trade-offs between energy density, costs and other performance characteristics.

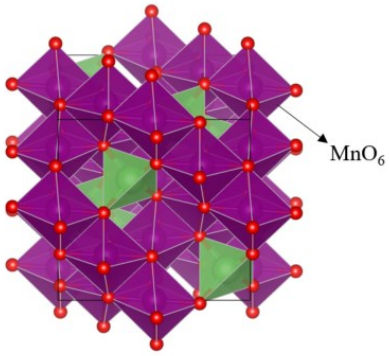

Figure 1.6. Spinel structure of $LiMn_2O_4$ [9]

1.1.2.2. Polyanionic compounds

A polyanionic compound is a material containing multiple negatively charged ions (anions) bonded together in a structured network. Such compounds typically feature a central atom, usually a transition metal, surrounded by oxygen atoms arranged in a tetrahedral configuration. The strong covalent bonds in this tetrahedral structure confer significant stability to the compound, contributing to its unique and valuable properties. These compounds have higher thermal stability than conventional layered transition metal oxides and are more suitable for LIBs. $LiMPO_4$ has an orthorhombic structure in which the transition metals (M) are interconnected with six oxygen atoms to form an edge-shared octahedron. Polyanionic compounds are safer and have longer cycling lives than layered oxides and spinels. Since the first report on $LiFePO_4$ electrochemical performance, polyanionic compounds have attracted significant research interest [9, 20].

The lithium iron phosphate battery (LFP) (general formula = $LiFePO_4$) was developed by John Goodenough in the late 1990s and has been commercially available since 2006. $LiFePO_4$ is attracting significant attention as a promising new cathode material for LIBs [16]. The crystal shape of olivine $LiFePO_4$ incorporates a polyanionic framework along with octahedral LiO_6, octahedral FeO_6 and tetrahedral PO_4 as shown in Figure 1.7 [21]. The specific characteristics of $LiFePO_4$ (e.g., cycle stability, safety, environmental friendliness and potential low cost) position this material to play a dominant role in the electric vehicle sector in the coming years [20]. The main drawback of olivine structures is their poor electronic and ionic conductivity, given their rigid and stable crystal framework, strong covalent bonding and narrow ion migration pathways.

Research to improve the electrochemical performance of the $LiFePO_4$ cathode electrode shows surface modification and coating with different materials (carbon nano fillers and conducting polymers, for example) to be the most effective and conventional approach [16].

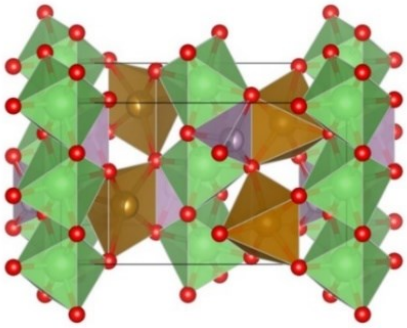

Figure 1.7. Crystal structure of olivine $LiFePO_4$ for Li-ion batteries [21]

1.2. Management of spent LIBs

In 2025, NMC batteries accounted for the biggest share of the worldwide LIB market (70%), followed by LFP (15%) and NCA (8%) batteries, as shown in Figure 1.8 [22]. With growth in demand for these LIBs for devices such as portable electronics and electric vehicles and for renewable energy storage, addressing their waste management is vital. The complex composition of these batteries, which contain a variety of metals and chemicals, makes their proper disposal crucial to prevent environmental contamination and resource depletion.

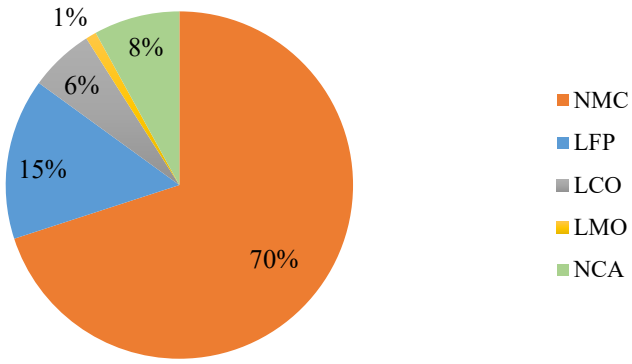

Figure 1.8. Five significant classes of cathode materials

(875 million metric tons, 2025) [22]

In the electric vehicle (EV) industry in particular there has been a substantial surge in demand for LIBs, now recognized as significant contributors to the upcoming wave of LIB waste [23]. Waste LIBs present numerous hazardous characteristics, including the potential for spontaneous ignition and release of hazardous chemicals when landfilled or incinerated [24, 25]. Accordingly, the management of spent LIBs is a critical aspect of modern waste management strategies requiring careful consideration to balance environmental impacts and resource recovery. Recycling spent LIBs promotes recovery of valuable metals and helps minimize the environmental impacts of hazardous waste as well as resource depletion [10]. The metals recovered could serve as valuable components in the battery production industry or in other industrial sectors.

1.3. Recycling spent LIBs

The recycling of spent LIBs has become increasingly critical as the demand for electric vehicles (EVs) and portable electronics continues to rise. These batteries contain valuable materials, such as Li, Co, Ni and Mn, making their recycling economically and environmentally beneficial. The recycling process typically involves several steps, including collection, pretreatment, separation of components and extraction of valuable metals through different methods.

1.3.1. Battery sorting

Sorting batteries is a critical step in the recycling process that entails classifying and separating batteries based on their composition, size and chemistry. The sorting of batteries based on their chemistry, whether manually or through optical and mechanical means, is crucial to prevent contamination in downstream processes, especially in the case of bulk delivery of mixed batteries. Technologies like Sortbat in Belgium have demonstrated good potential, achieving remarkable purity levels of up to 99.7% through a combination of manual pre-sorting, mechanical sorting and automated methods based on magnetic resonance response [26]. Nonetheless, sorting of the various LIB types based on their chemistry remains challenging due to differences in intrinsic composition and the evolving nature of the materials, necessitating ongoing research and development efforts [10]. For this reason, research groups have been working to develop flexible hydrometallurgical processes for recycling mixed-spent batteries. Otron et al. [27], for example, demonstrated the possibility of leaching and recovering metals (rare earth elements, zinc, manganese, nickel, cobalt, and cadmium) from unsorted batteries with high recovery efficiencies. Li et al. [28] achieved high recovery rates by leaching a blended stream of LIBs with hydrochloric acid, but their approach did not

provide a closed-loop solution for recycling spent mixed active materials into the production of new batteries.

1.3.2. Pretreatment

Pretreatment is crucial in recycling spent LIBs to separate battery components and prevent short-circuiting or spontaneous combustion [29]. Pretreatment processes fall into three categories: mechanical, thermal and chemical [30, 31].

A common method of pretreatment calls for manual battery pack dismantling and then discharging, crushing and shredding, material separation, electrolyte recovery and binder separation to separate the cathode, anode and other components [10]. Pretreatment produces a powder called "black mass" that contains the cathode materials. The next crucial step is to remove residues such as PVDF, carbon black and graphite from the cathode active materials by recovery processes such as thermal pyrolysis with froth flotation [32]. Thermal pyrolysis decomposes the PVDF binder and the carbon black, altering the material properties for effective froth flotation. This method separates graphite and carbon black, leaving behind purified cathode active materials. It also facilitates the efficient separation of cathode materials in LIBs, enhancing purity for further processing.

1.3.3. Recycling

There are three main methods of recycling spent LIBs: pyrometallurgy, hydrometallurgy and direct recycling.

Pyrometallurgy, a well-established technique, uses high-temperature smelting furnaces to incinerate carbon, plastic separators and electrolytes while reducing and recovering valuable metals as alloys [33]. With pyrometallurgy, valuable transition elements can be extracted for reintegration into the production chain. Pyrometallurgy is currently the method most commonly used in the recycling industry by major companies such as Umicore (Belgium), Batrec (Switzerland), Dowa and Sumitomo (Japan) [10]. Pyrometallurgy is a simple recycling approach that is highly efficient and productive. However, it does not recover Li and is not considered environmentally sustainable given the associated hazardous gas emissions and high energy consumption [34].

Hydrometallurgy uses aqueous solutions to extract, separate and purify valuable metals. It has attracted considerable interest in battery recycling research as it requires less energy than pyrometallurgy [10, 35]. Typical acids used in LIB leaching include inorganic acids such as sulphuric (H_2SO_4) [36], hydrochloric (HCl) [37], nitric (HNO_3) [38] and phosphoric (H_3PO_4) [39] acid and organic acids such as citric [40],

oxalic [41] and formic [42, 43] acid. Extraction by acid leaching can be assisted by reducing agents such as hydrogen peroxide (H_2O_2) [44-46], sodium bisulfite ($NaHSO_3$) [47], Fe^{2+} [48, 49] and glucose [50] to improve dissolution of metal ions such as Mn and Co from the solid material into the leaching solution and accelerate leaching kinetics [10]. The reducing agent promotes conversion of low-soluble metal compounds into more soluble forms, facilitates redox reactions and increases leaching efficiency. Separation is the next step in the recycling process. Different methods can be used, including selective precipitation by adjusting pH [51], liquid-liquid extraction [52] and crystallization [53]. Table 1.2 summarizes the advantages and disadvantages of these two methods for recycling spent batteries.

Table 1.2. Advantages and disadvantages of spent battery recycling methods

Method	Advantages	Disadvantages
Pyrometallurgy	Simple process Suitable for extensive industrial use Can efficiently recycle large quantities of spent batteries	Requires pretreatment processes High-energy consumption Produces large quantities of heavy-metal-containing solid waste Requires an off-gas treatment system Requires hydrometallurgy as well for metal recovery from slag
Hydrometallurgy	Low energy consumption Low toxic gas emissions Highly efficient High-purity products Suitable for large-scale industrial systems	Requires pretreatment processes Generates large quantities of wastewater

1.4. Hydrometallurgical recovery of valuable metals

After initial material separation during pretreatment, spent cathode active materials undergo metallurgical processing for recovery of valuable metals. Hydrometallurgy has emerged as a prominent technique for recycling valuable metals from spent LIB cathodes due to its high efficiency in selective leaching and metal recovery, lower energy requirements and friendlier environmental profile. Additionally, its adaptability has led to its widespread use in commercial-scale production. The recycling of spent LIBs in water-based solutions is typically categorized by battery type (NMC or LFP, for example) due to significant differences in cathode composition and leaching behaviour. Most research described in the literature focuses on treating these materials separately, with few studies of mixed cathode leaching. Though recyclers in commercial

plants can process mixed cathode materials simultaneously using existing hydromet methods, it is not an optimal solution as competing reactions and contamination of the pregnant leach solution with impurities increases operational costs.

1.4.1. NMC cathodes

As mentioned, NMC batteries are the most widely used type of LIB thanks to their high energy density, attributable to their valuable components. Recycling research to date has focused primarily on NMC batteries given the higher concentrations of valuable metals (such as Ni, Co and Mn) in these batteries than in other battery types. A number of different organic and inorganic acids can serve as leaching agents, with the notable advantages of eco-friendliness and higher leaching efficiency. The main factors affecting the leaching process are leaching agent concentration, reducing agent concentration, temperature, reaction time and solid-liquid ratio. Organic acids are attractive options as leaching agents because of their biodegradability [54]. However, despite their advantages and their high leaching efficiency, organic acids are more costly than inorganic acids, which means increased operating costs when used in commercial applications. Moreover, most organic acids have lower acidity levels than typical inorganic acids, decelerating the leaching reaction rate and consequently constraining productivity. Organic acids have not, accordingly, been widely adopted as leaching agents in the battery-recycling sector. Table 1.3 summarizes some of the studies that used organic acids to leach metals from spent NMC cathodes.

Inorganic acids have emerged as the preferred choice for leaching NMC cathode materials from LIBs because of their effectiveness, economic advantages, practicality and versatility. Table 1.4 summarizes several studies that used inorganic acids to leach metals from spent NMC. Among these acids, sulphuric acid stands out for its ability to efficiently dissolve metal oxides, yielding high metal recovery rates. In addition, its widespread availability and low cost make it economically viable for large-scale recycling operations, and established methodologies and infrastructure further enhance its practicality. Furthermore, sulphuric acid's flexibility in adjusting leaching conditions allows optimization tailored to different NMC cathode compositions, solidifying this acid’s position as an efficient solution for NMC leaching. Kim et al. [55] studied the physical/chemical recycling process for spent NMC from used hybrid electric vehicles. They report 99% leaching efficiencies for Mn, Ni, Co and Li with H_2SO_4 as leaching agent and H_2O_2 as reducing agent under conditions of 2 M H_2SO_4, 5 vol% H_2O_2, 60°C, stirring speed 300 rpm, S/L ratio 0.10 g/mL and reaction time 120 minutes. In another study, He et al. [56] obtained the recovery rate of 99.7 % for Li, Ni, Co and Mn under conditions of 1 M H_2SO_4, 1 vol% H_2O_2, S/L 0.04 g/L, 40°C and 60 minutes. Despite the high leaching rates with these acids, challenges (such as high consumption of reactants and energy and low S/L ratio) remain, suggesting areas for optimization.

Table 1.3. Use of organic acids for metal leaching from spent NMC

LIB type	Leaching agent	Reducing agent	Conditions: S/L ratio (g/mL) Temperature (°C) Time (min)	Efficiency (%)	Ref
NMC	3.5 M acetic acid	4 vol% H_2O_2	0.04 60 60	Mn = 96.3 Ni = 92.7 Co =93.6 Li = 99.97	[54]
NMC	1 M acetic acid	3 mL H_2O_2	NA 70 60	Mn = 97.07 Ni = 97.27 Co = 97.72 Li = 98.39	[57]
NMC	2 M maleic acid	2 mL H_2O_2	NA 70 60	Mn = 98.06 Ni = 98.05 Co = 98.41 Li = 98.24	[57]
NMC	2 M formic acid	6 vol% H_2O_2	0.05 60 45	Mn = 62.42 Ni = 49.80 Co = 37.77 Li = 99.93	[43]
NMC	1 M citric acid	12 vol% H_2O_2	0.08 60 40	Total metals > 98	[40]
NMC	0.5 M citric acid	1.5 vol% H_2O_2	0.02 90 60	Mn = 95.2 Ni = 98.7 Co = 99.8 Li = 99.1	[58]
NMC	1.5 M lactic acid	0.5 vol%H_2O_2	0.02 70 20	Mn = 98.4 Ni = 98.2 Co = 98.9 Li = 97.7	[59]

Table 1.4. Use of inorganic acids for metal leaching from spent NMC

LIB type	Leaching agent	Reducing agent	Conditions: S/L ratio (g/mL) Temperature (°C) Time (min)	Efficiency (%)	Ref
NMC	4 M HCl		0.02 80 60	Mn = 99 Ni = 99 Co = 99 Li = 99	[60]
NMC	0.5 M HNO_3 0.5 M ascorbic acid		0.02 85 10	Mn = 100 Ni = 100 Co = 100 Li = 100	[61]
NMC	2 M H_2SO_4	5 vol% H_2O_2	0.10 60 120	Mn = 99 Ni = 99 Co = 99 Li = 99	[55]
NMC	1 M H_2SO_4	1 vol% H_2O_2	0.04 40 60	Mn = 99.7 Ni = 99.7 Co= 99.7 Li = 99.7	[56]
NMC	3 M H_2SO_4	3 vol% H_2O_2	0.02 80 60	Mn = 97 Ni = 98.1 Co = 96.5 Li = 97.8	[62]
NMC	2 M H_2SO_4	30 g/L hydrazine sulfate	0.05 80 60	Mn = 86 Ni = 96 Co = 95 Li = 97	[63]
NMC	2.5 M H_2SO_4	0.8 M NH_4Cl	0.10 80 60	Mn =97.34 Ni = 97.49 Co = 97.55 Li = 99.11	[64]

1.4.2. LFP cathodes

LFP has attracted much attention since its discovery thanks to its unique olivine structure. Global demand for LFP batteries has grown rapidly, with China the leading producer and consumption market. The surge in EVs and hybrid electric vehicles (HEVs) has further fueled this demand, with market growth expected

to continue at a strong pace. This growing demand for LFP batteries is expected to lead to a significant increase in end-of-life disposal, potentially posing serious challenges in the near future. The recycling and recovery of valuable metals from spent LFP batteries is essential for resource conservation and environmental protection. Although extensive research has been conducted on recycling LCO and NMC batteries, few studies focus on recycling LFP batteries. Acid leaching is among the most common and effective recycling methods used to extract Li, Fe and P from LFP cathodes. Both inorganic and organic acids can be used in the leaching process, with organic acids offering advantages and drawbacks like those observed in NMC recycling. Table 1.5 summarizes studies of the use of organic acids for metal leaching from spent LFP.

Table 1.5. Use of organic acids for metal leaching from spent LFP

LIB type	Leaching agent	Oxidizing agent	Conditions: S/L ratio (g/mL) Temperature (°C) Time (min)	Efficiency (%)	Ref
LFP	1.25 M acetic acid		0.12 50 30	Li = 94.5 Fe = 99.3	[65]
LFP	0.1 M oxalic acid		0.01 25 30	Li = 99.3 Fe = 94	[66]
LFP	Citric acid	H_2O_2	0.06 25 90	Li = 94.8 Fe = 4.05	[67]
LFP	1 M formic acid	5% H_2O_2	0.10 30 30	Li=89.43 Fe<0.5	[68]

In acid leaching, using an inorganic acid such as H_2SO_4 as the leaching agent facilitates the recovery of Li^+. The efficiency and selectivity of the process can vary significantly depending on the leaching conditions, including acid concentration, temperature, S/L ratio and presence of oxidizing agents. However, recycling LFP is particularly challenging because of the lower intrinsic economic value of spent LFP batteries, which is based mainly on Li recovery. This makes LFP recycling less economically attractive than recycling other LIBs. Selective extraction of Li and transformation of the low-value iron and phosphate into a value-added heterosite $FePO_4$ product could be an attractive option [69]. Recovered heterosite $FePO_4$ (with an orthorhombic structure) can be used in new LFP production. This would offer a more energy-efficient,

environmentally sustainable and cost-effective alternative to traditional synthesis methods such as hydrothermal or carbothermal reactions. However, current hydrometallurgical processes for recycling LFP do not typically focus on recovery of orthorhombic $FePO_4$ as a valuable product. For example, Li et al. [70] report a 97% Li recovery rate with a highly selective process using diluted sulphuric acid as the leaching agent. However, the leach residue analysis indicated the $FePO_4$ obtained had a hexagonal rather than the required orthorhombic structure. In another study, Zheng et al. [71] achieved 97% leaching efficiency for Li recovery using 2.5 M H_2SO_4. Their process, however, involved complete dissolution of the LFP followed by use of ammonia to precipitate amorphous hydrated $FePO_4$, which is unsuitable for production of new LFP cathodes. In other words, developing a hydrometallurgical method that focuses on selective extraction of Li and recovery of heterosite $FePO_4$ for reuse in the manufacturing of LIBs remains a significant research gap. Table 1.6 summarizes studies that used inorganic acids for metal leaching from spent LFP.

Table 1.6. Use of inorganic acids for metal leaching from spent LFP

LIB type	Leaching agent	Oxidizing agent	Conditions: S/L ratio (g/mL) Temperature (°C) Time (min)	Efficiency (%)	Form of solid byproduct	Ref
LFP	0.3 M H_2SO_4 H_2SO_4/Li molar ratio 0.57	H_2O_2/Li molar ratio 2.07	NA 60 120	Li = 96.85 Fe = 0.03 P = 1.95	Hexagonal $FePO_4$	[70]
LFP	2.5 M H_2SO_4		0.10 60 240	Li = 97 Fe= 98	Amorphous $FePO_4 \cdot 2H_2O$	[71]
LFP	0.5 M H_3PO_4		0.04 25 40	LFP = 95	Monoclinic $FePO_4 \cdot 2H_2O$	[72]
LFP	1.3 M H_2SO_4	H_2O_2	0.20 20 90	LFP: 91.53	Al and $FePO_4$	[73]

1.4.3. Mixture of LIBs

With the growing use of electric vehicles, NMC and LFP batteries have become the most widely used battery types on the market and are expected to capture an even larger market share in the future. In addition, some studies have highlighted the advantages of blended NMC-LFP cathodes, which combine the high energy density of NMC with the excellent thermal stability and safety of LFP [74-76]. This rapid growth has also led to a significant increase in the number of spent batteries reaching the end of their life cycles. However, the current literature focuses on recycling individual types of cathode materials, such as NMC or LFP through hydrometallurgical processes, with little performed on recycling spent blended cathode materials, particularly those containing a combination of NMC and LFP. As mentioned, hydromet recycling plants process both types of cathode material either simultaneously or separately. However, in mixed leaching processes, conditions optimized for NMC can be detrimental to LFP, leading to increased operational costs. Separate leaching allows conditions to be tailored for each batch, but complicates process management and spent LIB feed stock management. In other words, developing and optimizing a flexible hydrometallurgical process capable of efficiently recycling mixed LIBs is a better option than focusing exclusively on individual battery chemistries.

A typical recycling process for recovering valuable metals from mixed LIBs involves the use of various organic or inorganic acids, often in combination with reducing or oxidizing agents to enhance metal extraction efficiency. Table 1.7 presents some research studies on recycling mixed streams of LIBs using different acids. In most studies, complete dissolution of transition metals such as Ni, Mn and Co is the main objective, with little focus on selective leaching of Li from LFP and recovery of $FePO_4$ for regenerating LFP. For example, Chen et al. [77] investigated the recycling of blended material from NMC and LFP batteries using phosphoric acid as a leaching solution. The study showed that 98.8% Mn, 99.5% Ni, 96.3% Co, 100% Li and 2.7% Fe were successfully dissolved into the leaching solution, while residual components remained as $FePO_4$ and carbon residue. Subsequent removal of carbon through calcination yielded hexagonal $FePO_4$. Similarly, Xu et al. [78] studied recovery of mixed LFP and NMC cathode materials using high-concentration $Fe_2(SO_4)_3$ (240 g/L) at a high temperature (90°C). The study indicated that Fe^{3+} serves as a Lewis acid facilitating $LiFePO_4$ to supply Fe^{2+} and reduce NMC and that 96.9% Mn, 97.9% Ni, 97.6% Co, 98.3% Li and 0.2% Fe were leached into the leaching solution. Meanwhile, the remaining leach residue precipitated as a complex mixture of $FePO_4$ and $Fe(OH)_3$, presenting challenges for both their separation and the subsequent regeneration of LFP.

Various investigations of acid-leaching methods for blended cathodes have explored recovery of Mn, Ni, Co and Li from mixed LIBs using sulphuric acid as the leaching agent with H_2O_2 as the reducing/oxidizing agent. These studies focus primarily on +99% recovery of transition metals, with limited attention to

removal of Fe through pH adjustment and no significant effort toward regeneration of LFP [79-81]. For example, Jiang et al. [82] reported the incomplete leaching of Co 92.4 %, while obtaining over 99% dissolution for Li, Fe and P from a mixture of LCO and LFP under the optimized conditions of 0.5 M H_2SO_4, S/L ratio of 0.03 mg/L, molar ratio of LCO/LFP 1:1 and 20 minutes. In their process, complete dissolution of LFP occurred, generating Fe (II) that acted as a reducing agent for Co. Subsequently, hexagonal $FePO_4$ was recovered by precipitation from the leachate at pH 2, followed by thermal treatment at 600 °C to obtain the final product. In another study, Tang et al. [83] used 1 M H_2SO_4 as the selective leaching agent to dissolve NMC and LFP under conditions of 30% H_2O_2 to raw material ratio 0.308 g/g, S/L ratio 0.19 g/mL, 300 minutes and 90°C. Leaching efficiencies achieved were 97.1%, 98.5%, 96.3%, 99.6%, 0.2% and 1.1%, respectively, for Mn, Ni, Co, Li, Fe and P, and the leach residue precipitated as the mixture $FePO_4 \cdot 2H_2O$ and carbon, which was then dissolved using HCl with recovery rates of 95.5% for P and 96.2% for Fe. Two-step leaching processes like this, however, suffer from slow kinetics (300 min) and complete dissolution of LFP. In another study, Song et al. [84] used high-concentration H_2SO_4, but dissolution of the cathode materials remained incomplete. Leaching efficiencies were 71.7%, 72.0%, 64.6% and 91.7% for Mn, Ni, Co and Li under conditions of 1.4 M H_2SO_4, 15 vol% H_2O_2, S/L ratio 0.25 g/mL, 60 minutes and 40°C. In addition, Zou et al. [85] studied the synergistic redox reaction of NMC and LFP in diluted H_2SO_4 by solubilizing more than 99% of transitional metals and 90% of Fe and P under conditions of 0.5 M H_2SO_4, S/L ratio 0.05 g/mL, NMC/LFP molar ratio 0.8 and leaching time 40 minutes at 25°C. $FePO_4$ was subsequently precipitated by adjusting pH and regenerating hexagonal $FePO_4$, which is not suitable for direct regeneration of LFP. Besides, the S/L ratio (0.05 g/mL) is low. In a subsequent study, Zou et al. [86] investigated the leaching of industrial black mass of NMC in the presence of LFP and obtained the leaching efficiency of 100 % for Co, 87.6 % for Ni, 91.1 % for Mn and 100 % Li under the optimum conditions of 2 M H_2SO_4, 180 minutes and 60°C. In this study, in addition to the incomplete leaching of NMC, the authors reported that all the added LFP was completely dissolved in the solution, and no $FePO_4$ was detected in the leach residue.

In sum, though various studies have reported high leaching efficiencies for transition metals and selective leaching of Li from blended LIB mixtures, the proposed processes still have certain drawbacks. Moreover, a research gap remains in preserving orthorhombic $FePO_4$ as a valuable by-product from mixed LIBs, enabling its direct reuse in LIB manufacturing. This route is less energy intensive than complete dissolution of LFP followed by the precipitation of hexagonal $FePO_4$.

Table 1.7. Use of inorganic/organic acids for metal leaching from spent mixtures

LIB type	Leaching agent	Conditions: S/L ratio (g/mL) Temperature (°C) Time (min)	Efficiency (%)	Form of solid byproduct	Ref
LCO, NMC, LFP	2 M HCl	0.10 95 80	LCO = 98 NMC = 100	None reported Recovery of $FePO_4$ by precipitation from leachate using NaOH	[87]
LCO, LMO, NMC, LFP	2 M H_3PO_4 4 vol% H_2O_2	0.05 60 60	Mn = 98.8, Ni = 99.5, Co = 96.3, Li = 100, Fe = 2.7	Recovery of hexagonal $FePO_4$ by thermal treatment at 600°C	[77]
NMC, LFP	0.88 M H_3PO_4	0.030 80 120	Mn = 97.3, Ni = 99.1, Co = 98.9, Li = 99.6	$FePO_4 \cdot 2H_2O$ Recovery of hexagonal $FePO_4$ by thermal treatment at 600°C	[88]
NMC, LFP	240 g/L $Fe_2(SO_4)_3$	0.14 90 60 LFP/NCM mass ratio: 1.33	Mn = 96.88, Ni = 97.9, Co = 97.65, Li = 98.32, P = 0.21	$FePO_4$ and $Fe(OH)_3$	[78]
NMC, LFP	0.3 M $NH_4Fe(SO_4)_2$	0.05 50 30	Mn = 98.3, Ni = 99, Co = 98.9, Li = 97.8	$FePO_4 \cdot 2H_2O$ Recovery of hexagonal $FePO_4$ by thermal treatment at 600°C	[89]
LCO, LFP	0.5 M H_2SO_4	0.03 50 20 LCO/LFP molar ratio 1	Co = 92.4, Li = 99.9, Fe = 99.8, P = 99.9	No solid residue Recovery of hexagonal $FePO_4$ by precipitation from leachate at pH 2 and thermal treatment at 600°C	[82]
LCO, LNO, NMC, LFP	Spent electrolyte 20% H_2O_2	0.025 90 90	Mn = 98.1, Ni = 99.8, Co = 99.2, Li = 99.5	FeOOH and $Al(OH)_3$	[90]
LCO, LNO, LMO, NMC, LFP	2.5 M H_2SO_4 Volume ratio H_2SO_4/H_2O_2 (30%): 5	0.10 60 60	Mn = 99.1, Ni = 99.1, Co = 99.2, Li = 99	Residual graphite, insoluble $LiFePO_4$ and the binder	[79]
LCO, LMO, NMC, LFP	4 M H_2SO_4 30 wt% H_2O_2	NA 80 120-180	Mn = 100, Ni = 100, Co = 100, Li = 100, Fe = partially dissolved	Residual insoluble $LiFePO_4$	[80]

LIB type	Leaching agent	Conditions: S/L ratio (g/mL) Temperature (°C) Time (min)	Efficiency (%)	Form of solid byproduct	Ref
LCO, LMO, NMC, LNO	2.5 M H_2SO_4 30 wt% H_2O_2	NA 90 150	Mn = 99, Ni = 99, Co = 99, Li = 99	None reported	[81]
NMC, LFP	1 M H_2SO_4 Ratio of 30% H_2O_2 to raw material: 0.308 g/g	0.19 90 300	Mn = 97.08, Ni = 98.52, Co =96.26, Li = 99.59, Fe = 0.24, P = 1.06	$FePO_4 \cdot 2\ H_2O$ and carbon	[83]
NMC, LFP	1.4 M H_2SO_4 15 vol% H_2O_2	0.25 40 60	Mn = 71.7, Ni = 72, Co = 64.6, Li = 91.7, Fe = 0.29	$FePO_4$ and $LiNi_xCo_yMn_{1-x-y}O_2$	[84]
NMC, LFP	1 M H^+	0.05 25 40 NMC/LFP molar ratio 0.8	Mn = 99.1, Ni = 99.5, Co = 98.9, Li = 99.8	Hexagonal $FePO_4$	[85]
NMC, LFP	1.5 M H_2SO_4	0.10 60 180	Mn > 95, Ni > 95, Co >95, Li >95	Graphite Recovery of $FePO_4$ by precipitation at pH 2.5	[76]
NMC, LFP	2 M H_2SO_4	NA 60 180	Mn = 91.1, Ni = 87.6, Co = 100, Li = 100, Fe=100	Graphite Nickle oxide Lithium manganese oxide Aluminum oxide hydroxide	[86]

1.5. Research hypothesis

The research hypothesis include:

- Acid leaching can reach to complete dissolution of NMC and selective leaching of LFP.
- Acid leaching can also reach to complete metal recovery from mixtures of NMC and LFP.
- Interactions among metals in mixed LIBs may further enhance the leaching efficiency of some metals.
- The addition of reducing or oxidizing agent can promote selective leaching of metals from mixed LIBs

1.6 Research goals

The main objective of this PhD project was to develop acid leaching processes for recovering valued metals from cathode materials of NMC and LFP LIBs, separated and mixed. Specific objectives were as follows:

- Characterization methods to determine the composition of solid samples
- Study the effects of acid leaching's main parameters on metal extraction from individual leaching of NMC and LFP cathode materials
- Study metal extraction efficiencies of sulphuric acid leaching of mixed NMC and LFP and analyze NMC-LFP interactions
- Study the action of soluble ferrous and ferric ions on leaching of NMC and LFP mixtures

1.7. Dissertation structure

The dissertation has six chapters:

- Chapter I offers an introduction to LIBs and to the recycling of spent LIBs. The state of the art and future outlook of LIB recycling are described briefly. This chapter also provides a synthetic literature review of the recycling of spent LIBs, with particular focus on hydrometallurgical methods of metal extraction.
- Chapter II describes the materials and methods used to achieve the study objectives.
- Chapter III describes the characterization of two cathode types, NMC and LFP, and explores the comparative study of metal extraction efficiencies from NMC and LFP using sulphuric acid.
- Chapter IV analyzes the effects of the main parameters of sulphuric acid leaching on the extraction of metals from mixture of NMC and LFP.
- Chapter V describes the study of the action of ferrous and ferric ions on leaching of NMC and LFP mixtures.
- Chapter VI outlines the conclusions of this research and makes some recommendations.

CHAPTER II

MATERIALS AND METHODS

2.1. Materials

The cathode material—$LiNi_xMn_yCo_zO_2$ (NMC) and carbon coated $LiFePO_4$ (LFP)—was provided in pure form by Hydro-Quebec (from Nano-One Materials, Canada) and used in this form to control composition during assays. Sulphuric acid (Fisher Scientific, Canada, 95-98% purity) was used to prepare the leaching solution for the cathode material. Hydrochloric acid (Fisher Scientific, Canada, 36-38% purity) was used for acid digestion of LFP and of residual solids to determine their composition. Hydrogen peroxide (Fisher Chemical, Canada, 30 wt%), ferrous sulfate heptahydrate ($FeSO_4 \cdot 7H_2O$) (Fisher Chemical, India, ≥ 99% purity) and iron (III) sulfate monohydrate ($Fe_2(SO4)_3 \cdot H_2O$) (Sigma Aldrich, USA, 97% purity) were used as reducing and oxidizing agents during the leaching assays.

2.2. Characterization methods

For solids characterization, the following properties were determined: crystallography, morphology and composition (metals and carbon-sulphur content). For the leaching solution, characterization involved determination of metal content and oxidation-reduction potential.

2.2.1. Crystallography

X-ray diffraction (XRD) was used to study the crystal structure of the initial solid and the solid residue. X-ray powder diffraction (XRD) is a method employed in analytical chemistry to identify crystalline phases in a material and determine their unit cell dimensions. X-ray diffraction is based on constructive interference of X-rays scattered by the periodic arrangement of atoms within a crystal lattice. These X-rays are generated using a cathode ray tube, filtered to generate monochromatic radiation and focused for greater coherence by aligning their phase, converging the beam and minimizing divergence. The resulting beam is then directed at the target sample. When a crystal is exposed to monochromatic X-rays, the atomic electrons within the crystal are excited by the incident X-rays and oscillate at the same frequency. These excited electrons scatter the X-rays in all directions. However, when reflected from the atomic planes of the crystal, the scattered X-rays can interfere with one another. Constructive interference occurs when the path difference between X-rays reflected from different atomic planes equals an integer multiple of the X-ray wavelength. This principle is accurately described by Bragg's Law:

$$(n\lambda = 2d \sin \theta) \quad (2.1)$$

Where, λ is the wavelength of electromagnetic radiation, θ is the diffraction angle and d is the lattice spacing in the crystalline sample. Figure 2.1 shows a schematic diagram of Bragg diffraction [91].

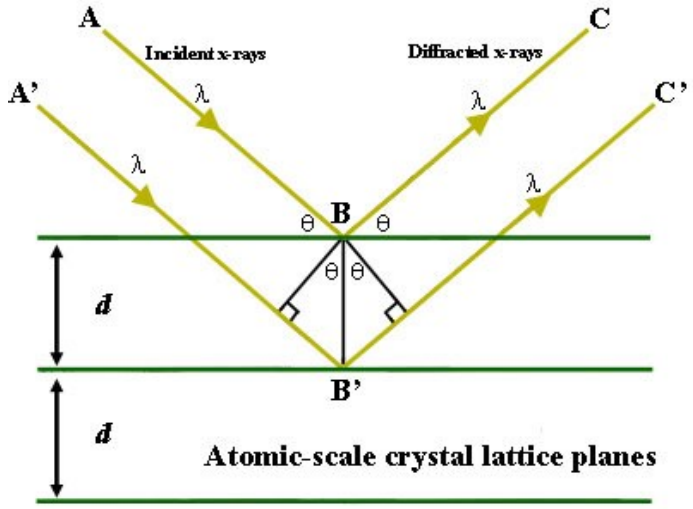

Figure 2.1. Schematic diagram of Bragg diffraction [91]

The diffracted X-rays are detected, processed and quantified. By systematically hit the sample through a range of 2θ angles, a complete set of lattice diffraction directions should be attained owing to the stochastic orientation of the powdered substance. The diffraction peaks are then converted into d-spacings for the purpose of phase identification, as each phase has a unique set of d-spacings. Typically, this process involves comparing the d-spacings obtained with standard reference patterns [92].

The spacing d_{hkl} between crystal planes, determined by the type of crystal structure. Each crystal system has a specific mathematical relationship that links this interplanar distance to the Miller indices (*hkl*) and the lattice parameters that define the crystal lattice. The Equation 2.2 for a cubic system is:

$$d_{hkl} = \frac{a}{\sqrt{\{h^2+l^2+k^2\}}} \quad (2.2)$$

where a is the lattice parameter of the cubic crystal, and *h,k,l* are the Miller indices corresponding to the Bragg planes.

For this PhD project, XRD patterns were recorded using a D2 PHASER desktop diffractometer for X-ray powder diffraction applications equipped with a Cu source (ƛ: 1.54184Å; LYNXEYE-XE-T detector) from 2θ: 10° to 80°. Data were collected by DIFFRAC.COMMANDER. The quantitative analysis of the

diffraction patterns was carried out with DIFFRAC.EVA V5.1 with crystallography open database (COD). Rietveld refinement of the initial cathode material samples was performed using Profex software.

2.2.2. Morphology and element distribution on particle surface

A scanning electron microscope (SEM) and energy dispersive X-ray spectroscopy (EDS) were used to analyze the morphology and elemental distribution of the samples. An SEM typically consists of an electron gun, magnetic lenses and detection systems, as shown in Figure 2.2 [93]. High-energy electrons are generated in the electron gun and accelerated through the column at a designated accelerating voltage, typically ranging from 1 keV to 30 keV. As the electrons travel through the column, condenser lenses and apertures work together to narrow the beam diameter. The final lens, the objective lens, focuses the electron beam on the surface of the sample. The sample is securely mounted on a stage in the chamber area, and the column and the chamber are maintained under vacuum through a combination of pumps. The positioning of the electron beam on the sample is meticulously controlled by scan coils located above the objective lens that allow the beam to be scanned across the sample surface in the X-Y plane. The interaction of the beam with the sample generates signals (including secondary electrons, backscattered electrons and characteristic X-rays) which are detected by specialized detectors for further analysis. Figure 2.3 illustrates interactions between the primary electrons and atoms within the sample [94].

Secondary electrons (SE) are emitted through inelastic scattering from atoms located on or near the surface of the sample. Backscattered electrons (BSE) are electrons reflected or deflected back by atoms in the sample through elastic scattering. Successive collisions can redirect an electron out of the material and back along its original path.

BSEs are generated from a deeper interaction volume because more collisions are needed to reverse direction. As a result, BSE images are lower resolution and do not show detailed surface features. The backscattering coefficient increases with the atomic number (Z) of the element, meaning that heavy elements produce more backscattered electrons than lighter elements, resulting in a brighter appearance in the image. BSE images, accordingly, show contrast between regions of different chemical composition, though they do not directly identify the elements present.

Characteristic X-rays are produced when a low orbital electron is ejected, creating a vacancy that is filled by a high orbital electron. This electron then emits a single photon (an X-ray) with energy equivalent to the energy difference between the low and high orbitals. The resulting X-ray energies are characteristic of the atom they originated from. Energy-dispersive X-ray spectroscopy (EDS) is a technique that uses

characteristic X-rays for chemical analysis, allowing examination of a single point or area within a specimen.

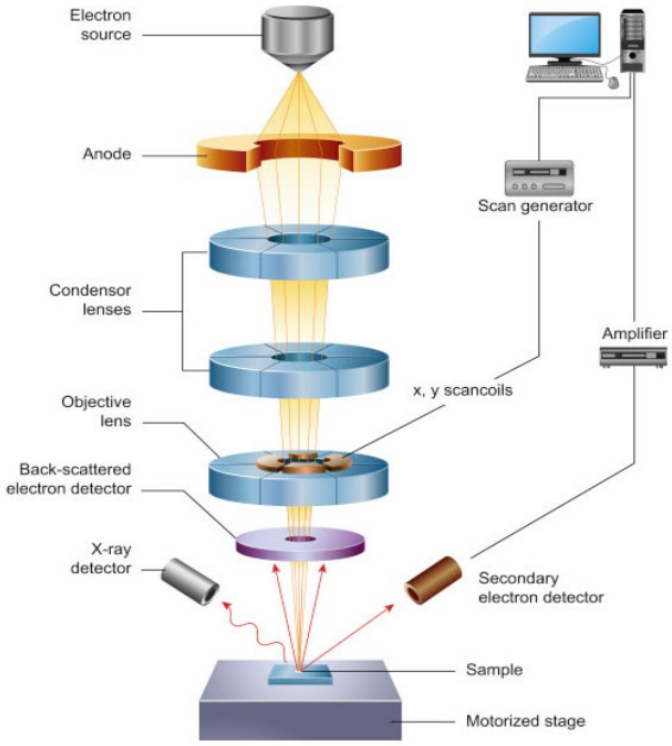

Figure 2.2. Schematic of a scanning electron microscope [93]

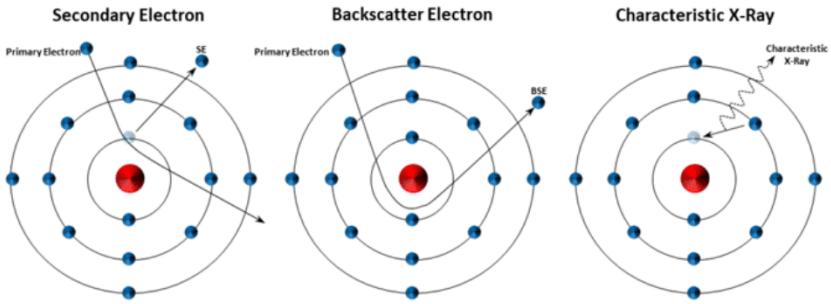

Figure 2.3. Schematics of emissions SEM: secondary electron (SE), backscattered electron (BSE) and characteristic X-ray [94]

For this PhD project, microstructure and chemical analyses were performed using a Hitachi SU9000 SEM (Japan) equipped with an EDS system from Oxford Instruments.

2.2.3. Carbon-sulphur content

Concentrations of carbon and sulphur in sample are determined by carbon-sulphur analysis, a fundamental technique in analytical chemistry. The measurements were conducted according to the ASTM E1019 standard procedure, which specifies the determination of carbon and sulphur in metals, ores, and related materials.

In this method, the sample is subjected to controlled combustion or reaction conditions that convert the carbon and sulphur into measurable gases such as carbon dioxide and sulphur dioxide. These gases are then quantified using analytical methodologies such as infrared spectroscopy or gas chromatography.

For this PhD project, carbon-sulphur analyses were carried out using a CS-2000 analyzer (Eltra GmbH, Germany), accuracy ± 0.05 to 0.1 wt% for carbon and sulphur content of organic and inorganic samples. Samples weighing around 0.5 g were placed in ceramic crucibles, weighed and placed in the analyzer's induction furnace. Combustion of the sample by a stream of oxygen at 1,350°C generated SO_2 and CO_2, which were detected and quantified by infrared absorption cells. SO_2 and CO_2 measurements were used to calculate total S and C content of the sample.

2.2.4. Metal content

Metal concentrations in leaching solutions and solid residue were analyzed using inductively coupled plasma-optical emission spectrometry (ICP-OES). ICP-OES instruments have two main parts: the inductively coupled plasma source and the optical emission spectrometry detector, as shown in Figure 2.4 [95].

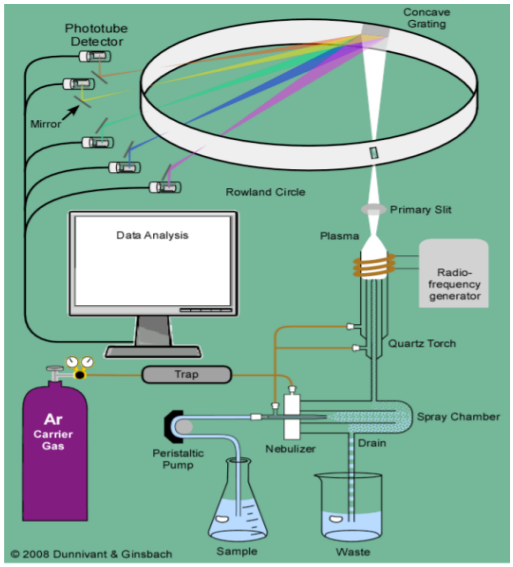

Figure 2.4. Schematic diagram of an ICP-OES system [95]

Inductively coupled plasma (ICP) is generated by passing argon gas through a quartz torch placed inside an induction coil and applying radio frequency (RF) power (750 to 1700 W) to the coil. A spark generated by a Tesla coil is then applied, causing electrons to be stripped from argon atoms. These electrons become trapped in the magnetic field and accelerate in closed circular paths, eventually forming the plasma through inductive coupling as shown in Figure 2.5 [96, 97]. The plasma atomizes, ionizes and excites elements in the sample, allowing precise analysis of their concentrations. In modern ICP-OES analysis, liquid samples, acid solutions or solids digested into aqueous forms are commonly introduced into the plasma through a nebulizer, where they undergo excitation and emit characteristic light for elemental analysis.

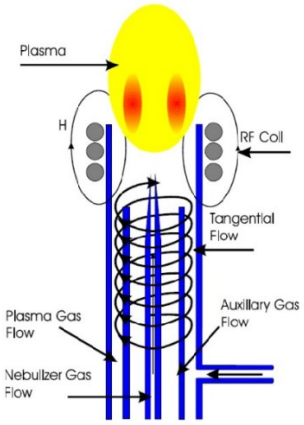

Figure 2.5. Plasma generation [96, 97]

Each element has a unique set of wavelengths in its emission spectrum that are characteristic of that element. Measurement of the emitted radiation of a particular component has many applications in the quantitative and qualitative analysis of metallic and quasi-metallic elements.

The frequency of the radiation emitted when an atom transitions from a higher energy level (Em) to a lower energy level (Ek) is given by [96]:

$$hv = E_m - E_k \quad (2.3)$$

where h is the Plank constant. In OES, wavelength ƛ is commonly used instead of frequency with:

$$ƛ = \frac{C}{V} \quad (2.4)$$

The intensity of a spectral line is proportional to:

$$I \sim (E_m - E_k)A\, n_m \quad (2.5)$$

where A is the transition probability and n_m is the population of electrons. The Boltzmann equation can be used to describe the relationship between the population n_m and the total population N, allowing the intensity of a spectral line to be expressed as:

$$I = \phi\left(\frac{hcg_m\, AN}{4\pi ƛz}\right)\exp(-E_m\ /kT) \quad (2.6)$$

where ϕ is a coefficient to account for the emission being isotropic over a solid angle of 4 π steradians. When a radiation source is stable enough to maintain a constant temperature, the partition function (Z) remains constant and the number of atoms (or ions) (N) is proportional to their concentration (c). In analyzing a specific element line, g_m, A, ƛ and E_m are constants, where g is the statistical weight (g = 2 J+ 1, J being the total electronic angular momentum quantum number), A is the transition probability, ƛ is wavelength and E_m is activation energy. I is accordingly proportional to c, which makes it possible to conduct precise quantitative analyses of metals [96]. An ICP-OES analyzer (Thermo Fisher Scientific, ICAP PRO Series) using a model 5110 ICP-OES optical emission spectrometer (Agilent technologies, Australia) was used to determine metal concentrations in all leachate samples and solids after acid digestion. The matrix for ICP analysis was a 5% v/v solution of HNO_3.

2.2.5. Oxidation-reduction potential (ORP)

Oxidation–reduction potential (ORP), or redox potential, is a fundamental parameter used to assess the electron transfer characteristics of a system. It provides quantitative information on the tendency of a solution or substance to gain or lose electrons, thus indicating its oxidizing or reducing capacity. Monitoring ORP during leaching processes offers valuable insight into the redox conditions that influence metal dissolution, speciation, and reaction kinetics, particularly for redox-sensitive elements such as iron.

In this study, the ORP of the leaching solution was measured using a platinum electrode with an Ag/AgCl KCl (3M) reference electrode (OAKTON WD-35805-13 ORP Electrode, USA). The measurements were conducted in situ throughout the leaching experiments to continuously monitor redox fluctuations.

The electrode assembly was immersed directly into the leachate, and the potential difference (in millivolts) was recorded using a digital multimeter or an integrated ORP meter. The ORP readings were automatically referenced to the Ag/AgCl electrode but were later converted to the standard hydrogen electrode (SHE) scale for comparison with literature values using the following relation:

$$E_{SHE}=E_{Ag/AgCl} + 210\ mV \quad (2.7)$$

The primary objective of these measurements was to determine the redox potential associated with the Fe(II)/Fe(III) couple during leaching. This allowed for the evaluation of oxidation–reduction dynamics, the stability of ferric and ferrous species, and their correlation with leaching efficiency.

2.3. Leaching of NMC and LFP materials

Leaching assays were conducted using a 500-mL three-neck flask equipped with a magnetic stirrer and placed in a temperature controllable water bath, as shown in Figure 2.6. The flask featured a reflux condenser to recover solvent vapours and prevent mass loss. A measured amount of NMC, LFP, or mixed powder was added to a preheated (75°C) sulphuric acid solution of known concentration under controlled stirring (330 rpm). During the leaching process, 3-mL liquid samples were collected at regular intervals to track the progress of the leaching. These samples were analyzed by ICP-OES to determine metal concentrations in the leachate. At the end of each assay, the suspension was filtered using a vacuum pump, a Buchner funnel and a 110-mm fibreglass filter. The filtrate was collected, and the cake was washed and then dried at 105°C for 24 hours. The dried cake was digested so its metal composition could be determined by ICP-OES analysis. To study the effect of reducing or oxidizing agents on the dissolution of NMC and LFP, H_2O_2 was added at the 60-minute mark of the leaching process. In some experiments involving leaching NMC and LFP mixtures, H_2O_2 was added at the 30-minute mark. To study how ferrous ions affect

metal leaching efficiency, ferrous sulfate heptahydrate ($Fe(II)SO_4 \cdot 7H_2O$) was added to the leaching solution at various reaction times. Similarly, to investigate the effect of ferric ions on the dissolution of LFP, iron (III) sulfate monohydrate ($Fe(III)_2(SO4)_3 \cdot H_2O$) was added to the leaching solution at different reaction times.

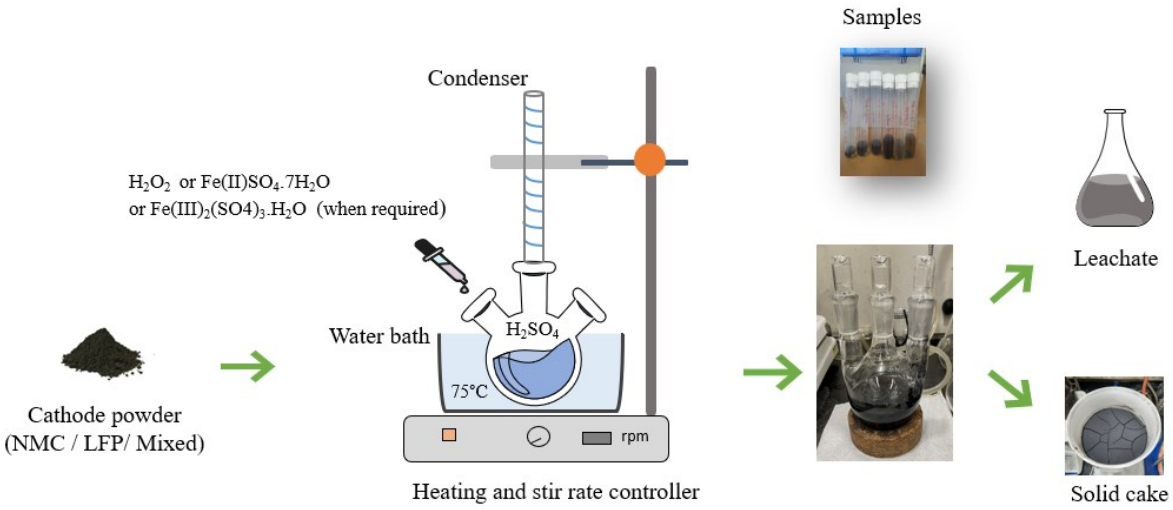

Figure 2.6. Schematic representation of leaching setup

2.3.1. Metal content of initial and final solids in leaching assays

NMC chemical composition was determined by acid digestion with 3.6 M H_2SO_4 (acid-to-dry sample v/w ratio 25:1) at 90°C for one hour then adding 3 mL of H_2O_2 for 30 minutes. The final solution was then filtered and diluted to 100 mL. Similarly, LFP chemical composition was determined by acid digestion with concentrated HCl (acid-to-dry sample v/w ratio 20:1) at 90°C for 1.5 hours, followed by dilution to 100 mL. This process was also used to determine the chemical composition of solid residues of NMC and LFP. The chemical composition of residues from the leaching of mixtures, however, was determined by acid digestion with 5 M H_2SO_4 (acid-to-dry sample v/w ratio 25:1) at 90°C for one hour followed by adding 3 mL of H_2O_2 for 30 minutes. The final solution was filtered and diluted to 100 mL.

2.3.2. Leaching efficiency

The leaching efficiency (η) of each metal was calculated using the following equation:

$$\eta\% = \frac{C_t \times V}{X^0 \times W^0} \quad (2.8)$$

where C_t is the concentration of the metal in the leachate (mg/L) at leaching time t (min), V is the volume of leachate (mL), X^0 is the chemical composition of the initial solid (mg/kg) and W^0 is the initial mass of the solid sample (g).

Total leaching efficiency was verified using the following equation:

$$\eta\% = \frac{(m_0 - m_1) \times 100\%}{m_0} \quad (2.9)$$

where, m_0 is the total amount of a specific element in the initial solid sample (g) and m_1 is the total amount of this element in the solid after leaching (g).

The selectivity ratio of LFP (Fe and P) to NMC (Mn, Ni and Co) was calculated from the ratio of elemental recoveries:

$$S_{LFP}/S_{NMC} = R_{LFP}/R_{NMC} \quad (2.10)$$

2.4. Errors and standard deviation

Calculation of analytical errors is crucial to ensure the reliability and validity of research findings. Several steps in the research process had to be considered to calculate analytical error: mass balancing of raw materials, volumetric flask usage, sample dilutions, and ICP analysis. Table 2.1 specifies the error associated with each of these steps.

Table 2.1. Breakdown of analytical errors

No.	Step	Error
1	Mass balancing of raw materials	0.2%
2	Dilution pipettes (DF 10: 9.0 mL nitric acid and 1.0 mL sample) (DF 100: 9.9 mL nitric acid and 0.1 mL sample) (DF 1000: 9.0 mL nitric acid and 1.0 mL DF 100)	 0.72% 0.8% 0.72%
3	Volumetric flask	±0.30%
4	ICP	±5%

The total error can be calculated using the root sum of squares method, which accounts for the individual errors from each step. The formula is as follows:

$$\sigma_{total} = \sqrt{\{\sigma^2_{Mass\ balance} + \sigma^2_{Dilution} + \sigma^2_{Volumetric} + \sigma^2_{ICP}\}} \quad (2.11)$$

Substituting the given values into the equation:

$$\sigma_{total} = \sqrt{\{0.2^2 + 0.72^2 + 0.8^2 + 0.72^2 + 0.3^2 + 5^2\}}$$

$$\sigma_{total} = 5.17\%$$

Total error is $\pm 5\%$.

Supplementary data related to calculation of analytical errors presented in Appendix B.

To calculate standard deviation of the leaching efficiency for each element, a single assay under conditions of 2 M H_2SO_4, S/L ratio 0.15 g/mL, NMC/LFP molar ratio 1.02, 75°C, 0.68 M H_2O_2, stirring speed 330 rpm and 51 minutes was selected, and the assay was repeated three times. Tables 2.2 and 2.3 show leaching efficiencies and standard deviations for Mn, Ni, Co, Li, Fe and P under these conditions.

Table 2.2. Leaching efficiencies (2 M H_2SO_4, NMC/LFP molar ratio 1.02, S/L ratio 0.15 g/mL, 0.68 M H_2O_2, 75°C, 51 minutes)

Assay	**Leaching efficiency (%)**					
	Mn	**Ni**	**Co**	**Li**	**Fe**	**P**
1	99.2	100	100	99.8	63.3	67.7
2	99.4	100	100	99.8	65.7	69.6
3	98.1	98.7	98.8	98.7	63.4	64.0

Table 2.3. Calculation of Standard Deviation for each element (2 M H_2SO_4, NMC/LFP molar ratio 1.02, S/L ratio 0.15 g/mL, 0.68 M H_2O_2, 75°C, 51 minutes)

Parameter	**Element**					
	Mn	**Ni**	**Co**	**Li**	**Fe**	**P**
Mean (μ)	98.9	99.6	99.6	99.4	64.1	67.1
Standard deviation (σ)	0.7	0.7	0.7	0.6	1.4	2.8
Result	98.9±0.7	99.6±0.7	99.6±0.7	99.4±0.6	64.1±1.4	67.1±2.8

CHAPTER III

CHARACTERIZATION OF MATERIALS AND METAL EXTRACTION BY ACID LEACHING OF SINGLE NMC AND LFP CATHODE MATERIALS

3.1. Introduction

This chapter describes the characterization of the two cathode materials, NMC and LFP, as well as the separate acid-leaching processes used to extract metals from each. Characterizing the cathode materials is essential to determine their metal content, a key factor in calculating metal leaching efficiency. The main objective of this study was to investigate the metal extraction from NMC and LFP and identify the key leaching parameters. The effect of sulphuric acid concentration, solid-liquid (S/L) ratio and H_2O_2 addition on metals leaching efficiency with both NMC and LFP materials was studied

3.2. Methodology

The leaching procedures for NMC and LFP were carried out following the method described in Chapter II. The sulphuric acid concentration was varied from 2 M to 6 M, and the S/L ratio ranged between 0.10 g/mL and 0.20 g/mL. The addition of 0.68 M H_2O_2 was selected. The choice of all leaching parameters was based on the optimal conditions previously established in research conducted at CNETE on the acid leaching of NMC black mass. In this regard, these ranges of sulphuric acid concentration, S/L ratio, and H_2O_2 concentration were chosen for the leaching of both NMC and LFP cathode materials.

Based on those results, all tests were conducted at a fixed temperature of 75 °C under atmospheric pressure ,time of 82 minutes and a stirring speed of 330 rpm, with H_2O_2 added after 60 minutes of leaching with sulphuric acid to allow sufficient time for the solubilization of metals.

3.3. Results

3.3.1. Characterization of NMC and LFP materials

Table 3.1 shows metal content results for NMC cathode material from two ICP-OES analyses. Ni was detected at the highest concentration, with an average content of 366.74 ± 0.89 g/kg.

Table 3.1. Metal content of NMC (g/kg), error +/- 5%

Cathode material	Mn (g/kg)	Ni (g/kg)	Co (g/kg)	Li (g/kg)	Al (g/kg)	Ca (g/kg)	Cu (g/kg)	Fe (g/kg)	K (g/kg)	Mg (g/kg)	Na (g/kg)
NMC (1)	115.25	367.37	118.59	68.91	1.18	0.081	0.033	0.052	0.041	0.017	0.510
NMC (2)	114.56	366.11	118.33	69.06	1.15	0.121	0.034	0.166	0.061	0.018	0.493

Ni (366.7 ± 0.9 g/kg), Mn (114.9 ± 0.5 g/kg), Co (118.5 ± 0.2 g/kg) and Li (69.0 ± 0.1 g/kg) were the main elements in the NMC material. Other elements observed were Al (1.17 ± 0.02 g/kg) and Na (0.50 ± 0.01 g/kg). The oxygen content of the NMC material was calculated by mass balance since most metals were in the form of oxides (nickel oxide (NiO), manganese oxide (MnO_2) and cobalt oxide (Co_2O_3)). Oxygen content was calculated as 328.9 ± 1.4 g/kg.

The stoichiometry of the NMC ($LiNi_xMn_yCo_zO_2$) was calculated from the average molar content of each element, determined by dividing the mass concentration of each element by its molecular weight, as shown in Table 3.2. Given molar content and calculated stoichiometry, the NMC cathode material was identified as $LiNi_{0.6}Mn_{0.2}Co_{0.2}O_2$ (NMC622).

Table 3.2. Calculated stoichiometry of NMC

Element	Molecular weight (g/mol)	Molar content (NMC) (mol/kg)	Approximate stoichiometry
Ni	58.69	6.248	
Mn	54.94	2.091	Ni:Mn ratio ~ 6:2
Co	58.93	2.010	Ni:Co ratio ~ 6.2:2

The crystal structure and lattice parameters of the NMC sample were analyzed by XRD. Figure 3.1 shows the XRD pattern for the crystal structure of the NMC sample, which corresponded to $LiNi_{0.333}Mn_{0.333}Co_{0.333}O_2$ (NMC111) with space group 166. This does not align with the stoichiometry results, however. For this reason, average lattice parameters were measured through Rietveld refinement

using Profex software, and they were calculated to be a = 2.869 Å, b = 2.869 Å and c = 14.223 Å. These values suggest NMC622 based on its stoichiometry [98], indicating that NMC111 and NMC622 share the same XRD patterns but differ in their lattice parameters. Given the lattice parameters obtained and the Ni:Mn:Co ratio being 6:2:2, it was concluded that the crystal structure of the NMC sample corresponded to NMC622 and not NMC111.

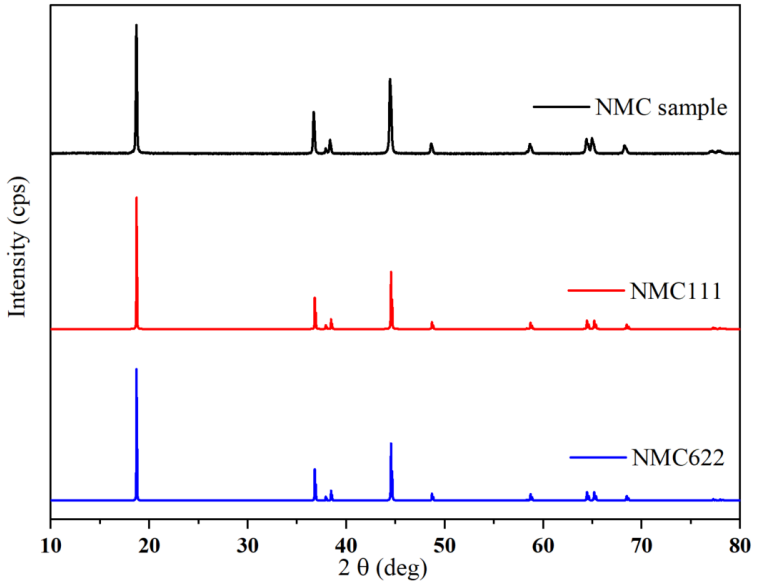

Sample	a, b (A°)	c (A°)	Ref
NMC sample	2.869	14.223	This work
NMC111	2.859	14.231	[98]
NMC622	2.868	14.218	[98]

Figure 3.1. XRD patterns of NMC sample and lattice parameters of NMC111, NMC622 reported by Azhari et al. [98]

LFP samples were characterized with the same procedure used for the NMC samples. Tables 3.3 and 3.4 show the chemical composition of LFP (ICP-OES) and the stoichiometry calculation. On average, Fe (337 ± 5 g/kg), P (191.5 ± 0.8 g/kg) and Li (42.7 ± 0.03 g/kg) were the main elements in the LFP cathode material. Other elements were Mn (1.22 ± 0.01 g/kg), Al (0.21 ± 0.01 g/kg), Ca (0.27 ± 0.08 g/kg) and K (0.27 ± 0.01 g/kg). Total carbon of the sample was 2.35% ± 0.22%. The oxygen content of the LFP cathode

was calculated by mass balance considering the metals were in the form of oxides (iron oxide (FeO), lithium oxide (LiO) and phosphorus oxide (PO_4)). Oxygen content was calculated as 403.08 ± 5.47 g/kg.

As Figure 3.2 shows, the XRD pattern of the LFP sample reveals a crystal structure corresponding to $LiFePO_4$ with the orthorhombic space group Pnma (62). Average lattice parameters, determined through Rietveld refinement using Profex software, were a = 10.322 Å, b = 6.005 Å and c = 4.693 Å, that is, consistent with the lattice parameters of the Crystallography Open Database (COD ID: 1101111): a = 10.333Å, b = 6.004 Å, c = 4.698 Å.

Table 3.3. Metal content of LFP (g/kg), error +/- 5%

Cathode material	Fe (g/kg)	P (g/kg)	Li (g/kg)	Al (g/kg)	Ca (g/kg)	Cu (g/kg)	K (g/kg)	Mg (g/kg)	Na (g/kg)	Zn (g/kg)	Mn (g/kg)
LFP (1)	340.35	192.10	42.75	0.204	0.215	<LD	0.285	0.031	0.071	0.072	1.211
LFP (2)	333.67	190.97	42.71	0.208	0.325	<LD	0.266	0.032	0.085	0.056	1.228

Table 3.4. Calculated stoichiometry of LFP

Element	Molecular weight (g/mol)	Molar content (LFP) (mol/kg)	Approximate stoichiometry
Fe	55.845	6.034	
P	30.974	6.183	Fe:P ~ 1:1
Li	6.941	6.156	Fe:Li ~1:1

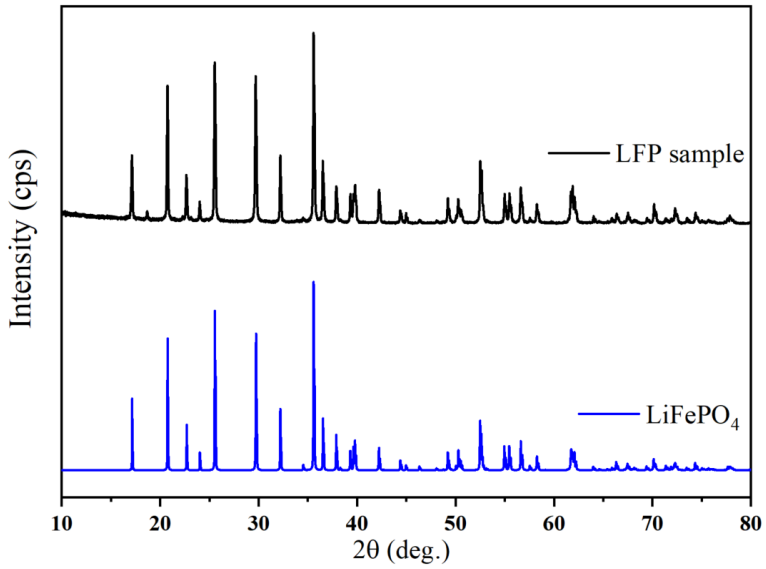

Figure 3.2. XRD patterns of LFP sample and $LiFePO_4$ with COD ID 1101111

3.3.2. Study of NMC acid leaching

As mentioned, leaching of Mn, Ni, Co and Li was studied by varying sulphuric acid concentration, S/L ratio and reducing agent (H_2O_2).

3.3.2.1. Effect of sulphuric acid concentration on leaching efficiency

Sulphuric acid (H_2SO_4) is widely used because of its exceptional ability to dissolve materials as well as its availability and price. For this study, H_2SO_4 concentrations of 2 M and 6 M were used at a fixed temperature of 75°C, an S/L ratio of 0.10 g/mL and a stirring speed of 330 rpm for 82 minutes. Figure 3.3 illustrates the effect of sulphuric acid concentration and time on leachate concentration. As the figure shows, the different concentrations of sulphuric acid produced slightly different patterns of Mn, Ni, Co and Li leaching.

Leaching efficiencies for Mn, Ni, Co and Li using sulphuric acid at 2 M and 6 M are shown in figures 3.4a and 3.4b, respectively. As Figure 3.4a shows, leaching efficiency for Li, Ni and Co increased rapidly in the first 30 minutes, remained relatively stable between 30 and 82 minutes and reached 97.8%, 46.7% and 43.0%, respectively, by the end of the leaching assay. Mn leaching efficiency, on the other hand increased only slightly during the first 30 minutes, decreased with time and then remained at around 0%. The same trends were observed for 6 M H_2SO_4, with final leaching efficiencies for Li, Ni, Co and Mn of 99.0%, 49.8%, 48.7% and 0%, respectively (Figure 3.4b). Based on these results, the 2 M solution was selected to

study the effect of sulphuric acid concentration on other parameters, because it is more economical, and operation risks are lower than with the 6 M solution.

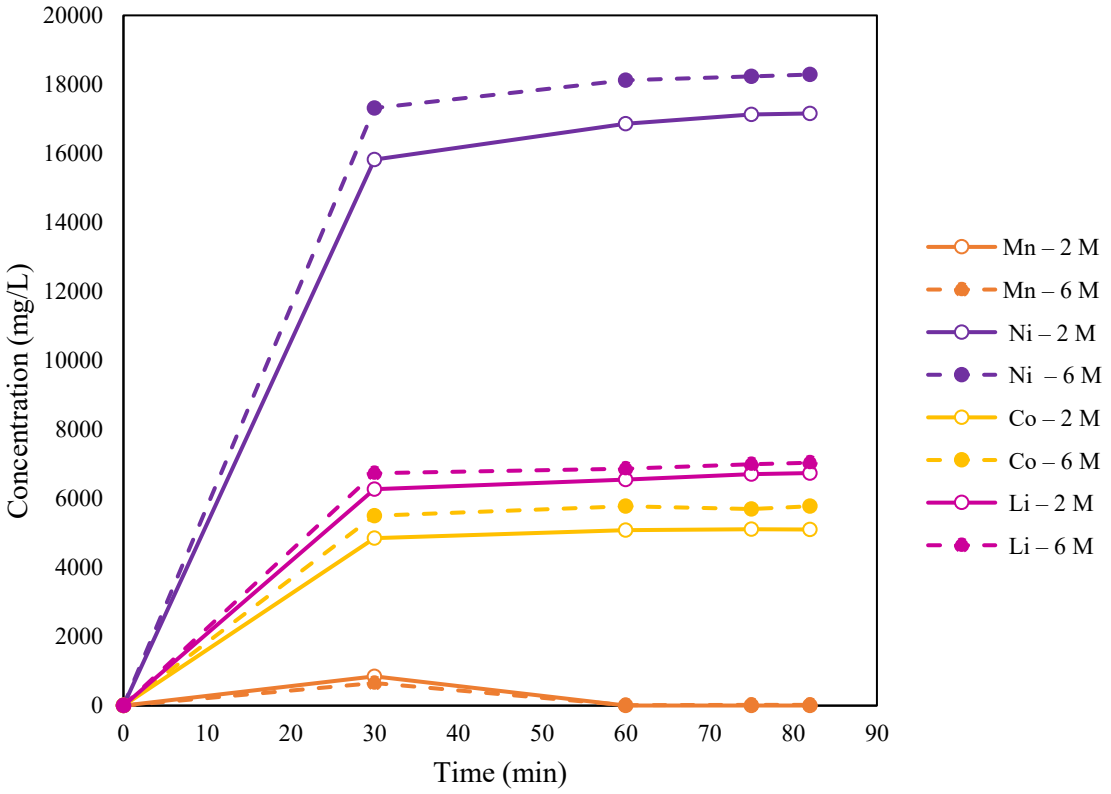

Figure 3.3. Effect of sulphuric acid concentration on leachate concentrations of Mn, Ni, Co and Li (2 M and 6 M H_2SO_4, S/L 0.10 g/mL, 75°C)

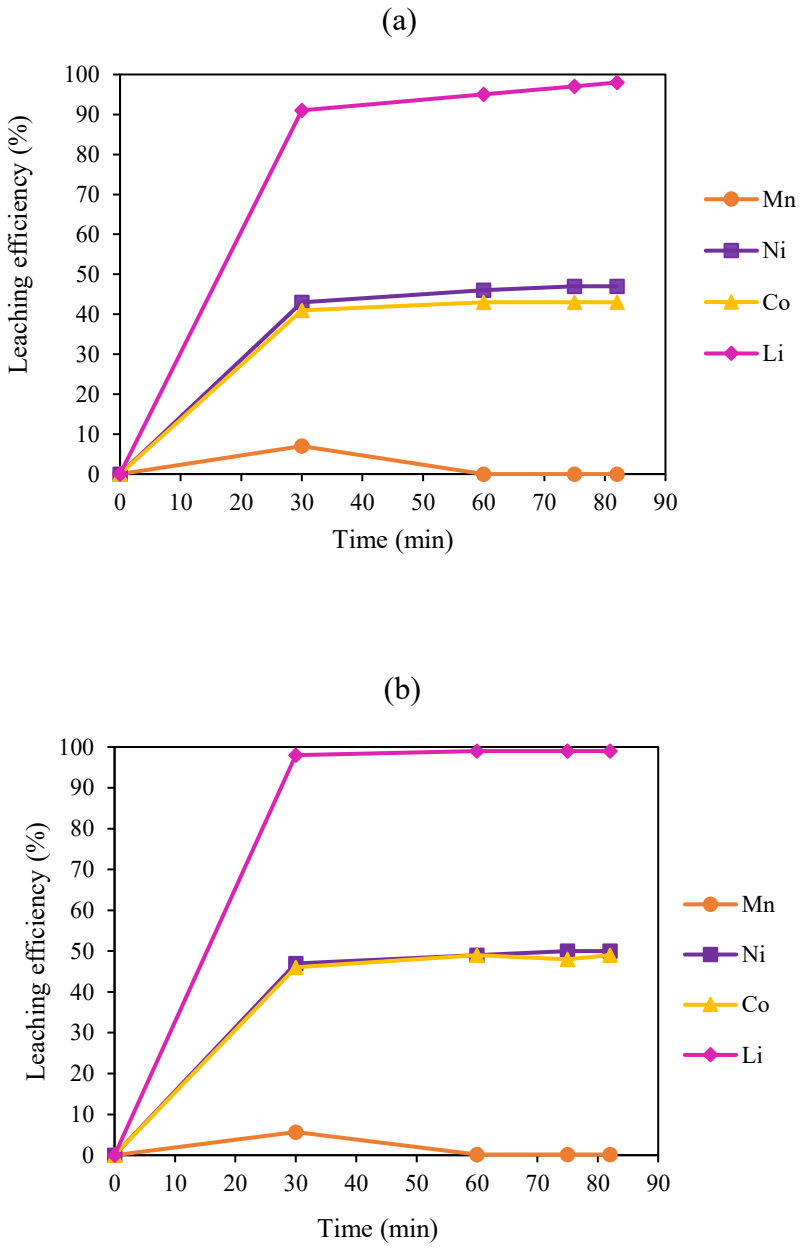

Figure 3.4. Leaching efficiencies for Mn, Ni, Co and Li (a) 2 M H_2SO_4, S/L 0.10 g/mL,75°C; (b) 6 M H_2SO_4, S/L 0.10 g/mL, 75°C

Table 3.5 and Figure 3.5 show metal content (mmol/g) and XRD analysis of solid leach residues obtained with both H_2SO_4 concentrations. Residues obtained with both acid concentrations show a similar metal composition and almost the same XRD pattern, which is consistent with the leaching efficiency results.

Table 3.5. Metal content (mmol/g) of leach residue (2 M and 6 M H_2SO_4, S/L 0.10 g/mL, 75°C)

Sample	Metal content (mmol/g)			
	Mn	Ni	Co	Li
Solid residue for 2 M H_2SO_4	3.67	5.69	1.94	0.45
Solid residue for 6 M H_2SO_4	3.80	5.66	1.86	0.18

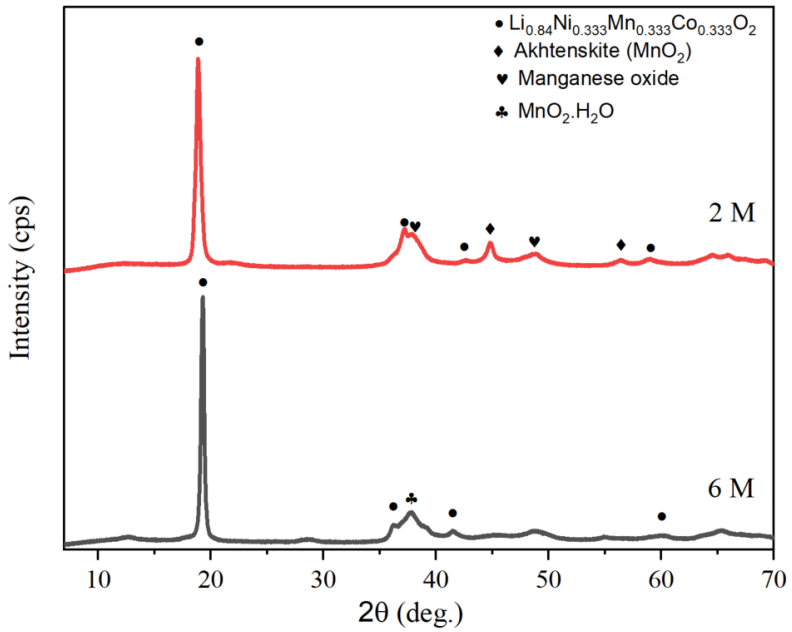

Figure 3.5. Solid leached residue XRD patterns (2 M and 6 M H_2SO_4, S/L 0.10 g/mL, 75°C)

3.3.2.2 Effect of solid-liquid ratio on leaching efficiency

To analyze the effect of S/L ratio on metal leaching, the leaching assays were performed at S/L ratios of 0.10, 0.15 and 0.20 g/mL at a fixed H_2SO_4 concentration of 2 M, temperature at 75°C and a stirring speed of 330 rpm for 82 minutes. Table 3.6 shows leaching efficiencies for Mn, Ni, Co and Li as a function of S/L ratio. Leaching efficiencies decreased with S/L ratio. Highest leaching efficiencies were observed with S/L ratio at 0.10 g/mL: 46.7% for Ni, 43% for Co and 97.8% for Li. Leaching efficiency for Mn was always nearly 0%. These findings clearly demonstrate that a low S/L ratio increases metal leaching efficiency.

Table 3.6. NMC leaching efficiencies with S/L ratios of 0.10, 0.15 and 0.20 g/mL (2 M H_2SO_4 at 75°C for 82 minutes)

S/L ratio (g/mL)	Leaching efficiency (%)			
	Mn	Ni	Co	Li
0.10	0.0	46.7	43.0	97.8
0.15	0.0	44.7	42.0	95.9
0.20	0.0	40.0	39.9	86.4

3.3.2.3 Effect of H_2O_2 addition on leaching efficiency

Hydrogen peroxide (H_2O_2) was used as a reducing agent. As shown in Equation (3.1), H_2O_2 has remarkable reducing capacity, enabling it to readily convert higher valence metals such as Mn^{4+}, Co^{3+} and Ni^{3+} to their lower valence states (Mn^{2+}, Co^{2+} and Ni^{2+}, respectively), which are more soluble [99].

$$H_2O_2 = O_2 + 2H^+ + 2e^- \qquad E^\circ = -0.68\ V \tag{3.1}$$

To examine the effect of H_2O_2 on metal dissolution, H_2O_2 was added to concentration 0.68 M after 60 minutes of leaching at 2 M H_2SO_4, 75°C, stirring speed 330 rpm and S/L ratio 0.10 g/mL. Figure 3.6 shows leachate concentrations with and without H_2O_2 as a function of time. As the figure shows, adding 0.68 M H_2O_2 improved Mn, Ni and Co dissolution but had a negligible effect on Li dissolution.

Figure 3.7 shows the effect of adding 0.68 M H_2O_2 on leaching efficiencies for Mn, Ni, Co and Li. Leaching efficiencies obtained for Ni, Co and Li in H_2SO_4 were 45.5%, 43.1% and 93.4%, respectively, at 60 minutes, but leaching efficiency for Mn remained close to 0. Leaching efficiencies for all metals increased by as much as 100% after H_2O_2 was added.

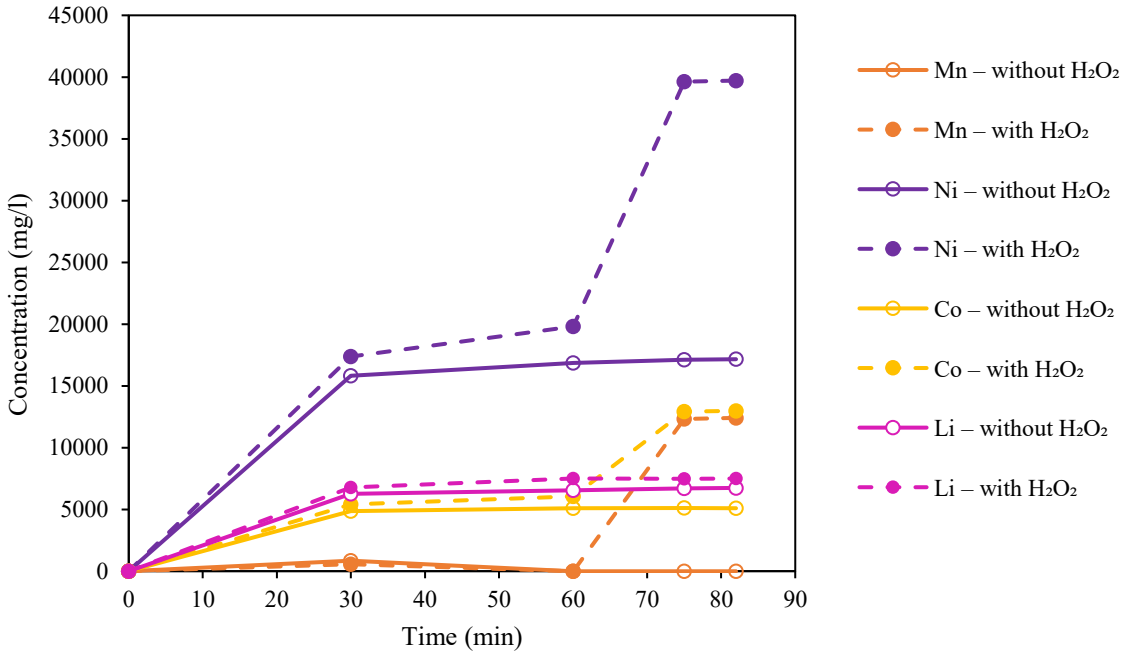

Figure 3.6. Effect of H_2O_2 on Mn, Ni, Co and Li leachate concentrations (0 M and 0.68 M H_2O_2, 2 M H_2SO_4, S/L 0.10 g/mL, 75°C, H_2O_2 added at 60 minutes)

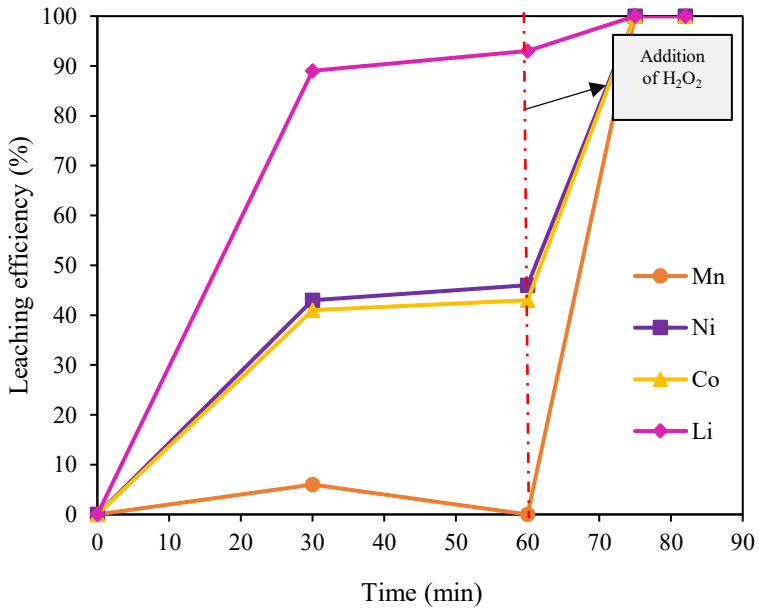

Figure 3.7. Leaching efficiencies for Mn, Ni, Co, Li (2 M H_2SO_4, S/L0.10 g/mL, 75°C, 0.68 M H_2O_2 added at 60 minutes)

Table 3.7 summarizes the effect of S/L ratio on leaching efficiencies for Mn, Ni, Co, Li when 0.68 M H_2O_2 was added. Leaching efficiencies decreased as S/L ratio increased. Highest leaching efficiencies (100% for all metals) were observed at S/L ratio 0.10 g/mL, clearly demonstrating that a low S/L ratio increases metal leaching efficiency in the presence of a reducing agent. Comparison of tables 3.6 and 3.7 shows that adding H_2O_2 increased leaching efficiency at all S/L ratios. The effect was most dramatic with Mn, where leaching efficiency increased from 0.0% to 100%, 72.4% and 27.5% at S/L ratios of 0.10, 0.15 and 0.20 g/mL, respectively. In other words, a reducing agent must be added when leaching Mn to convert Mn^{4+} to its soluble form Mn^{2+}.

Table 3.7. Leaching efficiency for NMC with S/L ratios 0.10, 0.15 and 0.20 g/mL (2 M H_2SO_4, 0.68 M H_2O_2, 75°C, 82 minutes, H_2O_2 added at 60 minutes)

S/L ratio (g/mL)	Leaching efficiency (%)			
	Mn	Ni	Co	Li
0.10	100	100	100	100
0.15	72.4	76.1	76.1	95.2
0.20	27.5	49.4	49.7	83.0

3.3.3. Study of LFP acid leaching

Leaching of Fe, P and Li was studied by varying sulphuric acid concentration, S/L ratio and H_2O_2 addition.

3.3.3.1. Effect of sulphuric acid concentration on leaching efficiency

The same conditions were used with the LFP cathode material as with the NMC material to study the effect of H_2SO_4 concentration on leaching efficiency: concentration of H_2SO_4 varied between 2 M and 6 M with temperature at 75°C, S/L ratio 0.10 g/mL, stirring speed 330 rpm and reaction time 82 minutes. Figure 3.8 illustrates the effect of H_2SO_4 concentration and time on leachate concentrations. As the figure shows, increasing H_2SO_4 concentration from 2 M to 6 M had little effect on P and Li leaching but caused a drop in Fe dissolution.

Leaching efficiencies for Fe, P and Li at 2 M and 6 M H_2SO_4 are shown in figures 3.9a and 3.9b, respectively. As Figure 3.9a shows, leaching efficiencies for Fe, P and Li at 2 M H_2SO_4 increased rapidly in the first 30 minutes, reaching about 100% by the end of the leaching assay. With 6 M H_2SO_4, however, leaching efficiencies increased slowly with time to 98.6% for P and 98.6% for Li, but only 91.3% for Fe

(Figure 3.9b). As a result, the 2 M concentration was selected to study the effect of other parameters because of its higher leaching efficiency.

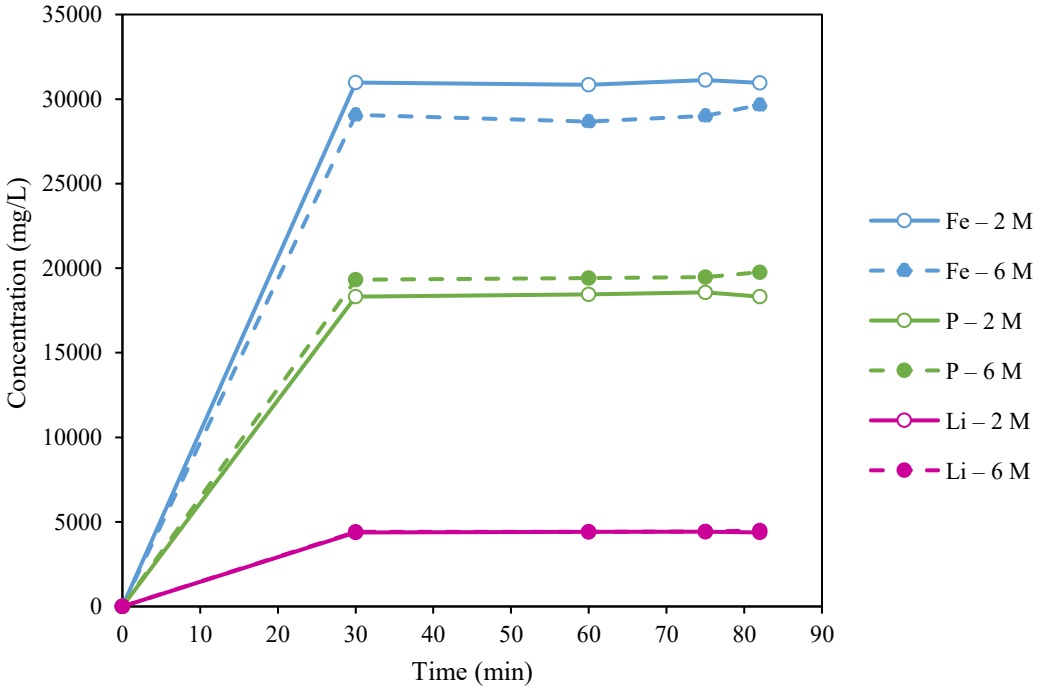

Figure 3.8. Effect of sulphuric acid concentration on leachate concentrations of Fe, P and Li (2 M and 6 M H_2SO_4, S/L 0.10 g/mL, 75°C)

(a)

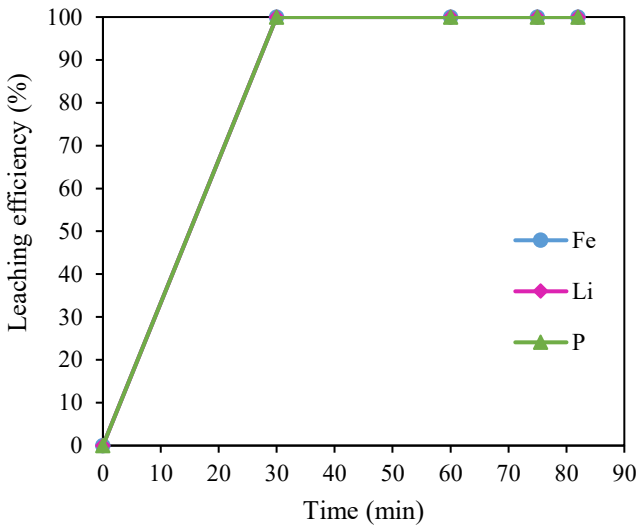

(b)

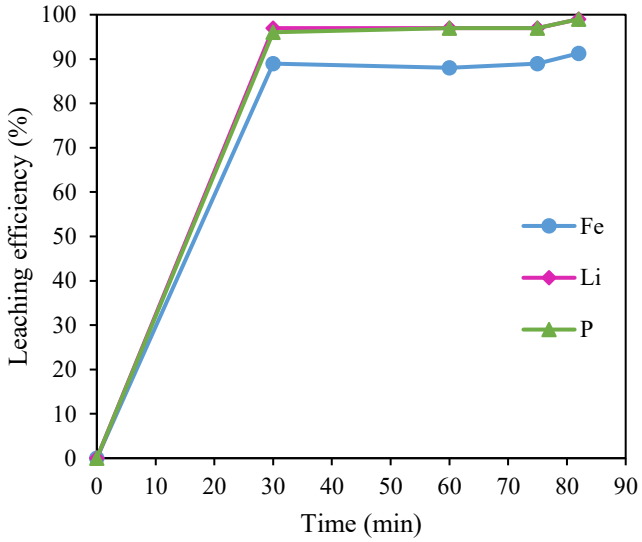

Figure 3.9. Leaching efficiency for LFP: a) 2 M H_2SO_4, S/L 0.10 g/mL, 75°C; (b) 6 M H_2SO_4, S/L 0.10 g/mL, 75°C

Table 3.8 and Figure 3.10 show metal content (mmol/g) and XRD pattern of the leach residue with 6 M H_2SO_4. The results show ferrous sulfate hydrate ($FeSO_4.H_2O$) precipitated in the leach residue.

Table 3.8. Metal content (mmol/g) of leach residue (6 M H_2SO_4, S/L 0.10 g/mL, 75°C)

Sample	Metal content (mmol/g)		
	Fe	P	Li
Leach residue, 6 M	3.11	0.49	0.52

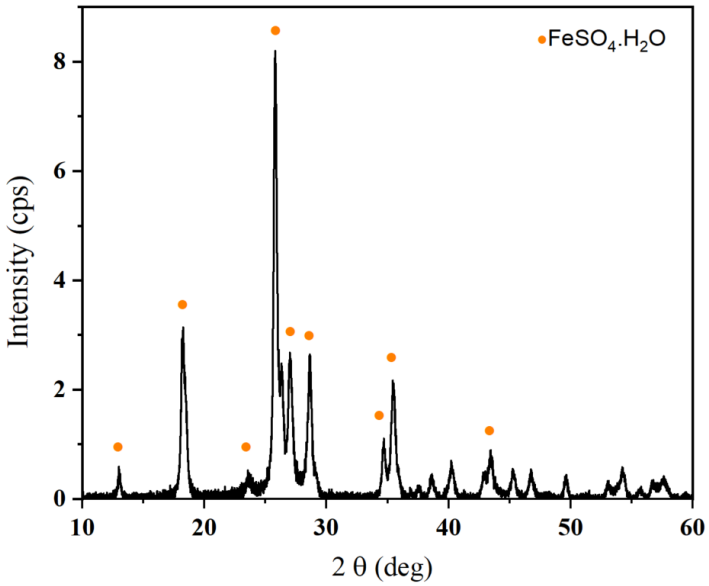

Figure 3.10. XRD pattern of leach residue (6 M H_2SO_4, S/L 0.10 g/mL, 75°C)

3.3.3.2. Effect of solid-liquid ratio on leaching efficiency

To examine the effect of S/L ratio on metal leaching, the leaching assays were performed with an S/L ratio of 0.10, 0.15 and 0.20 g/mL (2 M H_2SO_4, temperature 75°C, stirring speed 330 rpm, 82 minutes). Table 3.9 shows leaching efficiencies for Fe, P and Li as a function of S/L ratio. Leaching efficiency decreased as S/L ratio increased. The highest leaching efficiencies were observed at S/L ratio 0.10 g/mL (100% for Fe, P and Li). As the table shows, metal leaching efficiency decreased as S/L ratio increased.

Table 3.9. Leaching efficiencies for LFP at S/L ratios of 0.10, 0.15 and 0.20 g/mL (2 M H_2SO_4, 75°C, 82 minutes)

S/L ratio (g/mL)	Leaching efficiency (%)		
	Fe	P	Li
0.10	100	100	100
0.15	96.7	96.9	96.9
0.20	86.6	86.9	94.3

3.3.3.3. Effect of H_2O_2 addition on leaching efficiency

H_2O_2 can act as an oxidizing agent due to its high standard reduction potential (1.77 V), enabling it to readily accept electrons and oxidize other species under acidic conditions as demonstrated in Equation 3.2. [77]. To determine its effect on LFP dissolution, H_2O_2 was added at 60 minutes, for a concentration of 0.68 M H_2O_2 in the leachate, under conditions of 2 M H_2SO_4, 75°C, stirring speed 330 rpm and S/L ratio 0.10 g/mL. Figure 3.11 shows leachate concentrations with and without H_2O_2 as a function of time.

$$H_2O_2 + 2H^+ + 2e^- = 2H_2O \quad E^\circ = 1.77\ V \tag{3.2}$$

Concentration of Fe in the leachate increased rapidly in the first 30 minutes and then remained stable to 60 minutes. When H_2O_2 was added at 60 minutes, Fe concentration dropped, due to the dilution effect of adding 15 mL of H_2O_2 to the solution. A similar trend was observed for P and Li.

Figure 3.12 illustrates the effect of adding 0.68 M H_2O_2 on leaching efficiencies for Fe, P and Li: leaching efficiencies for Fe, P and Li reached 100% after H_2O_2 was added and the effect on leaching efficiencies for all metals was negligible.

To further study the effect of adding H_2O_2 on the leaching of LFP, two assays with high S/L ratios were carried out. Table 3.10 shows the effect of S/L ratio on leaching efficiencies for Fe, P and Li when 0.68 M H_2O_2 was added: leaching efficiencies dropped as S/L ratio increased. The highest leaching efficiencies were recorded for S/L ratio 0.10 g/mL (100% for all metals). Comparison of tables 3.9 and 3.10 shows that the addition of H_2O_2 had a negligible effect on leaching efficiencies for all metals at S/L ratios 0.10 g/mL and 0.15 g/mL. On the other hand, when H_2O_2 was added and S/L ratio was increased from 0.15 to 0.20 g/mL, leaching efficiency for Fe and for P dropped from 86.6% to 61.1% and from 86.9% to 61.2%, respectively, and for Li rose from 94.3% to 99.1%.

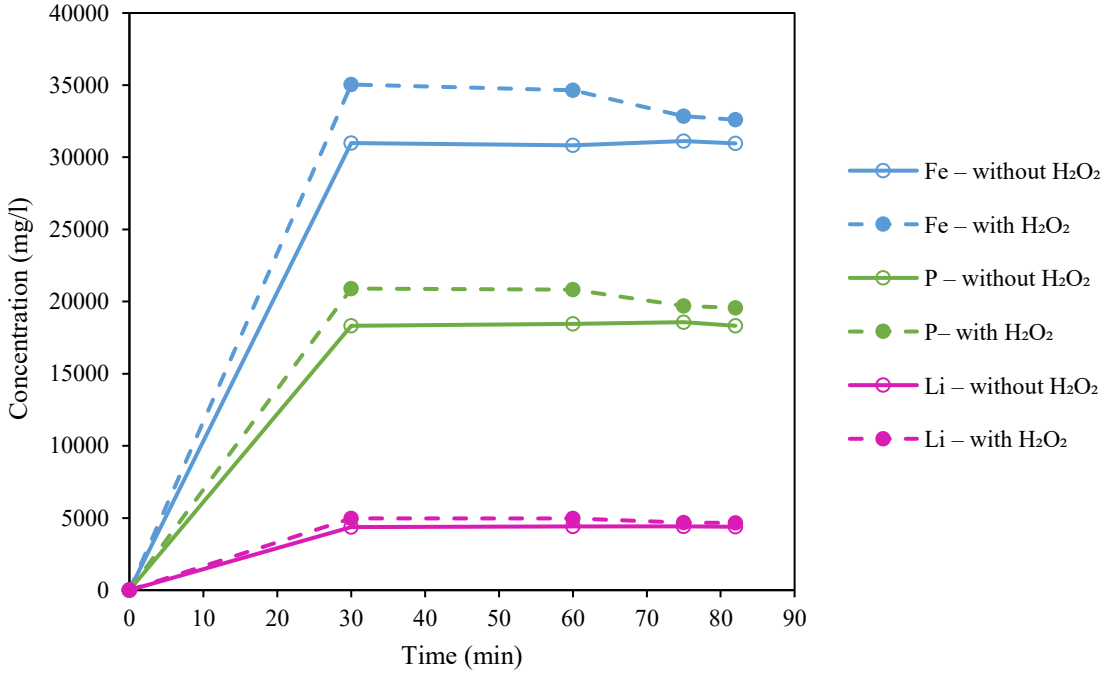

Figure 3.11. Effect of H_2O_2 on leachate concentrations of Fe, P and Li (0 and 0.68 M H_2O_2, 2 M H_2SO_4, S/L 0.10 g/mL, 75°C) with H_2O_2 added at 60 minutes

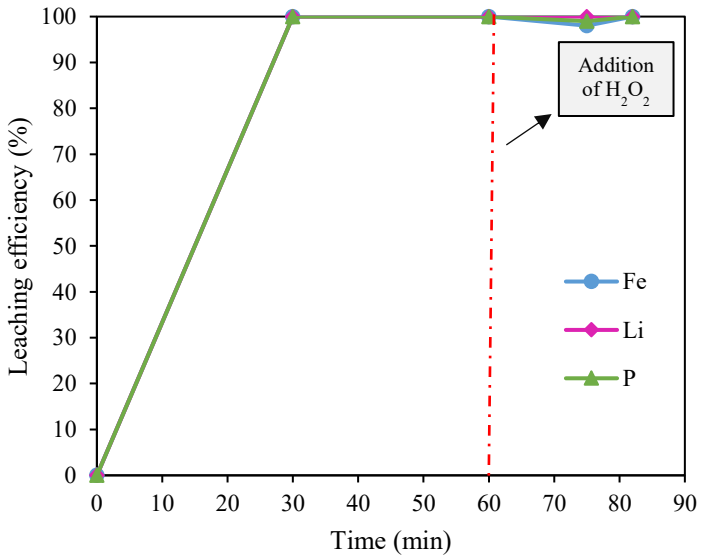

Figure 3.12. Leaching efficiencies for Fe, P and Li (2 M H_2SO_4, S/L 0.10 g/mL, 75°C, 0.68 M H_2O_2) with H_2O_2 added at 60 minutes

Table 3.10. Leaching efficiency of LFP (S/L ratio 0.10, 0.15 and 0.20 g/mL, 2 M H_2SO_4, 0.68 H_2O_2, 75°C, 82 minutes) with H_2O_2 added at 60 minutes

S/L ratio (g/mL)	Leaching efficiency (%)		
	Fe	P	Li
0.10	100	100	100
0.15	98.1	98.1	98.6
0.20	61.1	61.2	99.1

ICP and XRD analyses of the solid residues from leaching with and without H_2O_2 (2 M H_2SO_4, 75°C, S/L ratio 0.20 g/mL) were carried out. Table 3.11 shows metal content of the two leach residues. The results clearly indicate that Fe and P content is higher when H_2O_2 is added, while Li content is reduced due to greater dissolution.

Figure 3.13 shows the XRD pattern of the solid residue from leaching (2 M H_2SO_4, 75°C, S/L 0.20 g/mL) without H_2O_2. As the figure shows, the orthorhombic iron phosphate dihydrate ($FePO_4 \cdot 2H_2O$) was produced together with lithium sulfate monohydrate ($Li_2SO_4 \cdot H_2O$) and ferrous sulfate monohydrate ($FeSO_4 \cdot H_2O$). Figure 3.14 shows the XRD pattern of the solid leach residue under the same conditions but with the addition of 0.68 M H_2O_2. The XRD pattern matches two types of iron phosphate dihydrate ($FePO_4 \cdot 2H_2O$), orthorhombic and monoclinic. However, the XRD pattern of the sample is not a good fit for the first peak of the diffraction pattern for monoclinic $FePO_4 \cdot 2H_2O$ (011). Table 3.12 shows the lattice parameters refined based on the sample's diffraction pattern. The lattice parameters of the monoclinic system are in good agreement with those reported by Zaghib et al [75]. However, the lattice parameters of the orthorhombic system are different from those reported by Song et al. [100].

Table 3.11. Metal content (mmol/g) of leach residue with and without 0.68 M H_2O_2 (2 M H_2SO_4, 75°C, S/L 0.2 g/mL, 82 minutes)

Sample	Metal content (mmol/g)		
	Fe	P	Li
Leach residue, S/L ratio 0.20 g/mL without H_2O_2	3.54	3.53	1.52
Leach residue, S/L ratio 0.20 g/mL with 0.68 M H_2O_2	5.02	5.10	0.11

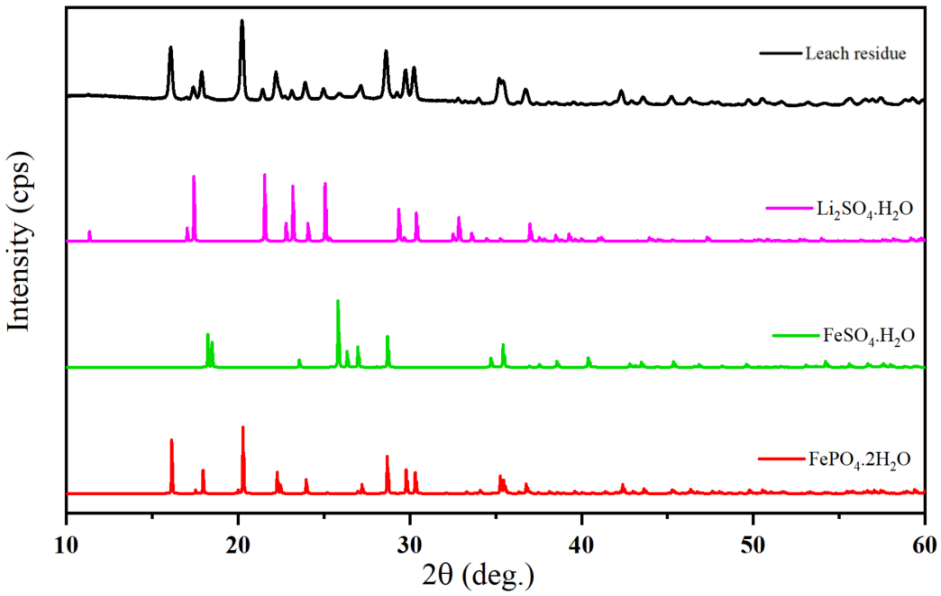

Figure 3.13. XRD patterns of leach residue (2 M H_2SO_4, 75°C, S/L 0.20 g/mL, 82 minutes) and of $Li_2SO_4 \cdot H_2O$ (COD ID: 1008190), $FeSO_4 \cdot H_2O$ (COD ID: 9004339) and $FePO_4 \cdot 2H_2O$ (orthorhombic COD ID: 9010007)

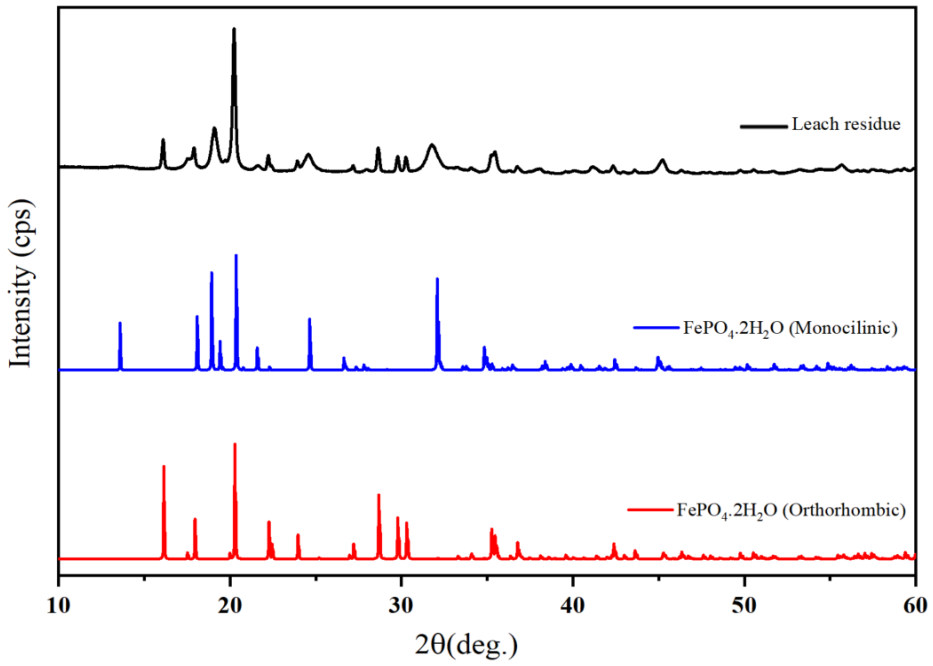

Figure 3.14. XRD patterns of leach residue (2 M H_2SO_4, 0.68 M H_2O_2, 75°C, S/L 0.20 g/mL, 82 minutes) and of $FePO_4 \cdot 2H_2O$ (monoclinic with COD ID: 9010008) and $FePO_4 \cdot 2H_2O$ (orthorhombic COD ID: 9010007)

Table 3.12. Phase identification and lattice parameters of $FePO_4.2H_2O$

Phase	System	Space group	Lattice parameters			Volume	Ref
			a	b	c		
$FePO_4{\cdot}2H_2O$	Monoclinic	$P2_1/n$ (14)	5.335 Å	9.808 Å	8.720 Å	456.26 $Å^3$	This work
$FePO_4{\cdot}2H_2O$	Orthorhombic	Pbca (61)	8.722 Å	9.878 Å	10.119 Å	871.79 $Å^3$	This work
$FePO_4{\cdot}2H_2O$	Monoclinic	$P2_1/n$	5.3125(6) Å	9.765(2) Å	8.683(7) Å	450.44 $Å^3$	[75]
$FePO_4{\cdot}2H_2O$	Orthorhombic	Pbca	9.8674 Å	10.0973 Å	8.7046 Å	867.27 $Å^3$	[100]

3.4. Discussion

- Characterization of NMC and LFP materials

Samples of NMC and LFP cathode materials were used to develop acid leaching procedures for these materials. The materials were first characterized for metal content. In the NMC samples, Ni content was the highest, averaging 366.7 ± 0.9 g/kg as shown in Table 3.1. The calculated stoichiometry of $Ni_{0.6}Mn_{0.2}Co_{0.2}$ agreed with the LIB manufacturers specifications such as NEI Corporation and by Peschel et al. [101]. Average lattice parameters obtained in this study align well with XRD results for NMC622 reported in the literature. Zhang et al. [102], for example, report lattice parameters a, b = 2.8704(2) Å and c = 14.2199(3) Å for NMC622. Additionally, the XRD data for the NMC sample were analyzed with Rietveld refinement using TOPAS software, confirming a space group 166 and lattice parameters a, b = 2.86741(4) Å and c = 14.2180(4) Å. These results agree with values reported in the literature, validating the reliability of the characterization and analysis.

The composition of the LFP cathode material used in this study (Table 3.3) is very similar to the one reported in the literature. Mahandra et al. [103], for example, found metal content (wt%) in spent cathode powder to be 32.50% Fe, 18.05% P, and 4.35% Li. XRD analysis of the LFP samples indicated an orthorhombic crystal structure with space group Pnma (62). Average lattice parameters closely aligned with those reported in the Crystallography Open Database (COD ID: 1101111). Comparative studies in the literature report similar lattice parameters for LFP. For example, Boiko et al. [104], report $LiFePO_4$ crystallizing in an orthorhombic structure with the space group Pnma (62) and lattice parameters a = 10.328 Å, b = 6.007 Å and c = 4.694 Å for LFP. In another study, Liang et al. [105] report LFP with an orthorhombic crystal structure with space group Pnma and the lattice parameters a = 10.3172 Å, b = 6.0096 Å and c = 4.6775 Å. These consistent results confirm the structural characterization of LFP in this study and suggest the analytical methods developed are correct.

- Effect of sulphuric acid concentration on leaching efficiency

Our findings indicate that switching from 2 M to 6 M sulphuric acid did not significantly affect leaching efficiency for Mn, Ni, Co and Li from NMC cathode material under conditions of S/L ratio 0.10 g/mL, 75°C and reaction time of 82 minutes. This suggests that 2 M H_2SO_4 provides sufficient protons (H^+) to dissolve transition metals and that further increases in acid concentration did not improve leaching efficiency.

Equation (3.3) describes the acid leaching of NMC622 batteries [106]. H_2SO_4 dissociates into H^+ and SO_4^{2-}, and the H^+ ions act as the primary agent in attacking the M-O bonds in the NMC lattice. This leads to reduction and dissolution of transition metals oxides and the formation of soluble sulfate salts.

$$20LiNi_{0.6}Mn_{0.2}Co_{0.2}O_2 + 30H_2SO_4 = 12Ni(II)SO_4 + 4Co(II)SO_4 + 4Mn(II)SO_4 + 10Li_2SO_4 + 30H_2O + 5O_2 \quad (3.3)$$

Reduction half-reactions and their standard potentials (E°) describe the reduction of Ni^{3+}, Co^{3+} and Mn^{4+} to their divalent states (Ni^{2+}, Mn^{2+} and Co^{2+}) [107]:

$$Ni^{3+} + e^- \rightarrow Ni^{2+} \quad E^\circ = +1.5\ V \quad (3.4)$$

$$Mn^{4+} + 2\ e^- \rightarrow Mn^{2+} \quad E^\circ = +1.23\ V \quad (3.5)$$

$$Co^{3+} + e^- \rightarrow Co^{2+} \quad E^\circ = +1.82\ V \quad (3.6)$$

Ni and Co showed the same trends and almost the same leaching efficiency at both H_2SO_4 concentrations, thanks to their higher redox potential. However, given their high valence states (Ni^{3+} and Co^{3+}) in ternary materials, the reduction reaction did not proceed to completion. Total dissolution typically requires an external reductant to transform the remaining cathode metal oxides to a soluble form.

Leaching results showed dramatically different behaviour for Mn due to its lower redox potential. Mn leaching efficiency initially (during the first 30 minutes) increased slightly but subsequently decreased and stayed nearly constant at around 0%. This can be explained by poor reduction of Mn^{4+} to Mn^{2+} in the first 30 minutes followed by oxidation of Mn^{2+} to Mn^{4+} and subsequent precipitation of manganese oxides (MnO_2). This hypothesis is supported by XRD analysis (Figure 3.5), which confirmed the formation of MnO_2 precipitates at both concentrations of H_2SO_4. This is also supported by the literature. Partinen et al. [108] report precipitation of MnO_2 at temperatures above 50°C, indicating a highly oxidative solution.

Li demonstrated a significantly higher leaching efficiency than Ni, Mn and Co, attributable to differences M-O in bond lengths and bonding energies. The Li-O bond has lower bond energy (336 kJ/mol) than the

Mn-O (402 kJ/mol), Ni-O (391 kJ/mol) and Co-O (400 kJ/mol) bonds, making is easier for the acidic solution to break the Li-O bonds and release Li^+ ions into the leachate [56, 109].

As documented in the literature, metal leaching rate typically increase with rising H_2SO_4 concentration up to an optimal level thanks to a higher collision frequency between the leaching agent and cathode material particles [63]. For example, Lv et al. [64] report that leaching efficiencies for Co, Ni, Mn and Li increased when H_2SO_4 concentrations were increased from 0 to 2.5 M but plateaued when concentrations were increased from 2.5 M to 3 M (conditions: S/L ratio 0.10 g/mL, 80°C, 60 minutes and 0.8 mol/L NH_4Cl. Similarly, Kim et al. [55] report that 2 M H_2SO_4 was the optimal concentration for dissolving 98% of Mn, Ni, Co and Li from NMC cathodes under conditions of 2.13 M H_2O_2 , 60°C, 120 minutes and S/L ratio 0.10 g/mL. They report that further increases in acid concentration did not improve metal leaching efficiency.

Similarly, for LFP, increasing H_2SO_4 concentration from 2 M to 6 M had little effect on the dissolution of Li and P but Fe leaching decreased. Equation (3.7) describes the dissolution reaction of LFP with H_2SO_4 [73]. The H^+ ions from the H_2SO_4 react with the LFP, dissolving it and releasing Li^+ and Fe^{2+} into the solution. These ions then react with the sulphate (SO_4) and form $Fe(II)SO_4$ and Li_2SO_4 [110].

$$2\,LiFe(II)PO_4\,(aq) + 3\,H_2SO_4 = 2\,Fe(II)SO_4\,(aq) + Li_2SO_4\,(aq) + 2\,H_3PO_4 \quad (3.7)$$

The results show that 2 M H_2SO_4 is sufficient to effectively dissolve LFP. However, dissolution of Fe decreased at 6 M H_2SO_4. Koblyn et al. [111] studied solubility in the H_2O-$FeSO_4$-H_2SO_4 system at 80°C and found that solubility of $FeSO_4$ decreased when H_2SO_4 molality was increased, as shown in Figure 3.15. This could be due to the common ion effect: the increase in SO_4^{2-} ion concentration shifts the solubility equilibrium backward, meaning less $FeSO_4$ will dissolve. In other words, the low leaching efficiency for Fe could be due to formation of insoluble $FeSO_4.H_2O$ at high concentrations of H_2SO_4, as suggested by XRD (Figure 3.10). Zheng et al. [71], however, demonstrated that when H_2SO_4 concentration was increased from 0.5 to 2.5 M, leaching efficiency increased from 25% to 97.2% for Li and from 46% to 98.5% for Fe but that increasing sulphuric acid concentration beyond 2.5 M had a negligible effect on leaching rates (conditions were S/L ratio 0.10 (g/mL), reaction time 4 hours and 60°C).

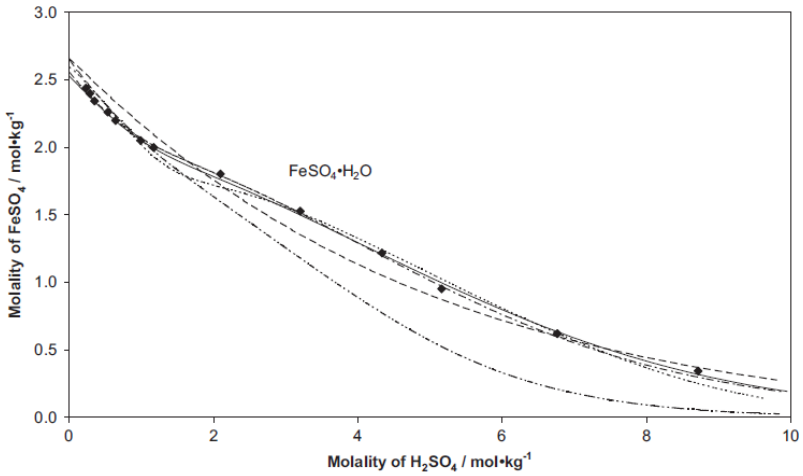

Figure 3.15. Assessed and experimental solubility data for the H_2O–$FeSO_4$–H_2SO_4 system at 80°C as reported by Koblyn et al. [109]

- Effect of solid-liquid ratio on leaching efficiency

Based on Equation (3.3), the stoichiometric ratio for complete leaching of NMC is 1.5 moles of H_2SO_4 per mole of NMC. Table 3.13 shows the calculation of the stoichiometric acid requirement for NMC leaching at different S/L ratios. At all S/L ratios, the amount of H_2SO_4 is theoretically sufficient to fully dissolve the NMC present. However, as Table 3.6 shows, leaching efficiencies for Ni, Co and Li decreased slightly when the S/L ratio was increased from 0.10 g/mL to 0.20 g/mL, while Mn remained consistently undissolved, its leaching efficiency 0%.

Highest leaching efficiencies were recorded for Li across all S/L ratios, with efficiencies dropping from 97.8% to 86.4% as S/L ratio was increased from 0.10g/mL to 0.20 g/mL. As discussed, this is attributed to Li having lower bond energy and being less redox-dependent than the other transition metals. Ni and Co leaching efficiencies decreased slightly, from 46.7% to 40.0% and from 43.0% to 39.9%, respectively, as S/L ratio was increased. As mentioned, both Ni^{3+} and Co^{3+} require sufficient redox potential for reduction to their divalent state, and the increased concentration of dissolved Ni^{2+} and Co^{2+} ions at higher S/L ratios caused a decrease in the system's redox potential. According to the Nernst equation (3.8) [112]:

$$E = E^{\circ} - \frac{RT}{nF} Ln \left(\frac{[M^{2+}]}{[M^{3+}]}\right) \quad (3.8)$$

where E is the electrode potential (V), E° is the standard electrode potential (V), R is the molar gas constant (J/mol.°K), T is the temperature (°K), n is the number of electrons transferred in the reaction and F is the

Faraday constant (C/mol). The reduction in redox potential decreases the driving force required for further dissolution of Ni and Co.

Final leaching efficiency for Mn was around 0% across all tested S/L ratios. This indicates that Mn^{4+} could not be reduced to the soluble Mn^{2+} state. Mn may require a higher redox potential for reduction than Ni and Co.

Table 3.13. Calculation of stoichiometric acid requirement for NMC622 leaching

S/L (g/mL)	NMC mass (g)	NMC (moles)	H_2SO_4 (moles)	Stoichiometric acid requirement (moles)
0.10	20	0.206	2	0.309
0.15	30	0.310	2	0.465
0.20	40	0.413	2	0.620

This decrease in NMC leaching efficiency at higher S/L ratios has been reported in the literature. For example, Yang et al. [63] report that increasing S/L ratio from 50 g/L to 100 g/L had an adverse impact on leaching efficiency for Mn, Ni, Co and Li under conditions of 2 M H_2SO_4, hydrazine sulfate 30 g/L, 80°C and leaching time 60 minutes. In their study, leaching of Li appeared to be less affected by S/L ratio.

The stoichiometric acid requirement for dissolution of LFP, based on Equation (3.7), was calculated as shown in Table 3.14. At all S/L ratios, the amount of sulphuric acid is theoretically sufficient to fully dissolve the LFP. However, as shown in Table 3.9, leaching efficiencies for Fe and P decreased when S/L ratio increased from 0.10 g/mL to 0.20 g/mL. This can be explained by the oxidation of Fe^{2+} to Fe^{3+} due to an increase in redox potential at the higher S/L ratio. The XRD pattern of the solid residue at S/L ratio 0.20 g/mL (Figure 3.15) confirms the presence of Fe^{3+} in the form of $FePO_4 \cdot 2H_2O$. The leaching of Li appears to be less affected by the increased S/L ratio, probably because Li-O bonding energy (341 kJ/mol) is significantly lower than the bonding energy of Fe-O (409 kJ/mol) or P-O (596.6 kJ/mol), which means Li can dissolve more easily than Fe or P even with less acid available. Zheng et al. [71] report a decrease of leaching efficiency for Fe and Li when S/L ratio was more than 0.10 g/mL under conditions of 2.5 mol/L H_2SO_4, 60°C and leaching time 4 hours.

Table 3.14. Calculation of stoichiometric acid requirement for LFP leaching

S/L (g/mL)	LFP mass (g)	LFP (moles)	H_2SO_4 (moles)	Stoichiometric acid requirement (moles)
0.10	10	0.124	2	0.186
0.15	20	0.186	2	0.279
0.20	30	0.248	2	0.372

- Effect of H_2O_2 addition on leaching efficiency

The effect of H_2O_2 on leaching efficiency was different for NMC and LFP. As discussed, H_2O_2 functions both as a reducing agent and an oxidizing agent. Equation (3.8) describes the chemical reaction during NMC leaching with H_2SO_4 in the presence of H_2O_2 [106]. As described in Equation (3.1) and half reactions (3.4-3.6), H_2O_2 oxidizes to O_2 and H^+ , donating electrons to reduce Mn^{4+}, Co^{3+} and Ni^{3+} to the more soluble Mn^{2+}, Co^{2+} and Ni^{2+} [46]. Adding H_2O_2 to the leaching system increases its reducing power, allowing reduction of these three metals and thereby enhancing their leaching efficiency. Adding H_2O_2 has no effect on Li leaching efficiency, however, as it does not alter the oxidation state of Li. Besides, Li is already completely dissolved in the acidic solution, as reported by Ferreira et al. [53].

$$20LiNi_{0.6}Mn_{0.2}Co_{0.2}O_2 + 30H_2SO_4 + 2H_2O_2 = 12Ni(II)SO_4 + 4Co(II)SO_4 + 4Mn(II)SO_4 + 10Li_2SO_4 + 32H_2O + 6\ O_2 \quad (3.8)$$

Zhu et al. [113] report that the addition of 2% H_2O_2 (volume fraction) significantly improved the Co and Li leaching efficiencies of a sulphuric acid leaching system: 96.3% of Co and 87.5% of Li were leached under conditions of 2 M H_2SO_4, S/L 33g/L, 60°C and 2 hours. Similarly, He et al. [56] demonstrated that adding H_2O_2 improved metal leaching by facilitating the reduction of high oxidation states of metal ions in NMC, and obtained the recovery rate of all metals to 99.7 % under conditions of 1 M H_2SO_4, 1 vol% H_2O_2, S/L 0.04 mg/L, 40°C and 1 hour. These results align with the findings of this study.

For LFP, H_2O_2 acts as an oxidation agent. Leaching of LFP in the presence of H_2SO_4 and H_2O_2 can be described by Equation (3.9) [70]. During the first 60 minutes of leaching, before H_2O_2 is added, Li^+, Fe^{2+} and PO_4^{3-} are released into the leaching solution. When H_2O_2 is added, its strong oxidizing potential (E°= + 1.77 V), as shown in Equation (3.2), drives the oxidation of Fe^{2+} to Fe^{3+} (E°= + 0.77 V), as described in

Equation (3.10). This reaction is energetically favorable because the difference in redox potentials is a significant driving force. The formation of Fe^{3+} promotes precipitation of $Fe(III)PO_4$ as a leach residue.

$$2\ LiFe(II)PO_4 + H_2SO_4 + H_2O_2 = Li_2SO_4 + 2\ Fe(III)PO_4 + 2H_2O \quad (3.9)$$

$$Fe^{3+} + e^- = Fe^{2+} \qquad E^\circ = 0.77\ V \quad (3.10)$$

As mentioned, the addition of H_2O_2 had a negligible effect on the solubility of Fe, P and Li at S/L ratios 0.10 g/mL and 0.15 g/mL under the specified conditions. The presence of H_2O_2, however, decreased leaching efficiencies for Fe and P at S/L ratio 0.20 g/mL, probably due to the effect of pH on the solubility of Fe and P, as shown in Equation (3.11). At pH values less 0.5, Fe^{3+} tends to form soluble $Fe(III)_2(SO_4)_3$ rather than precipitating in the leach residue as $Fe(III)PO_4$ [69, 114] . For this reason, at low S/L ratios (0.10 g/mL and 0.15 g/mL), where there is more available acid and therefore a lower solution pH, the addition of H_2O_2 oxidizes Fe^{2+} to Fe^{3+} in soluble form without changing its solubility.

$$10\ Fe(III)PO_4 + 15\ H_2SO_4 = 5\ Fe(III)_2(SO4)_3 + 10\ H_3PO_4 \ , pH < 0.5 \quad (3.11)$$

However, precipitation of Fe^{3+} as $FePO_4$ at S/L ratio 0.20 g/mL was confirmed by XRD analysis. Comparison of the XRD patterns of the leach residues obtained at S/L ratio 0.20 g/mL with and without addition of H_2O_2 showed that adding H_2O_2 promoted precipitation of iron phosphate dihydrate ($FePO_4 \cdot 2H_2O$) while facilitating dissolution of other phases, such as $Li_2SO_4 \cdot H_2O$ and $FeSO_4 \cdot H_2O$. The effect of H_2O_2 on LFP dissolution was studied by Li et al. [70] . These researchers report oxidation of Fe^{2+} by H_2O_2 and precipitation of $FePO_4$ over the expected pH range. In another study, Zou et al. [86] observed that H_2O_2 did not improve LFP dissolution but instead led to a rise in redox potential from 335 to 476 mV vs. Ag/AgCl as a result of the oxidation of Fe^{2+} to Fe^{3+} as H_2O_2 was added.

3.5. Conclusion

Acid leaching procedures were developed to extract metals from cathode materials of NMC and LFP individually. Characterization of the NMC and LFP cathode materials in this study validated their metal content and structural properties, which proved very similar to reported literature values. The effect of H_2SO_4 concentration, S/L ratio and addition of H_2O_2 on the dissolution of metals was studied. The results indicate that a 2 M H_2SO_4 solution is sufficient for dissolution of Mn, Ni, Co and Li from NMC as well as Li, Fe and P from LFP. Higher concentrations did not improve leaching efficiency for NMC and reduced Fe dissolution in LFP due to $FeSO_4 \cdot H_2O$ precipitation. Leaching efficiency with both NMC and LFP cathode materials was significantly influenced by S/L ratio. For NMC, lower S/L ratios (0.10 g/mL)

provided optimal conditions for dissolving Ni, Co and Li while higher ratios reduced leaching efficiency by lowering the redox potential in the system and decreasing acid availability. Similarly for LFP, the low S/L ratio (0.10 g/mL) facilitated 100% leaching efficiencies for Fe, P and Li, while the high ratio (0.20 g/mL) led to formation of $FePO_4 \cdot 2H_2O$. These findings emphasize the importance of optimizing the S/L ratio for efficient metal recovery. The addition of H_2O_2 influenced leaching efficiency differently for NMC and LFP. The results indicate that addition of H_2O_2 significantly improves leaching efficiencies from NMC cathodes for Mn, Ni and Co. Leaching efficiency for Mn, Ni, Co were 100%, when H_2O_2 was added under conditions of S/L ratio 0.10 g/mL and 2 M H_2SO_4, demonstrating its role as an effective reducing agent. Conversely, in LFP, H_2O_2 oxidized Fe^{2+} to Fe^{3+}. When the S/L ratio was high (0.20 g/mL), addition of 0.68 M H_2O_2 led to a decrease in efficiency for Fe and P leaching due to the increase in pH and the formation of hydrated $FePO_4$.

CHAPTER IV

STUDY OF METAL EXTRACTION EFFICIENCY OF SULPHURIC ACID LEACHING OF MIXED NMC AND LFP CATHODE MATERIALS

4.1. Introduction

This chapter describes the study of acid leaching of a mixture of NMC and LFP cathode materials. The main focus was to study the effect of various parameters on the comprehensive leaching rate of metals from a mixture of NMC and LFP materials, including S/L ratio, H_2O_2, NMC/LFP molar ratio and H_2SO_4 concentration. The goal was to identify leaching parameters that improved leaching efficiencies for Mn, Ni, Co and Li while ensuring formation of orthorhombic $FePO_4$ as a valuable leach residue.

4.2. Methodology

The leaching procedures for the mixed NMC and LFP were carried out following the method described in Chapter II. Based on the results obtained in Chapter III regarding the effect of sulphuric acid concentration on the individual leaching of NMC and LFP, an acid concentration of 2 M H_2SO_4 was selected for the leaching of the mixed materials. In this regard, the effects of the solid-to-liquid (S/L) ratio (ranging from 0.05 g/mL to 0.20 g/mL), 0.68 M H_2O_2 concentration, and NMC/LFP molar ratios between 0.05 and 4.1 on the acid leaching behavior of the mixed cathode materials were studied.

Subsequently, after identifying the best operating conditions for the S/L ratio, H_2O_2 concentration, NMC/LFP molar ratio, the effects of lower H_2SO_4 concentrations (0.25 M and 0.5 M) were examined.

In accordance with the procedures described in the previous chapter, all tests were conducted at a fixed temperature of 75 °C under atmospheric pressure and a stirring speed of 330 rpm. The resulting leach residues were subsequently characterized to assess their composition and phase structure.

4.3. Results

4.3.1. Effect of solid-liquid ratio on metal leaching efficiency

To examine the effect of the solid-liquid (S/L) ratio on metal leaching, the leaching assays were performed at S/L ratios of 0.05, 0.10, 0.15 and 0.20 g/mL under fixed conditions of 2 M H_2SO_4, 75°C, NMC/LFP mass ratio 1, which corresponded to a NMC/LFP molar ratio 1.67, stirring speed 330 rpm and reaction time 82 minutes. Table 4.1 shows the details of the experimental design.

Table 4.1. Experimental design for study of the effect of S/L ratio on metal leaching efficiency from mixed NMC and LFP

Assay	NMC mass (g)	LFP/C mass (g)	H_2SO_4 concentration (M)	H_2SO_4 Volume (mL)	Solid-liquid ratio (g/mL)	Temperature (°C)	Time (min)
1	5	5	2	200	0.05	75	82
2	10	10	2	200	0.10	75	82
3	15	15	2	200	0.15	75	82
4	20	20	2	200	0.20	75	82

Figure 4.1 shows the effect of S/L ratio on leaching efficiencies for Mn, Ni, Co, Li, Fe and P under conditions of 2 M H_2SO_4, 75°C and 82 minutes. Results show that leaching efficiencies for Mn, Ni and Co decreased slightly as S/L ratio increased. Leaching efficiency for Mn decreased from 85.9% to 73.6% when S/L ratio was increased from 0.05 to 0.20 g/mL. A similar trend was observed for Ni and Co, with leaching efficiencies decreasing from 86.3% to 74.4% and from 86.4% to 74.3%, respectively, with the same increase in S/L ratio. Li showed consistently high leaching efficiency across all S/L ratios, while Fe and P experienced sharp declines above an S/L ratio of 0.10 g/mL with low efficiencies of 55.6% and 57.4%, respectively, at S/L ratio 0.20 g/mL. As expected, the highest efficiencies obtained at S/L ratio 0.05 g/mL due to greater availability of free acid for leaching.

Table 4.2 shows metal content (mmol/g) of the leach residues obtained with different S/L ratios under the specified conditions. Figure 4.2 shows XRD results for S/L ratios 0.10, 0.15 and 0.20 g/mL. The mass of the leach residue at S/L ratio 0.05 g/mL was insufficient for XRD analysis to be performed. For all three S/L ratios, these results show distinct peaks corresponding to $FePO_4$ with orthorhombic space group Pnma (62) and lattice parameters a = 9.814 Å, b = 5.789 Å and c = 4.782 Å, $Li_{0.115}MnO_2$ with cubic space group Fd-3m (227) and lattice parameter a = 8.064 Å, and $LiNi_{0.6}Mn_{0.2}Co_{0.2}O_2$ with lattice parameters a = 2.867 Å, b = 2.867 Å and c = 14.218 Å corresponding to space group 166, indicating presence of these compounds in the leach residues.

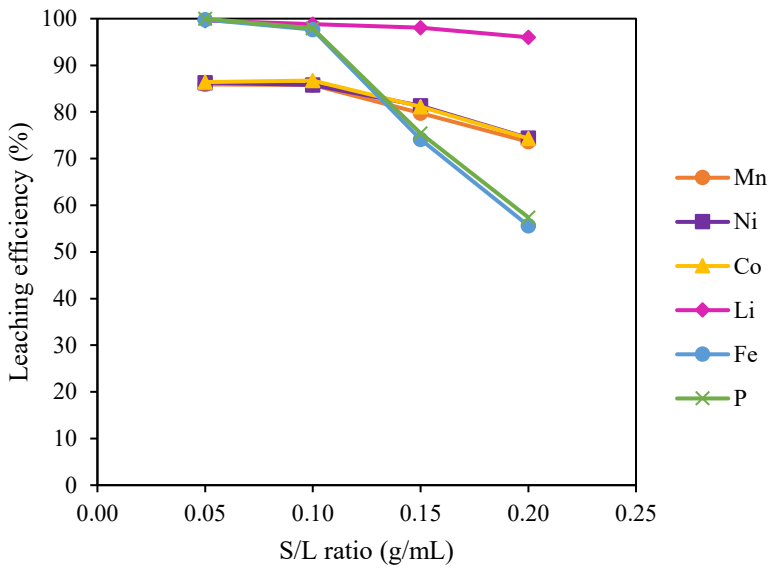

Figure 4.1. Leaching efficiencies for Mn, Ni, Co, Li, Fe and P with S/L ratios 0.10, 0.15 and 0.20 g/mL (2 M H_2SO_4, NMC/LFP mass ratio 1 (NMC/LFP molar ratio 1.67), 75°C and 82 minutes)

Table 4.2. Effect of S/L ratio on metal content (mmol/g) in leach residue (S/L ratios ranging from 0.05 to 0.20 g/mL, 2 M H_2SO_4, NMC/LFP mass ratio 1 (NMC/LFP molar ratio 1.67), 75°C, 82 minutes)

S/L (g/mL)	**Metal content (mmol/g)**					
	Mn	**Ni**	**Co**	**Li**	**Fe**	**P**
0.05	1.85	5.37	1.71	0.43	0.07	0.00
0.10	1.68	4.73	1.50	1.08	0.80	0.71
0.15	0.94	2.58	0.84	0.70	3.48	3.36
0.20	0.80	2.31	0.75	0.93	3.90	3.81

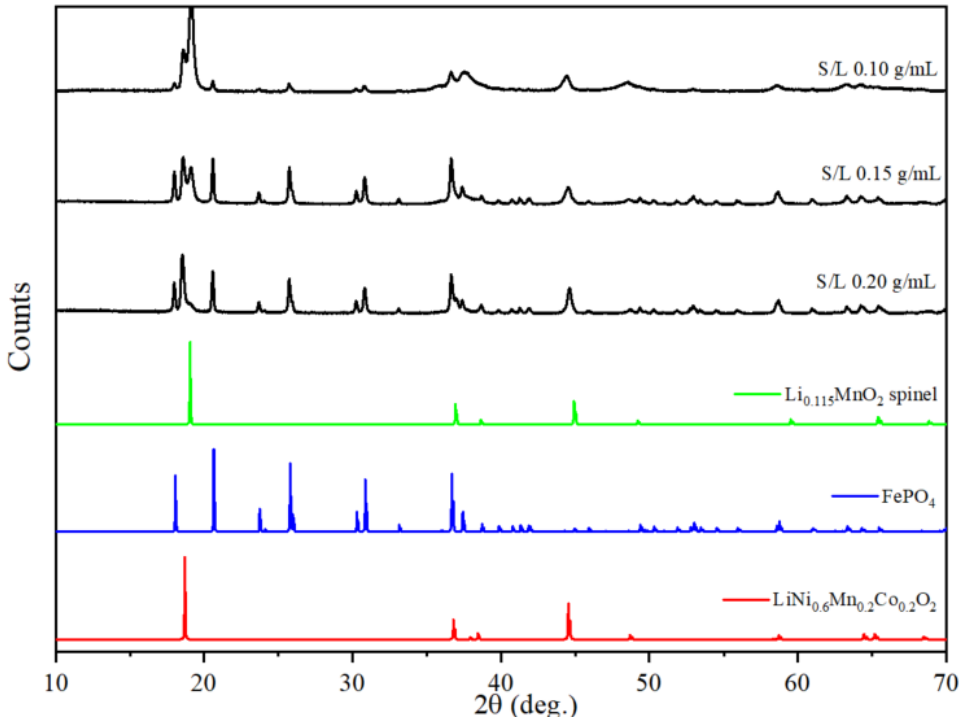

Figure 4.2. XRD patterns of leach residues with S/L ratios 0.10, 0.15, 0.20 g/mL (2 M H_2SO_4, NMC/LFP mass ratio 1 (NMC/LFP molar ratio 1.67), 75°C, 82 minutes) and of $Li_{0.115}MnO_2$ (COD ID: 8103495), $FePO_4$ (COD ID: 1525576) and $LiNi_{0.6}Mn_{0.2}Co_{0.2}O_2$ (COD ID: 4002443)

4.3.2. Effect of H_2O_2 addition on metal leaching efficiency

As discussed in Chapter 3, H_2O_2 was employed both as reductant and oxidant. To study the effect of H_2O_2 on metal dissolution in mixed NMC and LFP materials, H_2O_2 was added to reach a concentration of 0.68 M at 60 minutes of leaching under fixed conditions of 2 M H_2SO_4, 75°C, stirring speed 330 rpm, S/L ratio 0.10 g/mL and NMC/LFP mass ratio 1. Figure 4.3 shows leachate metal concentrations in the absence and presence of H_2O_2 as a function of time. As the figure shows, addition of 0.68 M H_2O_2 increased Mn, Ni and Co dissolution but on the contrary had a negligible effect on concentrations of Li, Fe and P.

As Figure 4.4 shows, leaching efficiencies for Mn, Ni, Co, Li, Fe and P increased rapidly in the first 30 minutes. From 30 to 60 minutes, leaching efficiencies for Mn, Ni and Co, Fe and P increased slowly, reaching 80.8%, 80.2%, 80.7%, 91.1% and 92.9%, respectively, while leaching efficiency for Li remained pretty much stable at around 99%. Leaching efficiencies for Mn, Ni and Co, however, increased to 100%

after 0.68 M H_2O_2 was added. These results indicate that around 80% of the NMC (Mn, Ni and Co) was reduced by Fe^{2+} during the first 60 minutes and the rest was reduced by H_2O_2. The addition of H_2O_2 had only a minor effect on dissolution of Fe, P and Li, and the final leaching efficiencies for these metals were 93.4%, 93.8% and 100%, respectively.

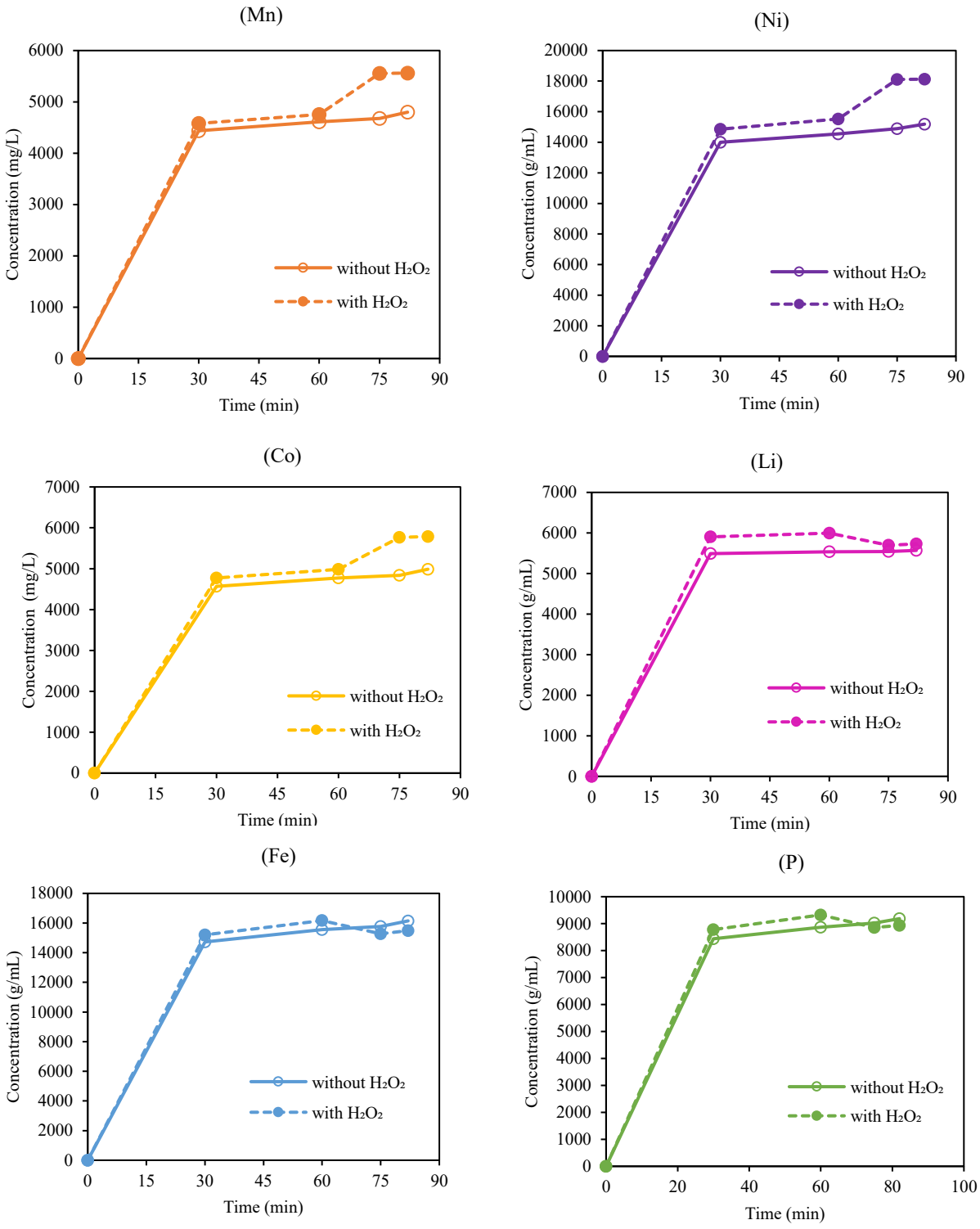

Figure 4.3. Concentrations of Mn, Ni, Co, Li, Fe and P (2 M H_2SO_4, S/L ratio 0.10 g/mL, NMC/LFP mass ratio 1 (NMC/LFP molar ratio 1.67), 75°C, 0 and 0.68 M H_2O_2) with H_2O_2 added at 60 minutes

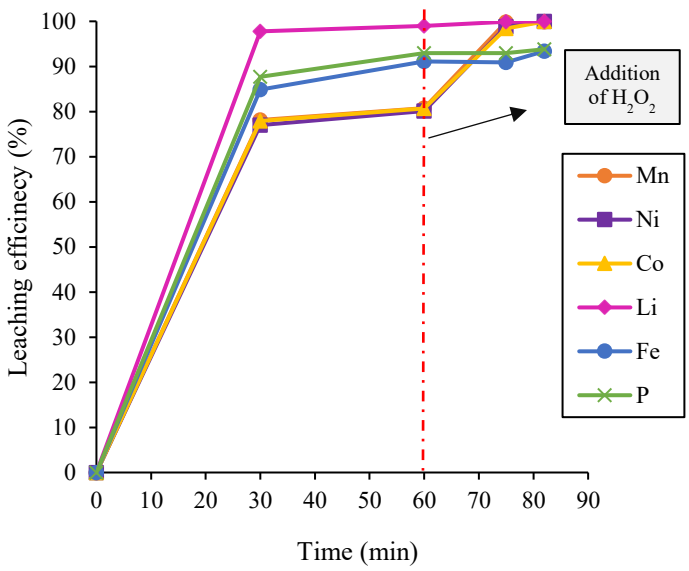

Figure 4.4. Leaching efficiencies for Mn, Ni, Co, Li, Fe and P (2 M H_2SO_4, S/L ratio 0.10 g/mL, NMC/LFP mass ratio 1 (NMC/LFP molar ratio 1.67), 75°C) with 0.68 M H_2O_2 added at 60 minutes

To further study the effect of H_2O_2 on leaching of a mixture of NMC and LFP, 0.68 M H_2O_2 was added at S/L ratios ranging from 0.05 g/mL to 0.20 g/mL. Figure 4.5 shows the effect of S/L ratio on leaching efficiencies for Mn, Ni, Co, Li, Fe and P under conditions of 2 M H_2SO_4, 0.68 M H_2O_2, 75°C and 82 minutes. As the figure shows leaching efficiencies decreased when S/L ratio increased, with highest efficiencies (100% recovery for all metals) recorded at S/L ratio 0.05 g/mL. These results are consistent with the statistical analysis of a one-way ANOVA ($p < 0.05$), followed by Tukey's Honestly Significant Difference (HSD) post-hoc test, presented in Appendix A. The statistical analysis indicates a significant effect of the S/L ratio on the leaching efficiencies of Mn, Ni, Co, Li, Fe, and P. Tukey's HSD test further revealed that an S/L ratio of 0.20 g/mL resulted in significantly lower leaching efficiencies compared with the other S/L ratios.

Comparison of figures 4.1 and 4.5 shows that addition of 0.68 M increased leaching efficiencies for Mn, Ni and Co at all S/L ratios, demonstrating the effectiveness of H_2O_2 in reducing metals from higher to lower oxidation states. With the addition of H_2O_2 leaching efficiency for Mn increased from 85.9%, 85.8%, 79.8% and 73.6% to 100%, 100%, 99.2% and 77.7% at S/L ratios of 0.05 g/mL, 0.10 g/mL, 0.15 g/mL and 0.20 g/mL, respectively. For Ni, leaching efficiency rose from 86.3%, 85.8%, 81.3% and 74.4% to 100%, 100%, 99.5% and 78.6% at the same respective S/L ratios. For Co, efficiency increased from 86.4%, 86.7%, 81.1% and 74.3% to 100%, 100%, 99.6% and 96.1%, respectively. For Li, addition of 0.68 M H_2O_2 had a minor

effect, with leaching efficiency increasing slightly, from 99.6%, 98.8%, 98% and 96% to 100%, 100%, 99.6% and 96.1% at the respective S/L ratios. The addition of 0.68 M H_2O_2 had a different effect on leaching efficiencies for Fe and P at the different S/L ratios, however. It was negligible at S/L ratios of 0.05 g/mL and 0.10 g/mL but at S/L ratios of 0.15 g/mL and 0.20 g/mL, it caused leaching efficiencies for Fe to decrease from 74.1% and 55.6% to 34.6% and 21.7%, respectively, and for P to decrease from 75.5% and 57.4% to 37.9% and 22.1%, respectively.

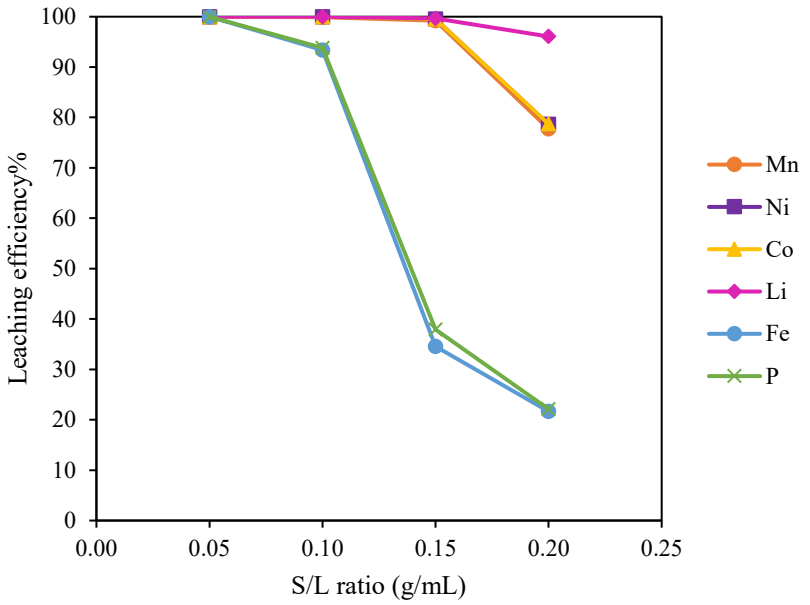

Figure 4.5. Effect of S/L ratio on leaching efficiencies for Mn, Ni, Co, Li, Fe and P (2 M H_2SO_4, 0.68 M H_2O_2, NMC/LFP mass ratio 1 (NMC/LFP molar ratio 1.67), 75°C, 82 minutes) with H_2O_2 added at 60 minutes

Table 4.3 shows metal content (mmol/g) of the solid residues obtained at different S/L ratios under the specified conditions. Figure 4.6 shows XRD results for S/L ratios ranging from 0.10 to 0.20 g/mL. The XRD pattern of the solid residue at S/L ratio 0.10 is compatible with $FePO_4$ with the orthorhombic space group Pnma (62) and lattice parameters a = 9.814 Å, b = 5.789 Å and c = 4.782 Å. All of the NMC was dissolved by adding H_2O_2, and only $FePO_4$ remained in the leach residue. The XRD patterns of the leach residues obtained at S/L ratios 0.15 g/mL and 0.20 g/mL, on the other hand, show distinct peaks corresponding to $FePO_4$ and $LiNi_{0.6}Mn_{0.2}Co_{0.2}O_2$. This suggests that when the S/L ratio was 0.20 g/mL, the leaching efficiency of both NMC and LFP decreased, with a selectivity ratio between LFP and NMC

(S_{LFP}/S_{NMC}) of 0.27. This reduction in efficiency led to the presence of unreacted NMC along with $FePO_4$ in the leach residue.

Table 4.3. Effect of S/L ratio on metal content (mmol/g) in leach residue (S/L ratios ranging from 0.10 to 0.20 g/mL, 2 M H_2SO_4, 0.68 M H_2O_2, NMC/LFP mass ratio 1 (NMC/LFP molar ratio 1.67), 75°C, 82 minutes)

S/L (g/mL)	Metal content (mmol/g)					
	Mn	Ni	Co	Li	Fe	P
0.10	0.02	0.03	0.01	0.00	4.63	4.42
0.15	0.02	0.04	0.01	0.08	5.76	5.56
0.20	0.45	1.29	0.41	0.61	4.60	4.65

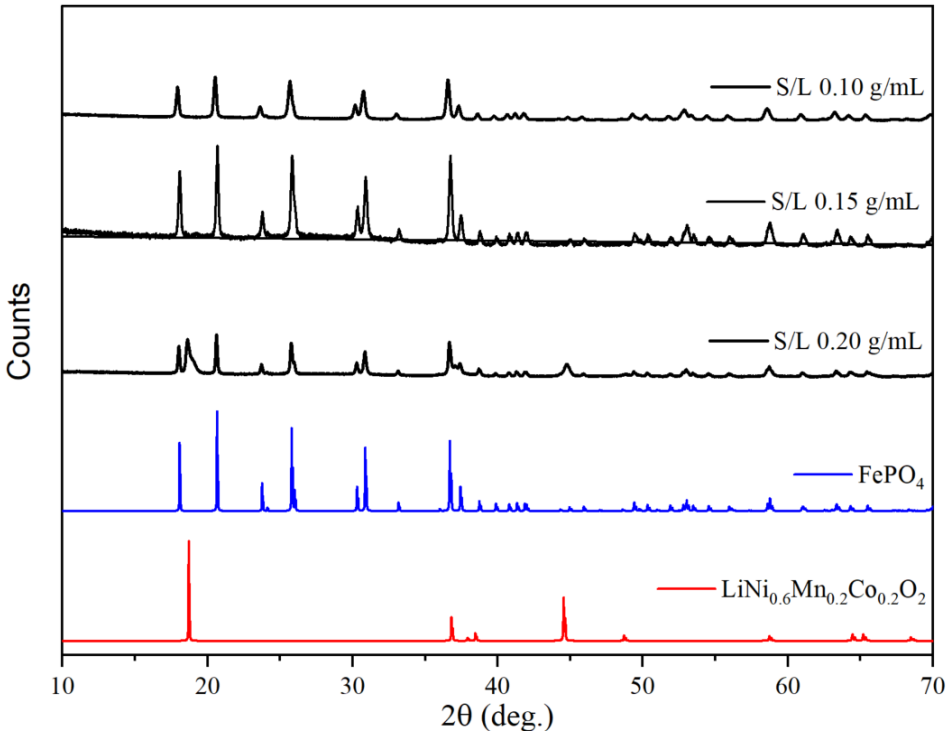

Figure 4.6. XRD patterns of leach residues with S/L ratios ranging from 0.10 to 0.20 g/mL (2 M H_2SO_4, 0.68 M H_2O_2, NMC/LFP mass ratio 1 (NMC/LFP molar ratio 1.67), 75°C, 82 minutes) and patterns of $FePO_4$ (COD ID: 1525576) and $LiNi_{0.6}Mn_{0.2}Co_{0.2}O_2$ (COD ID 4002443)

4.3.3. Effect of NMC/LFP molar ratio on metal leaching efficiency

To study the effect of the molar ratio of NMC to LFP, leaching assays were performed at NMC/LFP molar ratios ranging from 0.5 to 4 under conditions of 2 M H_2SO_4, 0.68 M H_2O_2, S/L ratio 0.15 g/mL, 75°C, stirring speed 330 rpm. Based on the results of previous assays and the observation that metal dissolution showed little variation between 30 and 60 minutes, the leaching reaction with H_2SO_4 was shortened to 30 minutes. Subsequently, H_2O_2 was added to the NMC and LFP solution after 30 minutes, and the solution was filtered 21 minutes later. Table 4.4 shows the details of the experimental design.

Table 4.4. Experimental design for studying the effect of NMC/LFP molar ratio on metal leaching efficiency in mixed NMC and LFP materials

Test	NMC Mass (g)	LFP/C Mass (g)	NMC/LFP molar ratio	H_2SO_4 concentration (M)	H_2O_2 concentration (M)	Solid-liquid ratio (g/mL)	Temperature (°C)	Time (min)
1	7.58	24.67	0.51	2	0.68	0.15	75	51
2	12.27	19.98	1.02	2	0.68	0.15	75	51
3	14.47	17.78	1.36	2	0.68	0.15	75	51
4	16.12	16.12	1.67	2	0.68	0.15	75	51
5	17.78	14.47	2.05	2	0.68	0.15	75	51
6	20.90	11.34	3.07	2	0.68	0.15	75	51
7	22.92	9.33	4.10	2	0.68	0.15	75	51

The effect of NMC/LFP molar ratio on leaching efficiencies for Mn, Ni, Co, Li, Fe and P as a function of time is shown in Figure 4.7. As the figure shows, leaching efficiency for Mn increased rapidly in the first 5 minutes and then remained nearly constant until 30 minutes for all tested NMC/LFP molar ratios. However, leaching efficiencies for Mn decreased as NMC/LFP molar ratio increased from 0.51 to 4.10. The addition of H_2O_2 significantly enhanced Mn dissolution, and a leaching efficiency above 97% was obtained at an NMC/LFP molar ratio of 4.10.

Leaching efficiencies for Mn, Ni and Co showed similar trends as a function of NMC/LFP molar ratio and time. Leaching efficiencies for Ni and Co increased rapidly in the first 5 minutes and then remained nearly constant until 30 minutes at all NMC/LFP molar ratios. The addition of H_2O_2 significantly increased leaching efficiencies for both Ni and Co, as observed for Mn. A leaching efficiency above 97% was obtained for both Ni and Co at an NMC/LFP molar ratio of 4.10.

The results show that Li leaching efficiency behaviour differs from that recorded for Mn, Ni and Co. Li leaching efficiency increased rapidly in the first 5 minutes and then remained nearly constant until 30 minutes, as was the case with Mn, Ni and Co. However, Li leaching rate was faster than that of the transition metals. The addition of H_2O_2 improved leaching efficiency for Li, which reached more than 99% at all NMC/LFP molar ratio.

The results show the same trend for dissolution of Fe and P over time. Both metals showed a rapid increase in the first 5 minutes, with dissolution then remaining constant until 30 minutes for all NMC/LFP molar ratios except 0.51. The effect of adding H_2O_2, however, differed depending on the NMC/LFP molar ratio. At molar ratios of 0.51, 1.02 and 1.36, the addition of H_2O_2 had a negligible effect on leaching efficiencies for Fe and P, but at NMC/LFP molar ratios above 1.36, it caused them to decrease. Final leaching efficiencies for both Fe and P were lower at higher NMC/LFP molar ratios, reaching lows of 1.4% for Fe and 5.7% for P at an NMC/LFP molar ratio of 4.10.

Figures 4.8 and 4.9 summarize the effect of NMC/LFP molar ratio on leaching efficiencies for Mn, Ni, Co, Li, Fe and P at 30 minutes and at 51 minutes under conditions of 2 M H_2SO_4, S/L ratio 0.15 g/mL and 75°C, with 0.68 M H_2O_2 added at 30 minutes. As these figures show, leaching efficiencies for Mn, Ni and Co decrease sharply as NMC/LFP molar ratio increases, reaching lows of 46.5%, 51.7% and 49.4%, respectively, at molar ratio 4.10 after 30 minutes, but increase across all molar ratios when H_2O_2 is added. For Li, on the other hand, the decrease in leaching efficiency as NMC/LFP molar ratio increases is relatively slight at 30 minutes but extraction improves with the addition of H_2O_2, and is nearly complete across all molar ratios at the end of 51 minutes. Fe and P dissolution, however, show a different trend. Leaching efficiencies at 30 minutes for Fe and P decrease sharply as NMC/LFP molar ratio increases from 0.51 to 1.02, remain nearly constant to molar ratio 1.67 and then increase to molar ratio 4.10. With the addition of H_2O_2, however, leaching efficiencies for Fe and P at 51 minutes decrease at NMC/LFP molar ratios above 1.67.

Table 4.5 shows the metal content (mmol/g) of leach residues obtained at NMC/LFP molar ratios ranging from 0.5 to 4.1. As Figure 4.7 shows, leaching efficiency did not vary as a function of time at molar ratios 1.02 and 1.36, and hence Fe and P did not precipitate when H_2O_2 was added. For this reason the solid residues from these two assays were selected for further crystallographic, morphological, and elemental distribution characterization. Figure 4.10 shows XRD results for these two assays, confirming that the XRD patterns of both leach residues corresponded to orthorhombic $FePO_4$ with space group Pnma (62) and lattice parameters a = 9.814 Å, b = 5.789 Å and c = 4.782 Å.

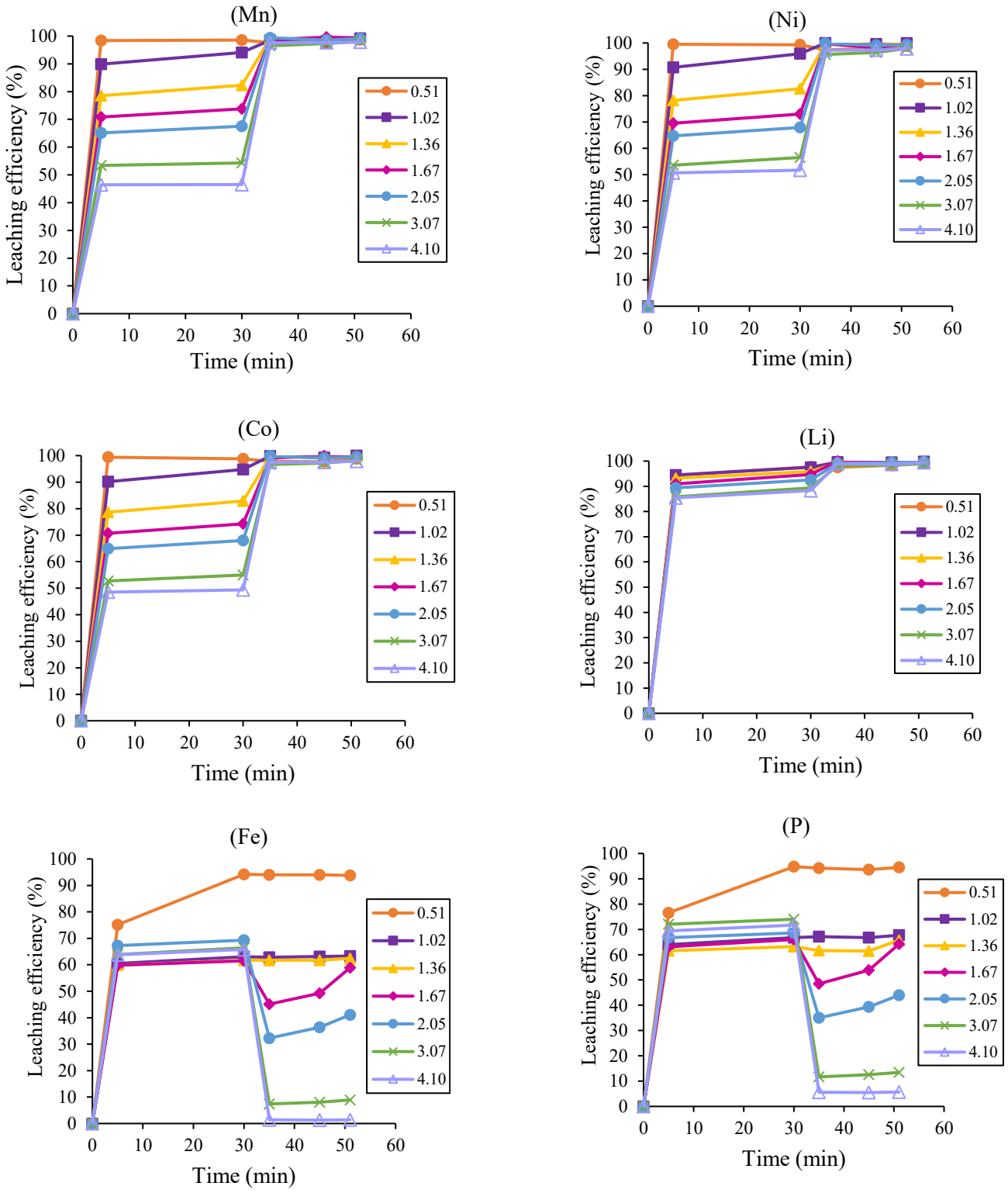

Figure 4.7. Leaching efficiencies as a function of time for Mn, Ni, Co, Li, Fe and P at NMC/LFP molar ratios ranging from 0.5 to 4.1 (2 M H_2SO_4, 0.68 M H_2O_2, S/L ratio 0.15 g/mL, 75°C, H_2O_2 added at 30 minutes)

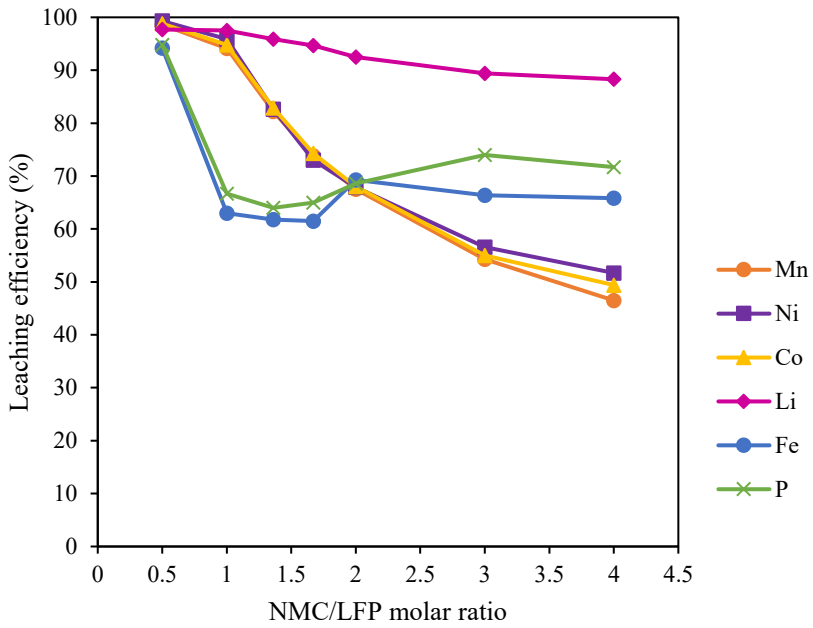

Figure 4.8. Effect of NMC/LFP molar ratio on leaching efficiencies for Mn, Ni, Co, Li, Fe and P (2 M H_2SO_4 75°C, 30 minutes)

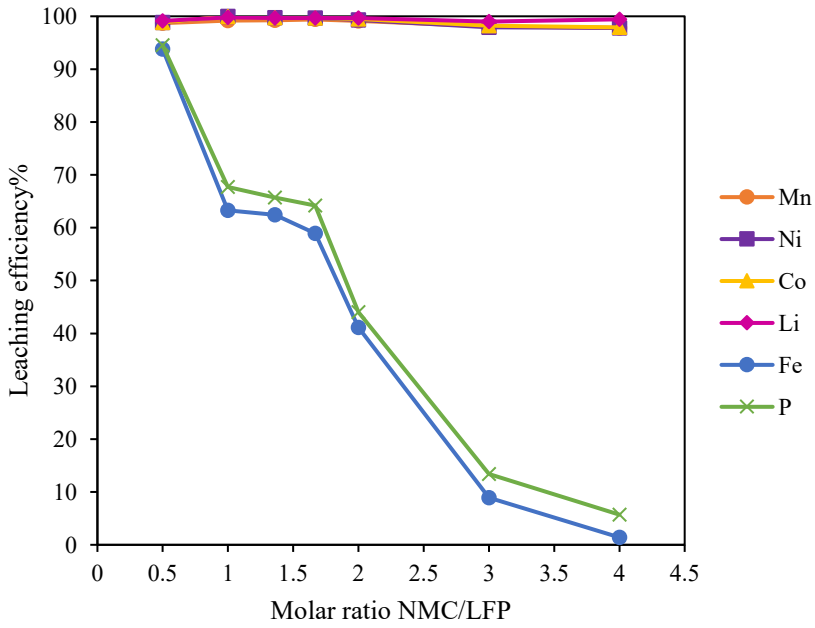

Figure 4.9. Effect of NMC/LFP molar ratio on leaching efficiencies for Mn, Ni, Co, Li, Fe and P (2 M H_2SO_4, 0.68 M H_2O_2, 75°C, 51 minutes)

Table 4.5. Effect of NMC/LFP molar ratio on metal content (mmol/g) in leach residue (NMC/LFP molar ratios ranging from 0.5 to 4.1, 2 M H_2SO_4, 0.68 M H_2O_2, S/L ratio 0.15 g/mL, 75°C, 51 minutes)

Molar ratio	Metal content (mmol/g)					
	Mn	Ni	Co	Li	Fe	P
0.51	0.08	0.22	0.07	0.81	3.71	3.33
1.02	0.03	0.00	0.00	0.07	6.58	5.89
1.36	0.04	0.04	0.01	0.13	6.34	5.89
1.67	0.03	0.04	0.01	0.12	6.63	5.88
2.05	0.04	0.08	0.02	0.08	5.86	5.54
3.07	0.08	0.25	0.07	0.25	5.86	5.30
4.10	0.10	0.33	0.10	0.17	5.87	5.12

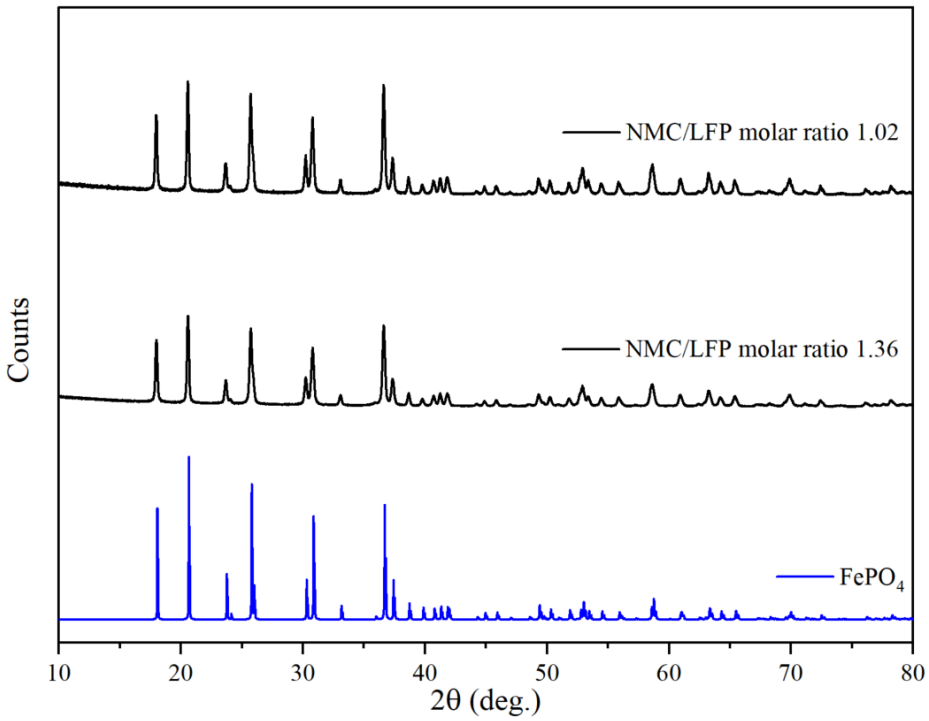

Figure 4.10. XRD patterns of leach residues at NMC/LFP molar ratios 1.02 and 1.36 (2 M H_2SO_4, 0.68 M H_2O_2, 75°C, 51 minutes) and pattern of $FePO_4$ (COD ID: 1525576)

Figure 4.11 shows SEM images of the leach residue obtained at NMC/LFP molar ratio 1.02 under the specified conditions. EDS mapping, as shown in Figure 4.12 and Table 4.6, reveals its chemical composition (in atomic percentages). EDS analysis indicated that no NMC was detected, that the leach residue consisted only of Fe, P, O and C from the carbon-coated LFP, along with Cu from the SEM grid.

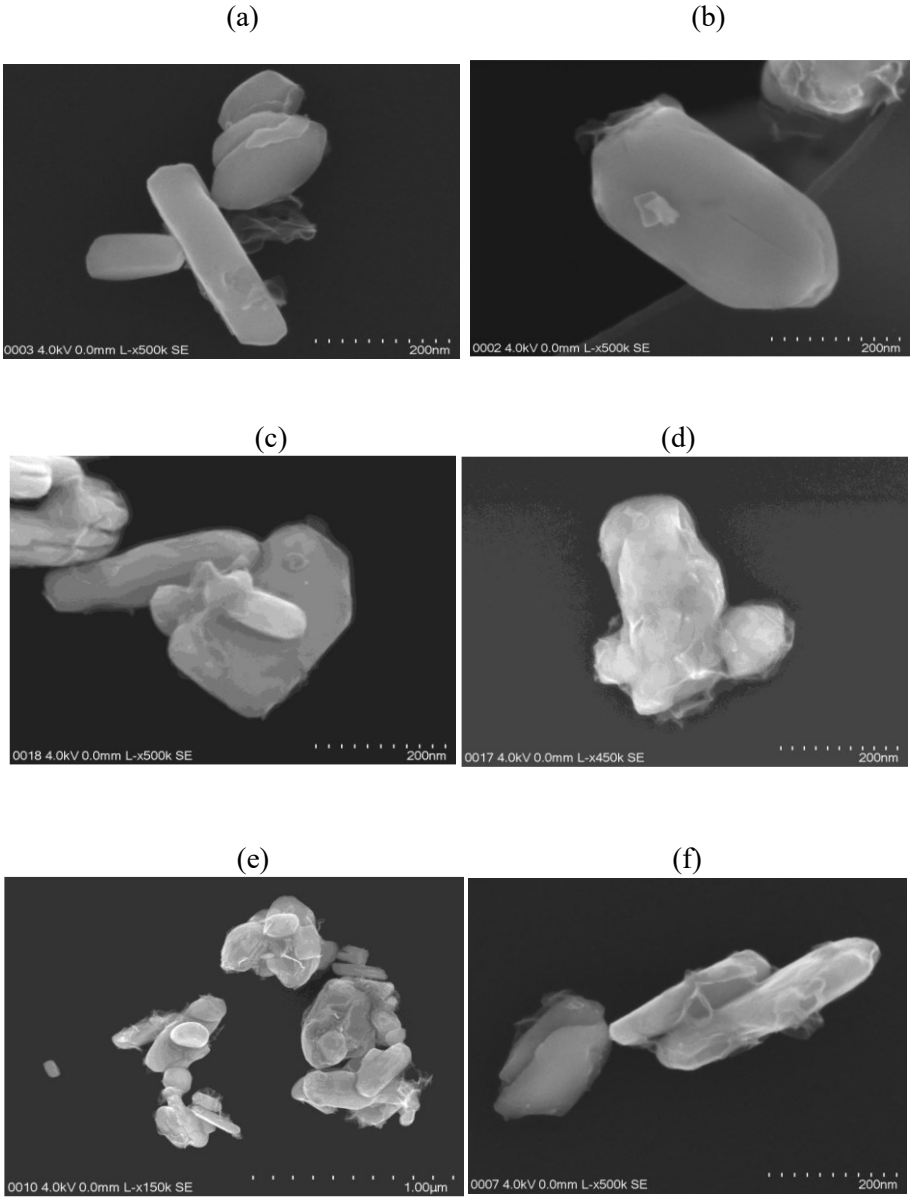

Figure 4.11. SEM images of leach residue (a-f) obtained under conditions of NMC/LFP molar ratio 1.02, 2 M H_2SO_4, 0.68 M H_2O_2, S/L ratio 0.15 g/mL, 75°C and 51 minutes

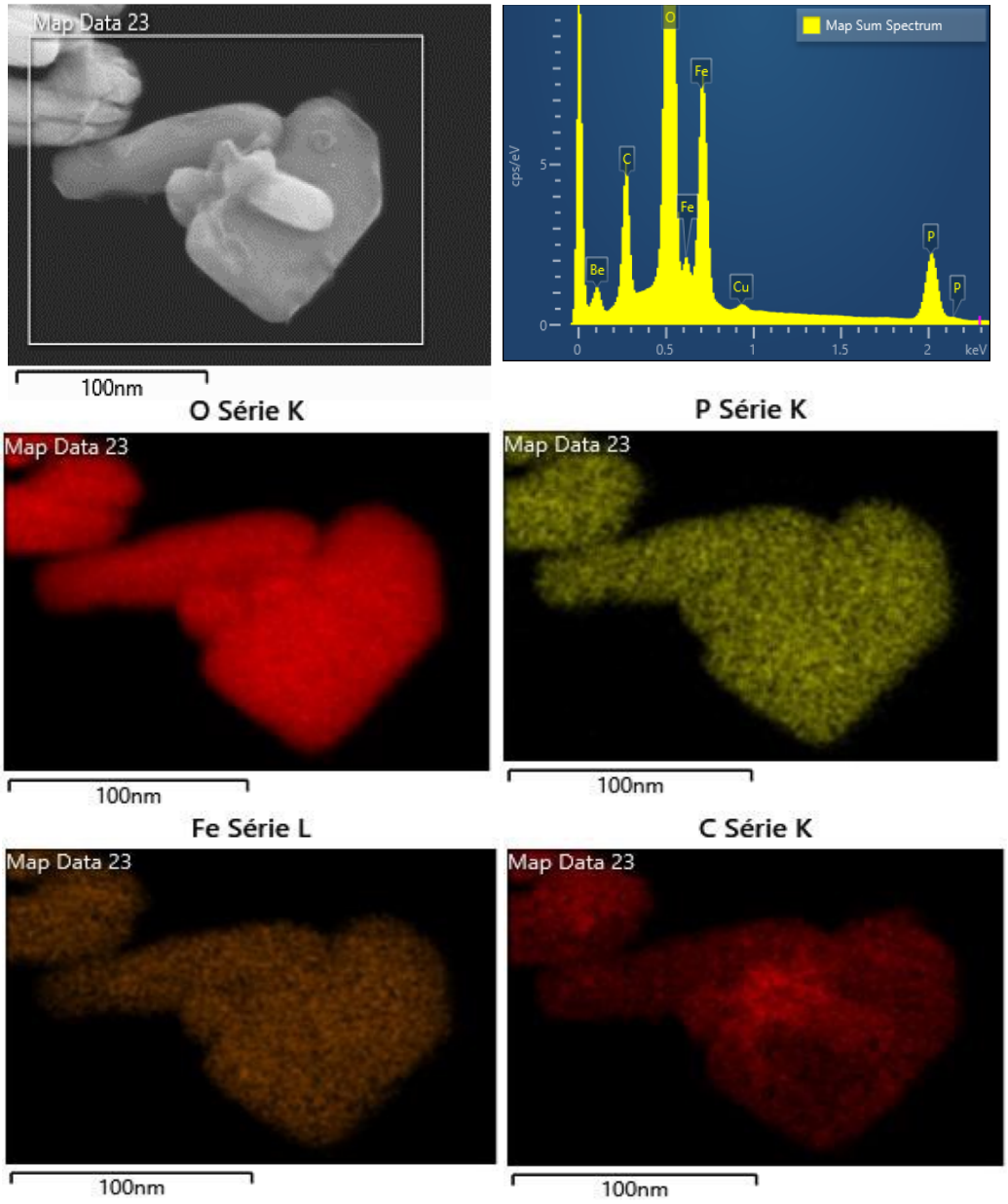

Figure 4.12. SEM (4.11.c) and EDS mapping images of leach residue obtained under conditions of NMC/LFP molar ratio 1.02, 2 M H_2SO_4, 0.68 M H_2O_2, S/L ratio 0.15 g/mL, 75°C and 51 minutes

Table 4.6. Elemental content determined by EDS analysis at 4 kV that corresponds to the SEM image (Figure 4.12) (NMC/LFP molar ratio 1.02, 2 M H_2SO_4, 0.68 M H_2O_2, S/L ratio 0.15 g/mL, 75°C, 51 min)

NMC/LFP molar ratio	O (at.%)	P (at.%)	Fe (at.%)	Cu (at.%)
1.02	48.94	12.5	18.94	0.28

Figure 4.13 shows SEM images of the leach residue obtained at NMC/LFP molar ratio 1.36 under conditions of 2 M H_2SO_4, 0.68 M H_2O_2, S/L ratio 0.15 g/mL, 75°C and 51 minutes. Its chemical composition (in atomic percentages) was determined by EDS mapping as shown in Figure 4.14 and Table 4.7. The leach residue contained only Fe, P, O and C from the carbon-coated LFP, along with Cu from the SEM grid.

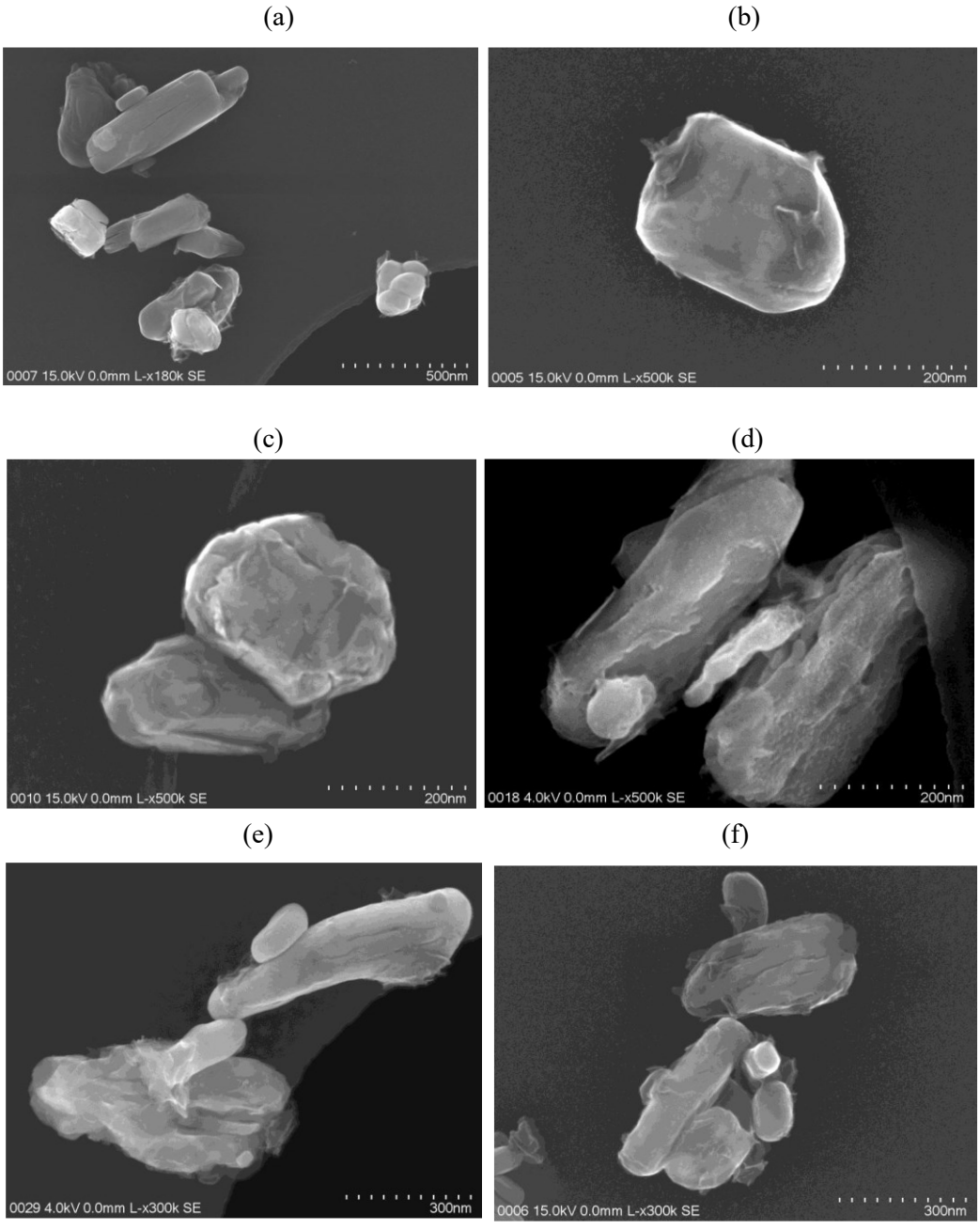

Figure 4.13. SEM image of leach residue (a-f) obtained under conditions of NMC/LFP molar ratio 1.36, 2 M H_2SO_4, 0.68 M H_2O_2, S/L ratio 0.15 g/mL, 75°C and 51 minutes

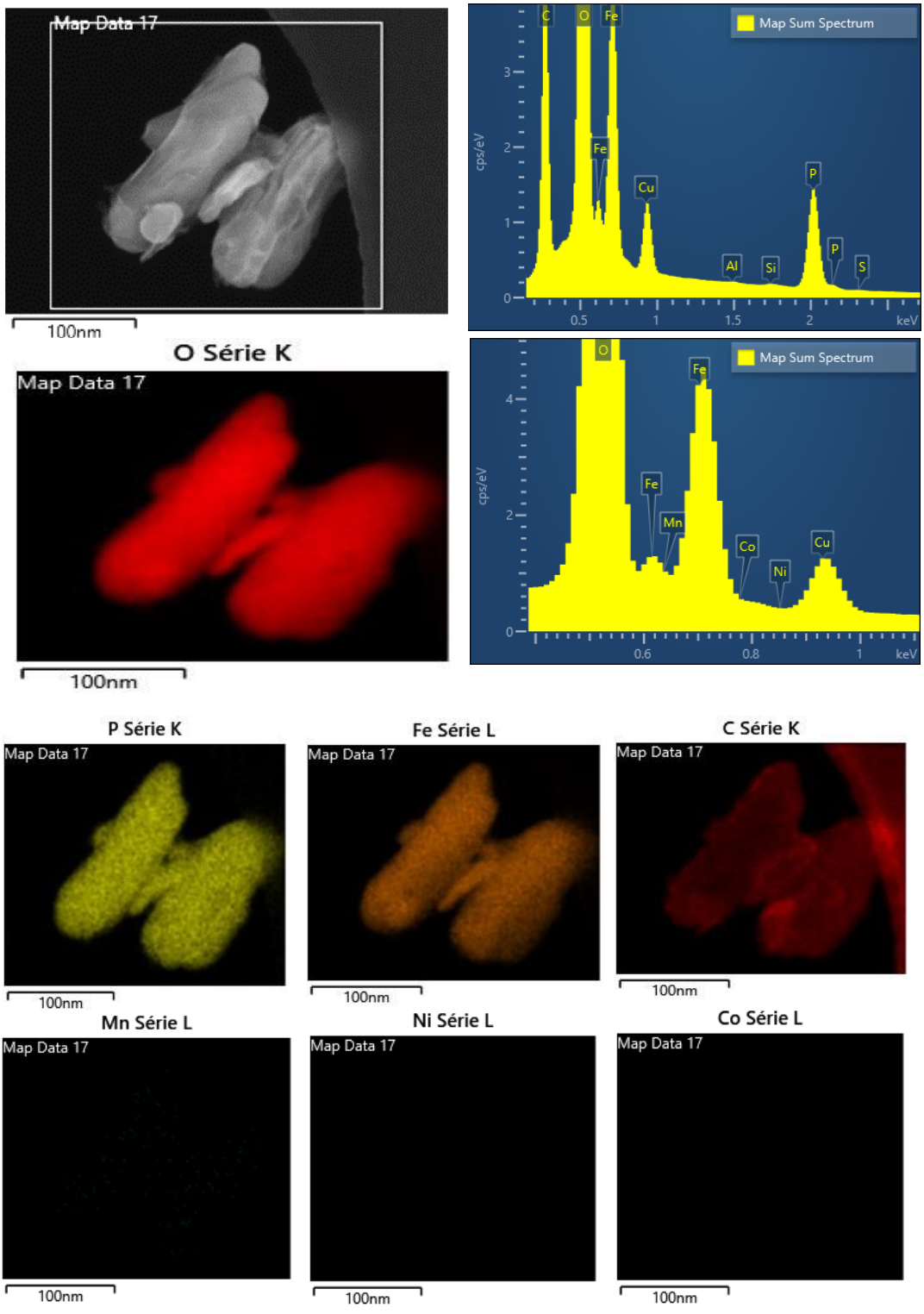

Figure 4.14. SEM image (4.13.d) and EDS mapping images of leach residue obtained under conditions of NMC/FLP molar ratio 1.36, 2 M H_2SO_4, H_2O_2 0.68 M, S/L ratio 0.15 g/mL, 75°C and 51 minutes

Table 4.7. Elemental content determined by EDS analysis at 4 kV that corresponds to the SEM image (Figure 4.14) (NMC/FLP molar ratio 1.36, 2 M H_2SO_4, 0.68 M H_2O_2, S/L ratio 0.15 g/mL, 75°C, 51 minutes)

NMC/LFP molar ratio	O (at.%)	P (at.%)	Fe (at.%)	Cu (at.%)	S (at.%)
1.36	30.58	6.87	9.79	3.87	0.18

4.3.4. Effect of sulphuric acid concentration on metal leaching efficiency

To study the effect of sulphuric acid concentration on metal leaching efficiency, the leaching assays were performed at three concentrations of H_2SO_4 (0.25, 0.5 and 2M) and the following best operating conditions: 0.68 M H_2O_2, S/L 0.15 g/mL, NMC/LFP molar ratio 1.36, 75°C, 51 minutes, stirring speed 330 rpm. H_2O_2 added at 30 minutes. Table 4.8 shows the details of the experimental design.

Table 4.8. Experimental design for studying the effect of H_2SO_4 concentration on metal leaching efficiency from mixed NMC and LFP materials

Test	Moles of NMC	Moles of LFP/C	NMC/LFP molar ratio	H_2SO_4 concentration (M)	H_2O_2 concentration (M)	Solid-liquid ratio (g/mL)	Temperature (°C)	Time (min)
1	0.149	0.110	1.36	0.25	0.68	0.15	75	51
2	0.149	0.110	1.36	0.5	0.68	0.15	75	51
3	0.149	0.110	1.36	2	0.68	0.15	75	51

Figure 4.15 shows the effect of H_2SO_4 concentration on leaching efficiencies for Mn, Ni, Co, Li, Fe and P under conditions of S/L ratio 0.15 g/mL, NMC/LFP molar ratio 1.36, 75°C and 51 minutes. Increasing H_2SO_4 concentration from 0.25 M to 0.5 M slightly improved leaching efficiencies for Mn, Ni, Co and Li, upping them from 9.2%, 8.5%, 8.6% and 36.4% to 15.7%, 22.0%, 18.2% and 52.8%, respectively. Increasing H_2SO_4 concentration to 2 M, however, significantly increased leaching efficiencies for Mn, Ni, Co and Li, upping them to 99.3%, 99.7%, 99.8% and 99.7%, respectively. Though leaching efficiencies for Fe and P were low at H_2SO_4 concentrations of 0.25 M and 0.5 M (around 8% for Fe and 13% for P), they

reached 62.4% and 65.7% at 2 M H_2SO_4. Table 4.9 shows metal content (mmol/g) of the leach residues obtained at H_2SO_4 concentrations of 0.25 M, 0.50 M and 2 M.

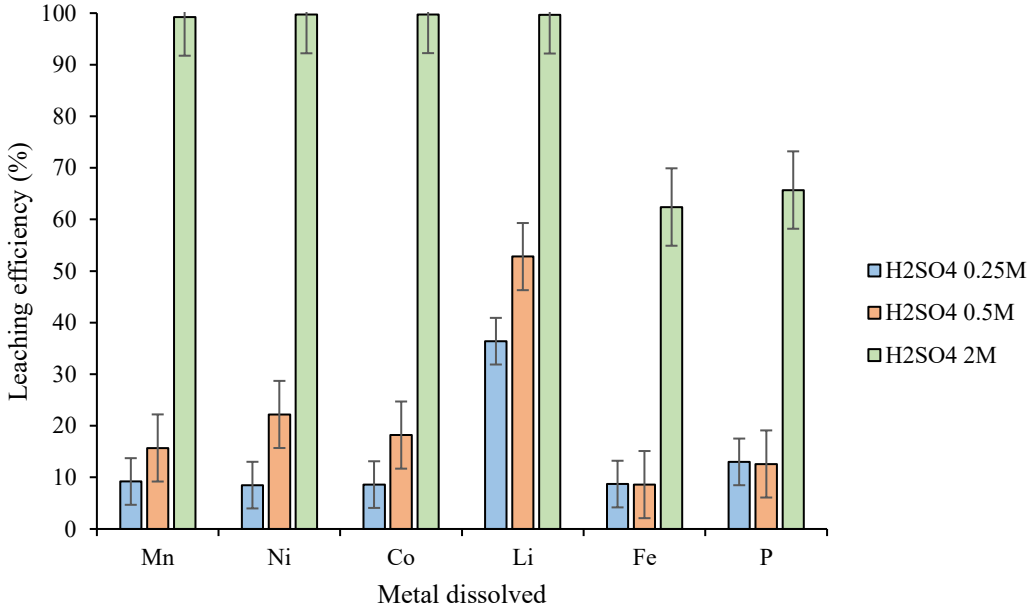

Figure 4.15. Effect of H_2SO_4 concentration on leaching efficiencies for Mn, Ni, Co, Li, Fe and P with 0.25 M, 0.50 M and 2 M H_2SO_4 (0.68 M H_2O_2, S/L ratio 0.15 g/mL, NMC/LFP molar ratio 1.36, 75°C, 51 minutes, H_2O_2 added at 30 minutes)

Table 4.9. Effect of H_2SO_4 concentration on metal content (mmol/g) in leach residue with 0.25 M, 0.50 M and 2 M H_2SO_4 (0.68 M H_2O_2, S/L ratio 0.15 g/mL, NMC/LFP molar ratio 1.36, 75°C, 51 minutes, H_2O_2 added at 30 minutes)

H_2SO_4 (M)	**Metal content(mmol/g)**					
	Mn	**Ni**	**Co**	**Li**	**Fe**	**P**
0.25	0.95	2.87	0.92	5.58	3.43	3.31
0.5	0.93	2.57	0.87	4.36	3.61	3.51
2	0.04	0.04	0.01	0.13	6.34	5.89

Figure 4.16 presents the XRD results for the three assays, confirming that NMC did not leach completely at the lower H_2SO_4 concentrations of 0.25 M and 0.5 M. The figure also shows that the XRD pattern of the leach residue obtained with 2 M H_2SO_4 corresponds to orthorhombic $FePO_4$ with a space group of Pnma (62) and lattice parameters a = 9.814 Å, b = 5.789 Å, and c = 4.782 Å.

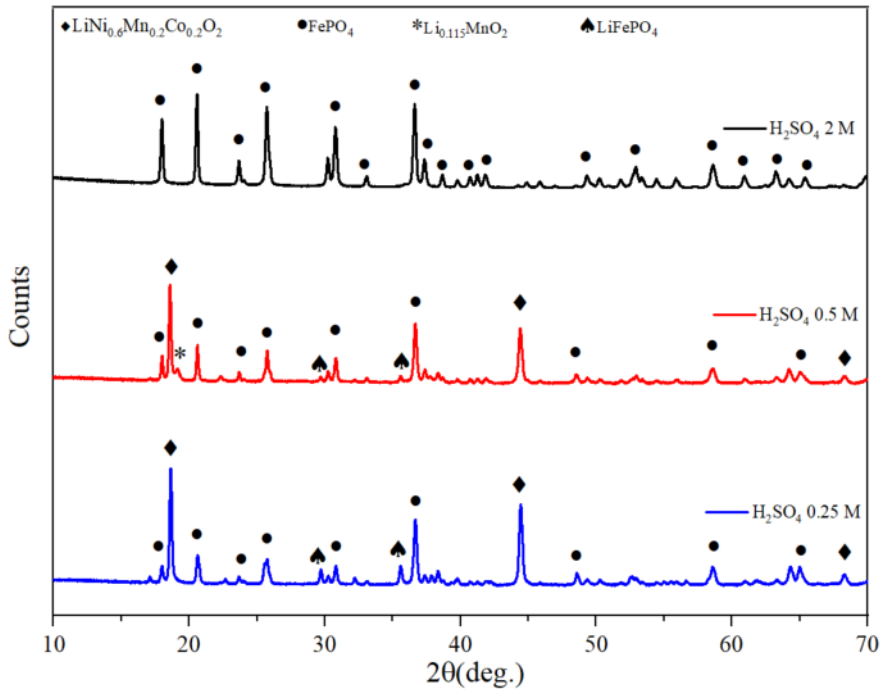

Figure 4.16. XRD patterns of leach residues with 0.25, 0.5 and 2 M H_2SO_4 (S/L ratio 0.15 g/mL, NMC/LFP molar ratio 1.36, 75°C, 82 minutes) and of phases $LiNi_{0.6}Mn_{0.2}Co_{0.2}O_2$ (COD ID: 4002443), $FePO_4$ (COD ID: 1525576), $Li_{0.115}MnO_2$ (COD ID: 8103495) and $LiFePO_4$ (COD ID: 1101111)

4.3.5. Effect of H_2O_2 concentration on metal leaching efficiency

To further investigate the impact of H_2O_2 concentration on metal dissolution with mixed NMC and LFP materials, two different concentrations of H_2O_2 (0.10 M and 0.68 M) were studied. H_2O_2 was added at 60 minutes of leaching under conditions of 2 M H_2SO_4, 75°C, stirring speed 330 rpm, S/L ratio 0.15 g/mL and NMC/LFP molar ratio 1.36. Table 4.10 shows the details of the experimental design.

Table 4.10. Experimental design for studying the effect of H_2O_2 concentration on metal leaching efficiency from mixed NMC and LFP materials

Test	Moles of NMC (g)	Moles of LFP/C (g)	NMC/LFP molar ratio	H_2SO_4 concentration (M)	H_2O_2 concentration (M)	Solid-liquid ratio (g/mL)	Temperature (°C)	Time (min)
1	0.149	0.110	1.36	2	0.10	0.15	75	51
2	0.149	0.110	1.36	2	0.68	0.15	75	51

Figure 4.17 shows metal leaching efficiencies at these two H_2O_2 concentrations. Results indicate that increasing H_2O_2 concentration from 0.10 M to 0.68 M slightly increased leaching efficiencies for Mn, Ni and Co, from 96.6%, 97.3% and 97.4% to 99.3%, 99.7% and 99.8%, respectively. However, the increase in H_2O_2 concentration had a negligible effect on dissolution of Li, leaching efficiencies for Fe and P decreased from 64.8% and 68.7% to 62.4% and 65.7%, respectively.

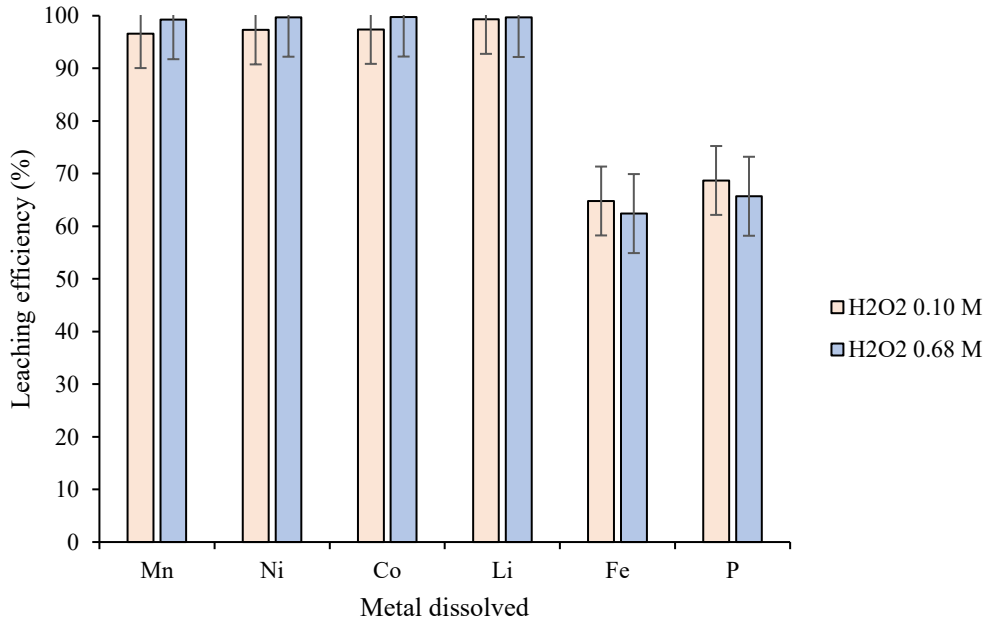

Figure 4.17. Effect of H_2O_2 concentration on leaching efficiencies for Mn, Ni, Co, Li, Fe and P with 0.10 M and 0.68 M H_2O_2 (2 M H_2SO_4, S/L ratio 0.15 g/mL, NMC/LFP molar ratio 1.36, 75°C, 51 minutes, H_2O_2 added at 30 minutes)

4.4. Discussion

- Reaction mechanism

To understand how NMC and LFP interact, the leaching assays with individual NMC and LFP materials discussed in Chapter 3 were compared with the mixed material assays discussed in this chapter. Leaching conditions selected for the comparison, as shown in Figure 4.18, are 2 M H_2SO_4, S/L 0.10 g/mL, 75°C and 82 minutes. In the first scenario (NMC leached with sulphuric acid, described in section 3.3.2), Mn did not leach effectively, while leaching efficiencies for Ni, Co and Li were 46.7%, 43.0% and 97.8% respectively. The incomplete leaching of Mn, Ni and Co can be attributed to the strong chemical bond between these metals and oxygen, requiring use of a reducing agent to improve leaching efficiencies. In the second scenario, discussed in section 3.3.3, LFP leaching under the same conditions resulted in nearly 100% extraction of Fe, P and Li, due to destruction of the LFP structure and release of Fe^{2+} into the solution. In the third scenario, a mixture of NMC and LFP (50% NMC and 50% LFP, NMC/LFP mass ratio 1) was leached with sulphuric acid under the same conditions, yielding leaching efficiencies for the NMC components (Mn, Ni and Co) higher than when the NMC was leached separately. This can be attributed to electron transfer and synergistic redox reactions between NMC and LFP in the sulphuric acid system. The overall reaction between LFP and NMC in the presence of sulphuric acid can be expressed as Equation 4.1 [83].

$$10\ LiFe(II)PO_4 + 10\ LiNi_{0.6}Mn_{0.2}\ Co_{0.2}O_2 + 20\ H_2SO_4 = 10\ Li_2SO_4 + 6Ni(II)SO_4 + 2Mn(II)SO_4 + 2Co(II)SO_4 + 10\ Fe(III)PO_4 + 20\ H_2O \quad (4.1)$$

In this reaction, 1 mole of LFP is leached with sulphuric acid, releasing 1 mole of Fe^{2+} into the solution. The Fe^{2+} then reduces 1 mole of NMC (Ni^{3+}, Mn^{4+} and Co^{3+}) to the soluble divalent ions Ni^{2+}, $Mn^{2+}$and Co^{2+}, while Fe^{2+} is oxidized to Fe^{3+}. This reaction increased the dissolution of Mn, Ni and Co from the NMC particles. Several studies in the literature report similar synergistic reactions between NMC and Fe^{2+}, using different leaching agents or parameters however. For example, Yunhui et al. [89] studied leaching of a mixture of LFP and NMC using 0.3 M $NH_4Fe(SO_4)_2$, under conditions of S/L ratio 0.05 g/mL, 50 °C and LFP/NMC622 ratio 1.8 g/g and obtained leaching efficiencies of 98.3% for Mn, 99% for Ni and 98.9% for Co. Similarly, Zou et al. [85] investigated the synergistic redox reaction between NMC and LFP in diluted sulphuric acid and obtained over 99% solubilization of transition metals and 90% leaching of Fe and P under conditions of 0.5 M H_2SO_4, S/L ratio 0.05 g/mL, NMC/LFP molar ratio 0.8 and leaching time 40 minutes at 25°C.

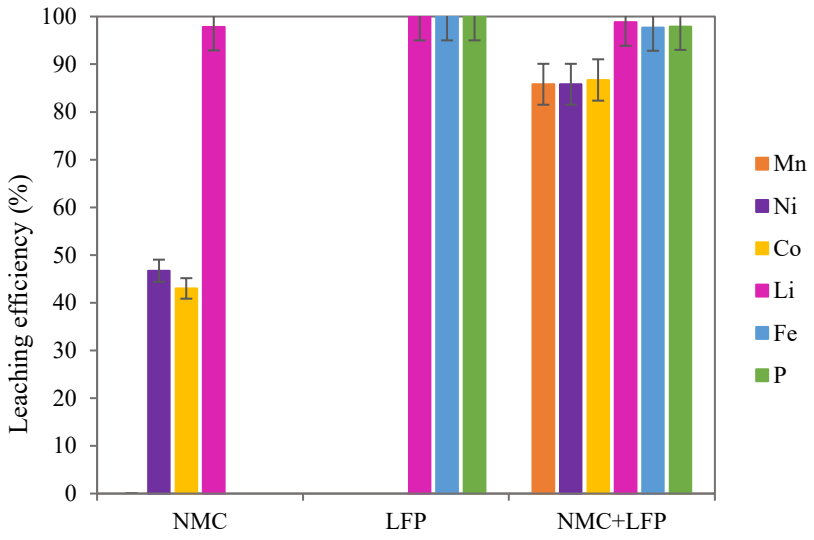

Figure 4.18. Comparison of leaching of separate and mixed NMC and LFP materials (NMC/LFP mass ratio 1) (2 M H_2SO_4, S/L: 0.10 g/mL, 75°C, 82 minutes)

- Effect of S/L ratio on metal leaching efficiency

Results show that leaching efficiencies for Mn, Ni, Co, Li, Fe and P decreased as S/L ratio increased from 0.05 to 0.20 g/mL under the standard conditions mentioned in the experimental section. Li demonstrated the highest leaching efficiency across all S/L ratios because its bonding energy is lower than that of the other metals in the LFP and NMC structures, making it more prone to dissolution in acidic conditions, even at higher S/L ratios [56]. However, Fe and P showed a sharper decline in leaching efficiency compared to the other transition metals as the S/L ratio increased. As discussed in Chapter 3, this decline was due to the increased acid consumption and a subsequent rise in the solution's pH. At higher S/L ratios, as a result, the reduced leaching efficiencies for Fe and P led to increased precipitation of orthorhombic $FePO_4$, as confirmed by the metal composition of the leach residues and the XRD results (Table 4.2 and Figure 4.2). Unreacted NMC622 and $Li_{0.115}MnO_2$ were observed in all leach residues for S/L ratios ranging from 0.10 g/mL to 0.20 g/mL. This could be due to the incomplete dissolution of NMC, likely caused by an insufficient amount of acid or reducing agent. The highest leaching efficiencies were achieved at the lowest S/L ratio (0.05 g/mL). This trend aligns with the findings of Jiang et al. [82], who report a similar effect of S/L ratio on metal dissolution from a mixture of LCO and LFP. In their study, Co and Li leaching rates gradually declined, while leaching efficiencies for Fe and P sharply decreased as S/L ratio increased from 10 to 50 g/L under conditions of 0.5 M H_2SO_4 and 50°C. This sharp decline was due to the likely precipitation of $FePO_4$, which is consistent with the results in our study.

- Effect of H_2O_2 on metal leaching efficiency

As discussed in Chapter 3, H_2O_2 acts as a reducing agent for NMC and as an oxidizing agent for LFP. In mixture leaching of NMC and LFP at S/L ratio 0.10 g/mL, addition of 0.68 M significantly enhanced the dissolution of Mn, Ni and Co by reducing them to more soluble lower valence state soluble ions, with full dissolution achieved by the end of the assay. However, adding 0.68 M H_2O_2 had a negligible effect on the leaching of Li, Fe and P. In this assay, as discussed in the context of the interactions between NMC and LFP, the Fe^{2+} from the LFP is oxidized to Fe^{3+} (93% in solution and 7% in leach residue), which in turn reduced around 80% of the Mn, Ni and Co in the first 60 minutes. When the H_2O_2 was added, the remaining unreacted Mn, Ni and Co was further reduced and dissolved completely. However, the addition of H_2O_2 did not lead to significant acid consumption during the dissolution of Mn, Ni and Co, and the pH of the solution remained unchanged. As a result, the addition of H_2O_2 had no impact on Fe and P dissolution. The XRD results confirmed $FePO_4$ in the leach residue (Figure 4.6).

A similar trend was noted for all metals at the lowest S/L ratio (0.05 g/mL), where Fe and P were already dissolved. However, at higher S/L ratios of 0.15 and 0.20 g/mL, the addition of H_2O_2 increased leaching efficiencies for Mn, Ni and Co but decreased them for Fe and P. This decrease could be attributable to changing the pH of the solution and the ORP, promoting precipitation of $FePO_4$ as shown in Figure 4.6 (S/L ratios 0.15 and 0.20 g/mL). If the goal of black mass leaching is to recover as much metal as possible, an S/L ratio of 0.15 g/mL could be regarded as the optimum condition. This effect has been observed by other researchers. For example, Song et al. [84] report a decrease in Fe leaching efficiency from approximately 40% to 10% when S/L ratio increased from 0.125 g/mL to 0.5 g/mL due to precipitation of $FePO_4$ in mixed leaching of LFP and NMC materials under conditions of 1.4 M H_2SO_4, 5% vol H_2O_2, 60°C and 60 minutes. In another study, Tang et al. [83] selected H_2O_2 as reducing and oxidizing agent and obtained higher leaching efficiencies for Mn, Ni, Co and Li and lower leaching efficiencies for Fe and P from an NMC/LFP mixture than with other agents such as oxygen and fortified air. Leaching efficiencies obtained for Mn, Ni, Co and Li were 97.1%, 98.5%, 96.3%, 99.6% and 99.6%, respectively, under conditions of 1 M H_2SO_4, ratio of 30% H_2O_2 to raw material 0.308 g/g, 90°C and 5 hours.

- Effect of NMC/LFP molar ratio on metal leaching efficiency

Results show that LFP provides Fe^{2+}, which serves as a reducing agent and improves NMC leaching efficiency up to 30 minutes. Dissolution of Mn, Ni, Co and Li decreased, however, when NMC/LFP molar ratio increased from 0.51 to 4.10, because there are more NMC moles and less LFP available to reduce them at higher NMC/LFP molar ratios. With the addition of H_2O_2, however, overall leaching efficiency

improved and remained high, with nearly complete recovery across all molar ratios from 0.51 to 4.10. Although Mn, Ni and Co have different redox potentials, they eventually exhibit similar leaching characteristics and were simultaneously released into the solution in the presence of a reducing agent [89]. Fe and P showed different trends up to 30 minutes with NMC/LFP molar ratios. Highest leaching efficiencies for Fe and P were observed at NMC/LFP molar ratio 0.5, after which they decreased and then remained almost constant between molar ratios 1.02 and 4.10. When H_2O_2 was added, Fe and P precipitated at NMC/LFP molar ratios above 1.36, leading to decreased leaching efficiency for these elements. This may be attributable to increased acid consumption by NMC dissolution, changing the pH of solution and hence promoting precipitation of $FePO_4$. The characterization of leach residues at NMC/LFP molar ratios 1.02 and 1.36 confirmed the complete dissolution of NMC and presence of orthorhombic $FePO_4$ (Figure 4.10). These findings are further supported by SEM and EDS results, which showed no traces of NMC in the leach residues. Zoe et al. [86] reported a similar effect of the NMC/LFP molar ratio on the dissolution of Mn, Ni, Co and Li. As the NMC/LFP molar ratio increased from 1.1 to 3.3, leaching efficiencies for Mn, Ni, Co and Li decreased from 90%, 86.9%, 100% and 100% to approximately 55%, 50%, 60% and 80%, respectively, under the conditions of 2 M H_2SO_4, 60°C and 120 minutes. These findings align with our results up to 30 minutes. Similarly, Zou et al. [85] studied the effect of NMC/LFP molar ratios between 0.5 and 2, reporting a gradual decrease in leaching rates of Li, Ni, Co and Mn as molar ratio increased, while leaching rates of Fe and P remained almost constant. Leaching rates close to 100% for Li, Ni, Co and Mn and over 90% for Fe and P were achieved under conditions of NMC/LFP molar ratio 0.8, 1 M H^+ solution, S/L ratio 0.05 g/mL, 25°C and 40 minutes. In our assays, however, increasing molar ratio of NMC/LFP from 0.5 to 1.67 led to a decrease in all metal leaching efficiencies up to 30 minutes; that is, our results for Fe and P differed from those of Zou et al.

- Effect of H_2SO_4 concentration on metal leaching efficiency

Results show that H_2SO_4 concentration plays a crucial role in the efficiency of metal leaching from NMC and LFP cathode materials. Table 4.11 shows SO_4^{2-}/metal molar ratios under the specified experimental conditions. As the table demonstrates, SO_4^{2-}/metal ratios increase with the increase in H_2SO_4 concentrations. At low H_2SO_4 concentrations (0.25 M and 0.5 M), leaching efficiencies for Mn, Ni, Co and Li were relatively low, due to the low acidity of the solution and the low SO_4^{2-}/metal molar ratio. A significant improvement in leaching efficiency was observed at 2 M H_2SO_4, however, with complete recovery of these metals obtained. Leaching efficiencies for Fe and P remained low at the lower acid concentrations but increased substantially at 2 M. These results indicate the importance of optimizing H_2SO_4 concentration to maximize the recovery of critical metals such as Mn, Ni, Co and Li. This study

highlights the need for precise control of H_2SO_4 concentration to maximize selective recovery of valuable metals from NMC and LFP cathode materials. Song et al. [84] observed similar trends, noting that increasing H_2SO_4 concentration from 0.8 M to 1.8 M significantly improved leaching efficiencies for Mn, Ni, Co and Li under conditions of 5 vol% H_2O_2, S/L ratio 0.25 g/mL, 60°C and 60 minutes. Fe leaching efficiency, however, remained low at lower concentrations of H_2SO_4 up to 1.4 M, after which it significantly increased from around 20% to 50% at 1.8 M H_2SO_4.

Table 4.11. SO_4^{2-}/metal molar ratios of initial solid with 0.25 M, 0.50 M and 2 M H_2SO_4 (0.68 M H_2O_2, S/L ratio 0.15 g/mL, NMC/LFP molar ratio 1.36, 75°C, 51 minutes, H_2O_2 added at 30 minutes)

H_2SO_4 (M)	**SO_4^{2-}/metal molar ratio**					
	Mn	**Ni**	**Co**	**Li**	**Fe**	**P**
0.25	1.65	0.55	1.72	0.20	0.46	0.45
0.5	3.29	1.10	3.43	0.40	0.92	0.91
2	13.18	4.42	13.74	1.58	3.69	3.63

- Effect of H_2O_2 concentration on metal leaching efficiency

As discussed, to solubilize the transitional metal oxides, the oxidation states of Mn^{4+}, Ni^{3+} and Co^{3+} must be reduced to Mn^{2+}, Ni^{2+} and Co^{2+} with the help of a reducing agent. H_2O_2 at a high concentration (0.68 M) can completely reduce Mn^{4+}, Ni^{3+} and Co^{3} by providing electrons to drive the reduction process. As discussed, dissolution of Li remains unchanged at higher H_2O_2 concentrations given the ease with which Li dissolves in acidic solutions and the fact that the Li^+ ion remains unchanged in solution. For Fe and P, increasing the concentration of H_2O_2 from 0.10 M to 0.68 M will mean oxidation of more Fe^{2+} to Fe^{3+}, which then precipitates with PO_4^{3-} to produce more $FePO_4$.

4.5. Conclusion

This chapter describes the development of an innovative acid leaching process for mixed NMC and LFP cathode materials. The study contributes new knowledge about the redox interaction between NMC and LFP in sulphuric acid, which affects leaching efficiencies for Mn, Ni and Co through electron transfer involving Fe^{2+} released from LFP. This interaction can be interpreted as a synergistic reaction that facilitates

NMC leaching while leading to $FePO_4$ formation. The findings emphasize the importance of optimizing S/L ratio, with 0.15 g/mL identified as the optimal value for best possible metal recovery from NMC as well as production of $FePO_4 \cdot H_2O_2$ addition significantly improves the dissolution of transition metals, but its concentration must be carefully adjusted to optimize efficiency while managing costs and risks. NMC/LFP molar ratio also influences leaching extraction, with a ratio of 1.36 yielding the best results. A sulphuric acid concentration of 2 M proved most effective, achieving nearly complete dissolution of all metals. Under the best operating conditions of 2 M H_2SO_4, 0.68 M H_2O_2, S/L ratio 0.15 g/mL, NMC/LFP molar ratio 1.36, temperature 75°C and a reaction time of 51 minutes, NMC dissolved completely and the orthorhombic $FePO_4$ was recovered, demonstrating the potential for sustainable recycling strategies for mixed LIBs.

CHAPTER V

SYNERGISTIC ACTION OF FERROUS AND FERRIC IONS ON LEACHING OF MIXED NMC AND LFP MATERIALS

5.1. Introduction

In the recycling of mixed NMC and LFP materials, selective recovery of metals like Ni, Mn, Co and Li from the cathodes is a critical challenge. Reductive leaching-based hydrometallurgy is currently the primary method for recovering metals from mixed NMC and LFP materials. Since most metals in NMC cathode materials are in high oxidation states, a reducing agent is required for their effective leaching. Conversely, for selective leaching of LFP, an oxidizing agent is necessary to dissolve Li and form $FePO_4$ as a valuable byproduct. Efficient selective leaching of NMC-LFP mixtures can decrease the number of separation and purification steps, as well as costs, time and energy. In hydrometallurgy, H_2O_2 is commonly used to drive both reduction and oxidation reactions. However, due to its instability and decomposition, often catalyzed by metal ions, excess amounts are typically required. This has led to a demand for alternative reducing and oxidizing agents that can efficiently achieve selective leaching of Mn, Ni, and Co while preserving the olivine structure of LFP, ultimately leaving orthorhombic $FePO_4$ as a valuable solid residue. In recent years, salt leaching using $Fe(II)SO_4$ or $Fe(III)_2(SO_4)_3$ has gained increasing attention cost-effective and technically feasible alternative to conventional reducing agents like H_2O_2 [78, 115]. However, their use has not been studied focusing on the selective leaching of mixed NMC and LFP cathode materials.

In this context, this chapter shows the study of the effect of adding $Fe(II)SO_4$ and $Fe(III)_2(SO4)_3$ on the acid leaching of NMC and LFP cathode materials. The study focuses also on interactions among LFP, NMC and ferrous sulfate as leaching agent.

5.2. Methodology

The leaching procedures for the mixed NMC and LFP materials were carried out following the general method described in Chapter II. To study the effect of ferrous ions on metal leaching efficiency, two main approaches were considered under the optimal operating conditions of 2 M H_2SO_4, S/L ratio 0.15 g/mL, and NMC/LFP molar ratio of 1.36.

In the first approach, the effect of $Fe(II)SO_4$ addition after 30 minutes of leaching on metal leaching efficiency was examined. Two concentrations of $Fe(II)SO_4$, 0.095 M and 0.285 M, were selected based on a comparison with H_2O_2 to provide approximately the same number of electrons as a reducing agent. However, according to the calculations, it was not possible to maintain identical electron equivalents for

$Fe(II)SO_4$ and H_2O_2 while keeping the same S/L ratio, therefore the lower $Fe(II)SO_4$ concentrations were tested instead.

The second approach focused on investigating the effect of LFP addition on NMC leaching in a ferrous sulfate solution. For this purpose, LFP was added at two different reaction times: first, after 10 minutes of leaching, and second, at the beginning of the assay. Each case included two experiments with Fe^{2+}/NMC molar ratios of 0.27 and 0.74.

Finally, to investigate the effect of ferric ions on metal leaching efficiency, one experiment was designed under the same optimal operating conditions (2 M H_2SO_4, S/L ratio 0.15 g/mL, NMC/LFP molar ratio 1.36). In this test, $Fe(III)_2(SO4)_3 \cdot H_2O$ was first added to the sulphuric acid solution at 2 M, followed by the addition of LFP. After 10 minutes of reaction, NMC was introduced into the mixture.

All experiments were performed at 75 °C under atmospheric pressure with a stirring speed of 330 rpm. The leach residues obtained were then characterized to determine their composition and phase structure.

5.3. Results

5.3.1. Effect of $Fe(II)SO_4$ addition on metal leaching efficiency

To study the effect of $Fe(II)SO_4$ addition on metal leaching, assays were performed at two concentrations of $Fe(II)SO_4$, 0.095 and 0.285 M with the other assay conditions being 2 M H_2SO_4, 75°C, NMC/LFP molar ratio 1.36, S/L ratio 0.15 g/mL, stirring speed 330 rpm, and 51 minutes. Table 5.1 shows the details of the experimental design. Figure 5.1 shows a simplified flow sheet with $Fe(II)SO_4$ added to the leaching solution at 30 minutes.

Table 5.1. Experimental design for study of the effect of adding $FeSO_4$ on metal leaching efficiencies

Assay	H_2SO_4 concentration (M)	$FeSO_4$ concentration (M)	Moles of $FeSO_4$ (Fe^{2+})	NMC/LFP molar ratio	Solid-liquid ratio (g/mL)	Temperature (°C)	Time (min)
1	2	0.095	0.0204	1.36	0.15	75	51
2	2	0.285	0.0612	1.36	0.15	75	51

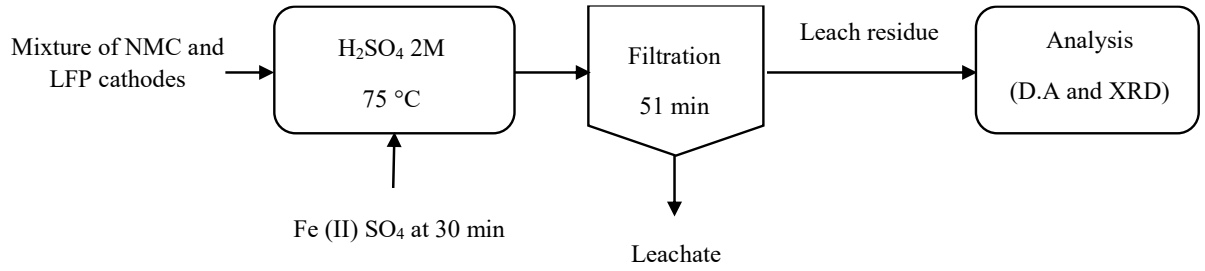

Figure 5.1. Simplified flow sheet for study of the effect of adding Fe(II)SO_4 on metal leaching efficiencies

Figure 5.2 shows the effect of the addition of 0.095 M Fe(II)SO_4 on leaching efficiencies for Mn, Ni, Co, Li, Fe and P as a function of time. As the figure shows, leaching efficiencies for Mn, Ni, Co, Li, Fe and P increased rapidly in the first few minutes and then slowly up to 30 minutes, being 79.7%, 79.7%, 81.6%, 97.9% 66.5% and 65.5%, respectively. With the addition of Fe(II)SO_4 at 30 minutes, the leaching efficiencies for Mn, Ni, and Co increased respectively up to 92.6 %, 91.5% and 94.5% at the end of the leaching assay. For Li, the leaching efficiency increased sharply within the first minute, and then it stayed stable at around 97.9% at 30 minutes. With the addition of Fe(II)SO_4, the Li leaching efficiency slightly increased to 99%. Fe and P behaved similarly, with a leaching efficiency of 66.5 % and 65.5%, respectively, at 30 minutes, and a increasing slightly to 67.2% and 68% at 51 minutes. Despite the improvements of transition metals leaching, the Fe(II)SO_4 concentration used was insufficient to reduce all the metals of NMC material. This indicates that the Fe(II)SO_4 dosage should be increased to completely leach these metals.

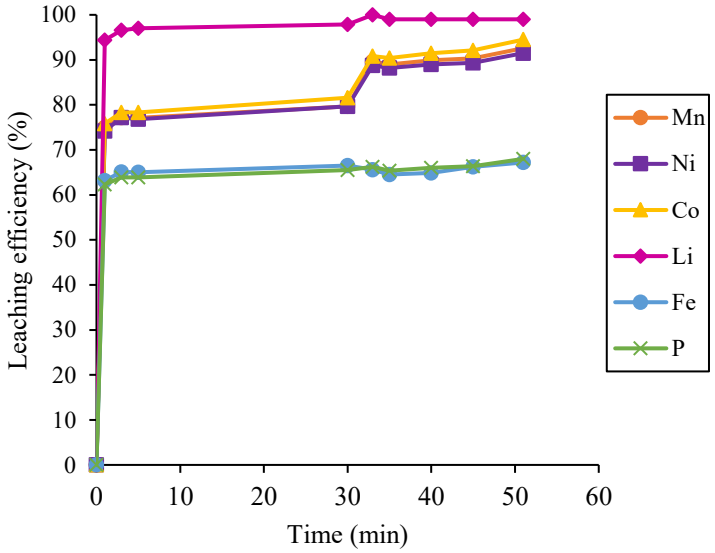

Figure 5.2. Leaching efficiencies for Mn, Ni, Co, Li, Fe and P (2 M H_2SO_4, 0.095 M Fe(II)SO_4, NMC/LFP molar ratio 1.36, S/L ratio 0.15 g/mL, 75°C, Fe(II)SO_4 added at 30 minutes)

In the second assay, the initial concentration of Fe(II)SO_4 was 0.190 M, and after 30 minutes it was increased by steps of 0.019 M every 2 minutes up to reach an equivalent total concentration of 0.285 M. Figure 5.3 shows leaching efficiencies for Mn, Ni, Co, Li, Fe, and P under these conditions. Up to 30 minutes, leaching efficiencies for these metals showed similar trends to those of previous assay, with values of 83.8%, 84.3%, 86.3%, 100%, 66.2%, and 65.5% respectively. Following the addition of 0.190 M of Fe(II)SO_4, the leaching efficiencies of Mn, Ni, and Co increased to 100% by the 35 minutes, whereas for Li, Fe, and P the increase was negligible. The subsequent increments of Fe(II)SO_4 every 2 minutes were also negligible for the leaching efficiencies of Li, Fe and P. These results show that the leaching efficiencies of Mn, Ni, and Co can be effectively increased to 100% using Fe(II)SO_4 as reducing agent being semi-selective for Fe and P.

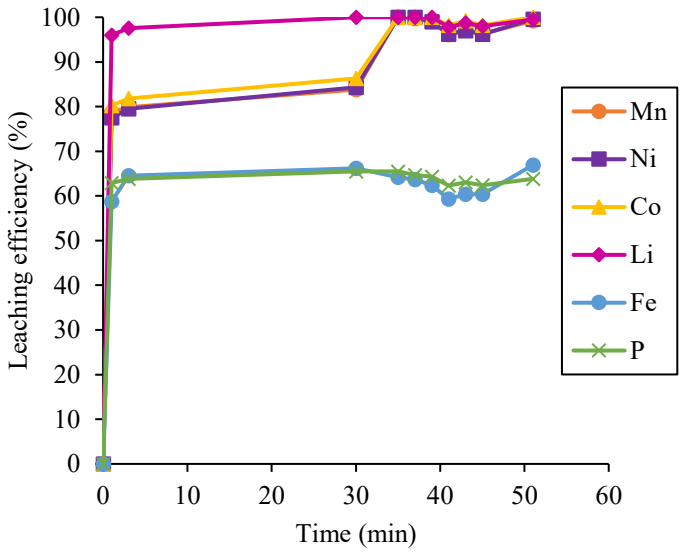

Figure 5.3. Leaching efficiencies for Mn, Ni, Co, Li, Fe and P (2 M H_2SO_4, 0.285 M Fe(II)SO_4, NMC/LFP molar ratio 1.36, S/L ratio 0.15 g/mL, 75°C) with 0.190 M Fe(II)SO_4 added at 30 minutes followed by incremental additions of 0.019 M Fe(II)SO_4 every 2 minutes

To determine the oxidation sate of Fe during the reaction, the oxidation-reduction potential (ORP) of the assay was registered, as shown in Table 5.2. Figure 5.4 shows the Eh-pH diagram of the Fe-Li-P-H_2O system, indicating that the potential corresponding to Fe^{3+} is greater than 0.7 V at acidic pH [88]. The results show that ORP increased from 0.891 V to 1.032 V during the first 30 minutes, indicating the oxidation of Fe^{2+} from LFP to Fe^{3+}. With the addition of 0.190 M Fe(II)SO_4 at 30 minutes, the ORP decreased to 0.717 V at 35 minutes, indicating the oxidation of Fe^{2+} from Fe(II)SO_4 to Fe^{3+}. With subsequent additions of 0.019 M Fe(II)SO_4 every two minutes from 37 to 45 minutes, the ORP gradually decreased from 0.690 V to 0.652 V, reflecting the accumulation of Fe^{2+} in the solution.

Table 5.2. Effect of $FeSO_4$ concentration on ORP (V) under conditions of 2 M H_2SO_4, 0.285 M Fe(II)SO_4, NMC/LFP molar ratio 1.36, S/L ratio 0.15 g/mL, 75°C, Fe(II)SO_4 added at 30 minutes and first sample taken at 35 minutes and followed by incremental additions of 0.019 M Fe(II)SO_4 every 2 minutes.

Time (min)	Fe(II)SO_4 concentration (M)	ORP (V)
1	0	0.891
3	0	0.970
5	0	0.937
30	0	1.032
35	0.190	0.717
37	0.019	0.690
39	0.019	0.675
41	0.019	0.666
43	0.019	0.658
45	0.019	0.652

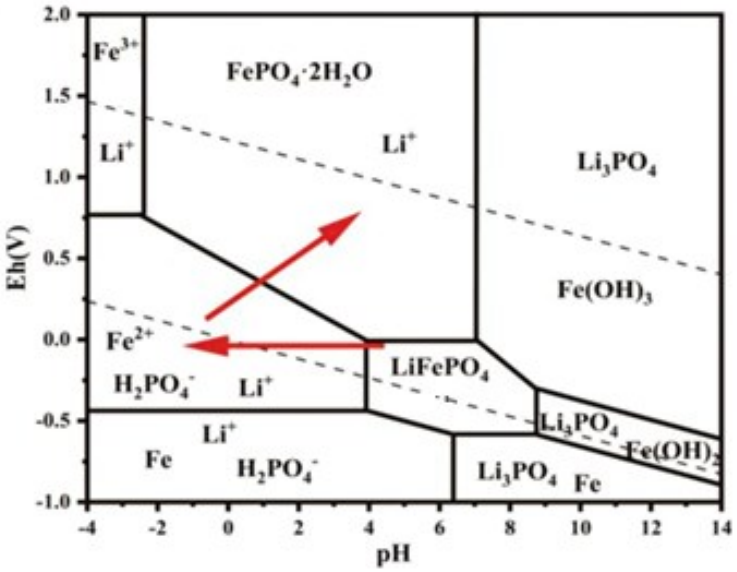

Figure 5.4. Eh-pH diagram of Fe-Li-P-H_2O system at 25°C and one atmosphere of pressure [85]. *The use of this figure was permitted by Elsevier*

Table 5.3 shows the metal content (mmol/g) in the leach residue obtained at $Fe(II)SO_4$ concentration of 0.095 and 0.19 M. At 0.095 M $Fe(II)SO_4$, the leach residue retained relatively high amounts of transition metals with Mn (0.35 mmol/g), Ni (0.96 mmol/g), Co (0.30 mmol/g) and Li (0.55 mmol/g), suggesting that the NMC was not leached completely. When the $Fe(II)SO_4$ concentration was increased to 0.285 M, the content of Mn, Ni, Co, and Li in the leach residue decreased to 0.04, 0.06, 0.02, and 0.21 mmol/g, respectively. This means that increasing $Fe(II)SO_4$ concentration improved the leaching efficiency and led to the nearly complete dissolution of the NMC. In contrast, the Fe and P contents increased slightly from 5.35 mmol/g and 4.94 mmol/g to 5.89 mmol/g and 5.72 mmol/g, respectively, due to the decrease of their leaching efficiency and the precipitation of Fe and P in the leach residue. Figure 5.5 shows the XRD patterns for these two leach residues. It shows that increasing the concentration of $Fe(II)SO_4$ from 0.095 to 0.285 M, results in the complete disappearance of NMC 622 peaks, leaving only $FePO_4$ with the orthorhombic space group Pnma (62), which is consistent with the leaching efficiency and the metal content.

Table 5.3. Effect of $Fe(II)SO_4$ concentration on metal content (mmol/g) in leach residues with 0.095 M and 0.285 M $Fe(II)SO_4$ (2 M H_2SO_4 NMC/LFP molar ratio 1.36, S/L ratio 0.15 g/mL, 75°C, 51 minutes)

$Fe(II)SO_4$ concentration (M)	**Metal content (mmol/g)**					
	Mn	**Ni**	**Co**	**Li**	**Fe**	**P**
0.095	0.35	0.96	0.30	0.55	5.35	4.94
0.285	0.04	0.06	0.02	0.21	5.89	5.72

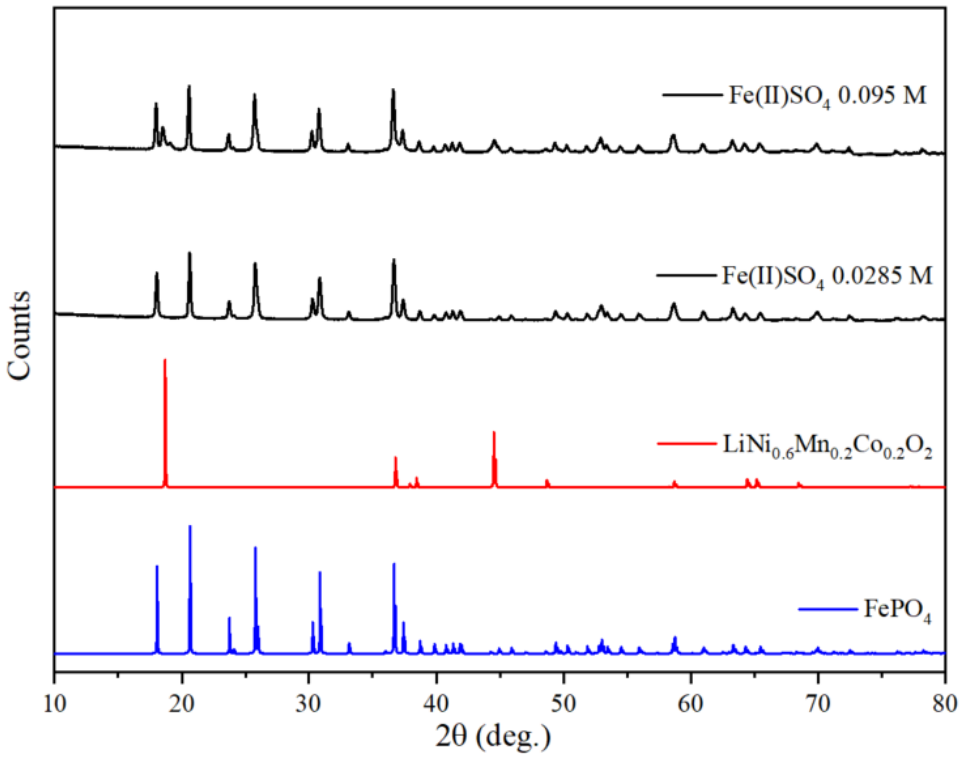

Figure 5.5. XRD patterns of leach residues with 0.095 M and 0.285 M Fe(II)SO_4 (2 M H_2SO_4, NMC/LFP molar ratio 1.36, S/L ratio 0.15 g/mL, 75°C, 51 minutes) and of $LiNi_{0.6}Mn_{0.2}Co_{0.2}O_2$ (COD ID: 4002443) and $FePO_4$ (COD ID: 1525576).

5.3.2. Effect of LFP addition on NMC leaching in a ferrous sulfate solution

To study the effect of LFP addition on NMC leaching in a ferrous sulfate solution on leaching efficiency and individual reactions between NMC/Fe^{2+} ions and LFP/Fe^{3+} ions, two experimental conditions were used. In the first condition, LFP was added to an initial mixture of Fe(II)SO_4 and NMC. In the second condition, Fe(II)SO_4, NMC and LFP were added at the beginning of the assay. Previous assays indicated reaction kinetics were fast, so reaction time was decreased to 36 minutes.

5.3.2.1. Addition of LFP to an initial mixture of Fe(II)SO_4 and NMC

To analyze the effect of adding LFP to an initial mixture of Fe(II)SO_4 and NMC as well as the initial reaction of Fe^{2+} ions and NMC, two assays were designed with two different Fe^{2+}/NMC molar ratios. Table 5.4 shows the experimental design. In these tests, Fe(II)SO_4 was added to an H_2SO_4 solution and heated to

75°C, after which NMC was added. The reaction was allowed to proceed for 10 minutes, and then LFP was introduced into the mixture, as shown in Figure 5.6.

Table 5.4. Experimental design for study of addition of LFP to an initial mixture of $Fe(II)SO_4$ and NMC

Assay	H_2SO_4 concentration (M)	$FeSO_4$ concentration (M)	Moles of $FeSO_4$ (Fe^{2+})	Fe^{2+}/NMC molar ratio	NMC/LFP molar ratio	Solid-liquid ratio (g/mL)	Temperature (°C)	Time (min)
1	2	0.190	0.0408	0.27	1.36	0.15	75	36
2	2	0.512	0.1101	0.74	1.36	0.15	75	36

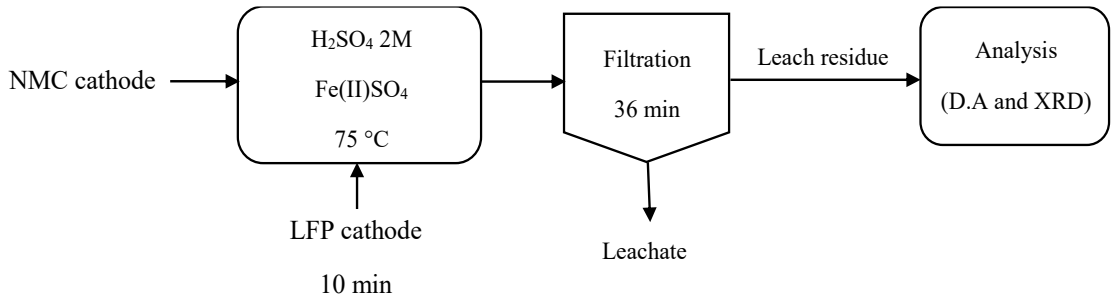

Figure 5.6. Simplified flow sheet for addition of LFP to an initial mixture of $Fe(II)SO_4$ and NMC

Figure 5.7 shows leaching efficiencies as a function of time for Mn, Ni, Co, Li, Fe and P with Fe^{2+}/NMC molar ratio 0.27. As the figure shows, leaching efficiencies for Ni, Co and Li increased rapidly to 55.9%, 56.0% and 95.3%, respectively, in the first minute and then remained constant to 10 minutes. For Mn, the leaching efficiency increased at first to 54.8 %, but it decreased slowly, hitting 42.5% at 10 minutes. Adding LFP at 10 minutes caused leaching efficiencies for Mn, Ni and Co to increase to near 100% for all NMC metals by the end of leaching. After the addition of LFP, the leaching efficiency of Li increased slightly to 99.2% by the end of the assay. By the addition of LFP to the leaching solution, the leaching efficiency of Fe and P increased to 43.3 % and 46.2% at 12 minutes and stayed nearly stable for the rest of the assay.

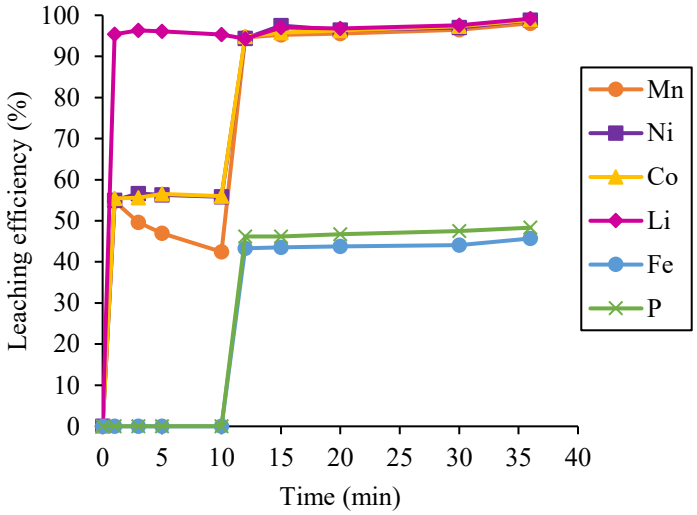

Figure 5.7. Leaching efficiencies for Mn, Ni, Co, Li, Fe and P (2 M H_2SO_4, NMC/LFP molar ratio 1.36, Fe^{2+} /NMC molar ratio 0.27, S/L ratio 0.15 g/mL, 75°C) with addition of LFP to initial mixture of Fe(II)SO_4 and NMC at 10 minutes

Table 5.5 shows ORP data measured during the reaction. As the table shows, all Fe^{2+} from the Fe(II)SO_4 effectively reduced the NMC, resulting in its oxidation to Fe^{3+} in the first 10 minutes. With the addition of LFP, Fe^{2+} from the LFP was similarly oxidized to Fe^{3+}, as the ORP measurements suggest.

To further study the reaction of NMC and Fe^{2+}, their molar ratio was increased to 0.74 in the second assay. Figure 5.8 shows leaching efficiencies for Mn, Ni, Co, Li, Fe and P for this molar ratio as a function of time. Leaching efficiencies for Mn, Ni and Co improved significantly within the first minute, sharply increasing to around 80% and then remaining relatively constant to reach 80.1%, 82.5% and 82.9%, respectively, at 10 minutes. The addition of LFP at 10 minutes further improved leaching efficiencies for these metals followed by a gradual increase to nearly 100% for all three metals by the end of the leaching assay. Li leaching from NMC presented a trend similar to the previous assay, with leaching efficiency rising to 94.8% within the first 10 minutes. After the addition of LFP, Li dissolution from both NMC and LFP cathodes increased to 100% by 36 minutes. Fe and P leaching also presented a trend similar to the previous assay but initial leaching efficiencies were lower and gradually rose to 28.3% and 34.5%, respectively, by the end of the assay.

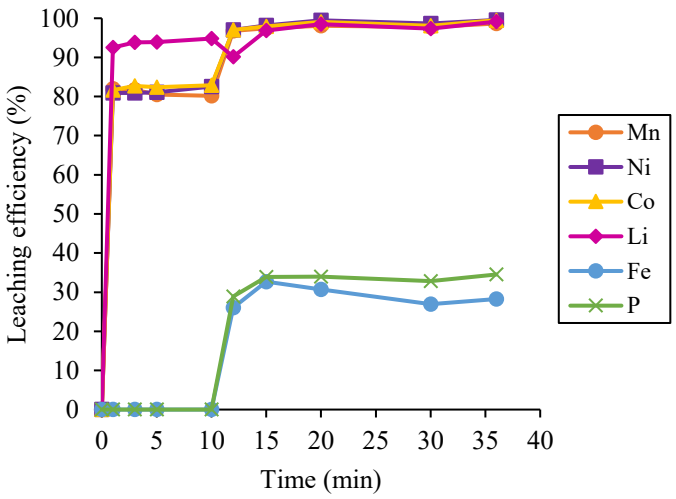

Figure 5.8. Leaching efficiencies for Mn, Ni, Co, Li, Fe and P (2 M H_2SO_4, NMC/LFP molar ratio 1.36, Fe2+/NMC molar ratio 0.74, S/L ratio 0.15 g/mL, 75°C) with addition of LFP to initial mixture of Fe(II)SO_4 and NMC at 10 minutes

ORP results for these two tests show oxidation of Fe^{2+} to Fe^{3+} in the first 10 minutes, leading to significant reduction of NMC. This aligns with the increase in leaching efficiency noted during this period. After addition of LFP at 10 minutes, ORP decreased in both tests. In the assay with Fe^{2+}/NMC molar ratio 0.74, ORP values reflect the presence of Fe^{2+} in the solution.

Table 5.5. Effect of Fe^{2+}/NMC molar ratio on ORP (v) with Fe^{2+}/NMC molar ratios 0.27 and 0.74 (2 M H_2SO_4, NMC/LFP molar ratio 1.36, S/L ratio 0.15 g/mL, 75°C, addition of LFP to initial mixture of Fe(II)SO_4 and NMC at 10 minutes)

Time (min)	Fe^{2+}/NMC molar ratio 0.27 ORP (V)	Fe^{2+}/NMC molar ratio 0.74 ORP (V)
0	0.568	0.573
1	1.403	1.366
3	1.418	1.376
5	1.414	1.369
10	1.412	1.363
12	0.832	0.689
15	0.910	0.665
20	0.947	0.654
30	0.916	0.647

Table 5.6 shows the metal content (mmol/g) in the leach residues obtained at of Fe^{2+}/NMC molar ratio 0.27 and 0.74. Under both conditions, the amounts of Mn, Ni, Co and Li in the leach residue were negligible, indicating that the NMC was completely leached. In contrast, Fe and P remained in both leach residue, with slightly higher contents observed at the Fe^{2+}/NMC molar ratio of 0.74 than 0.27. Figure 5.9 shows XRD results for these two leach residues. In both cases, the XRD are a match for $FePO_4$ with the orthorhombic space group Pnma (62). At the higher Fe^{2+}/NMC molar ratio, however, a larger mass of $FePO_4$ was produced.

Table 5.6. Effect of Fe^{2+}/NMC molar ratio on metal content (mmol/g) in the leach residues with Fe^{2+}/NMC molar ratios 0.27 and 0.74 (2 M H_2SO_4, NMC/LFP molar ratio 1.36, S/L ratio 0.15 g/mL, 75°C) and LFP added to the initial mixture of Fe(II)SO_4 and NMC at 10 minutes

Fe^{2+}/NMC molar ratio	**Metal content (mmol/g)**					
	Mn	**Ni**	**Co**	**Li**	**Fe**	**P**
0.27	0.06	0.11	0.03	0.22	6.10	5.90
0.74	0.03	0.03	0.01	0.19	6.59	6.12

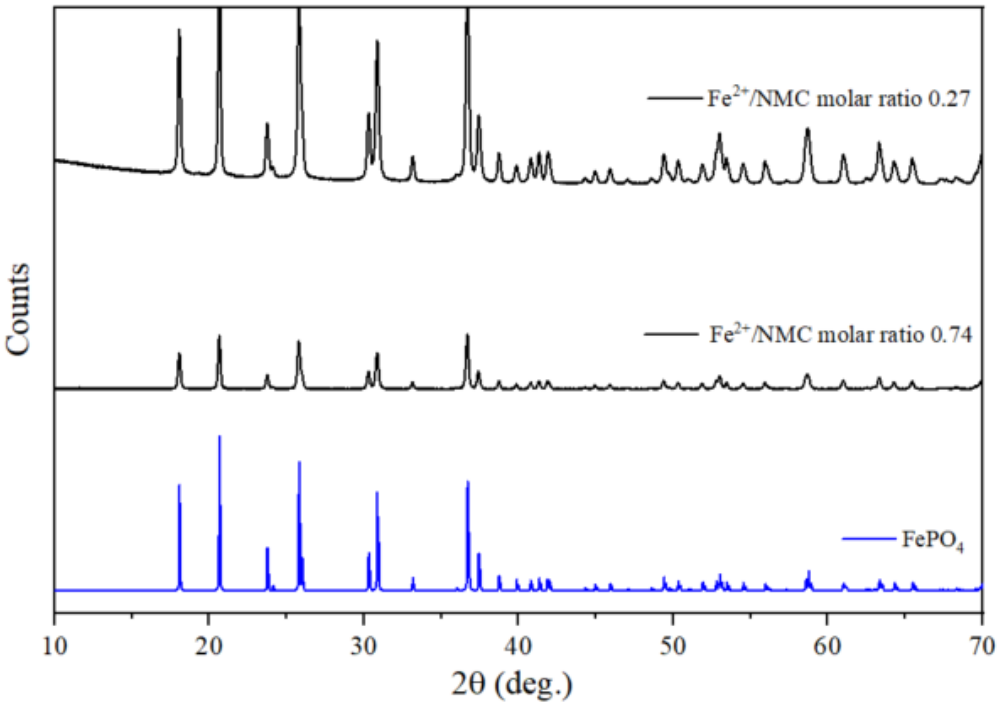

Figure 5.9. XRD patterns of leach residues with Fe^{2+}/NMC molar ratios 0.27 and 0.74 (2 M H_2SO_4, NMC/LFP molar ratio 1.36, S/L ratio 0.15 g/mL, 75°C, LFP added to initial mixture of Fe(II)SO_4 and NMC at 10 minutes) and pattern of $FePO_4$ (COD ID: 1525576)

5.3.2.2. Initial simultaneous addition of Fe(II)SO_4, NMC and LFP

To analyze the simultaneous reaction of NMC, LFP and Fe(II)SO_4, two assays were designed using the same Fe^{2+}/NMC molar ratios as in the experiments described above. The Fe(II)SO_4 was solubilized in a sulfuric acid solution and the NMC and LFP mixture was added as shown in Figure 5.10. The Table 5.7 shows the experimental design for this study.

Table 5.7. Experimental design for study of initial simultaneous addition of $FeSO_4$, NMC and LFP

Assay	H_2SO_4 concentration (M)	$FeSO_4$ concentration (M)	Moles of $FeSO_4$ (Fe^{2+})	Fe^{2+}/NMC molar ratio	NMC/LFP molar ratio	Solid-liquid ratio (g/mL)	Temperature (°C)	Time (min)
1	2	0.190	0.0408	0.27	1.36	0.15	75	36
2	2	0.512	0.1101	0.74	1.36	0.15	75	36

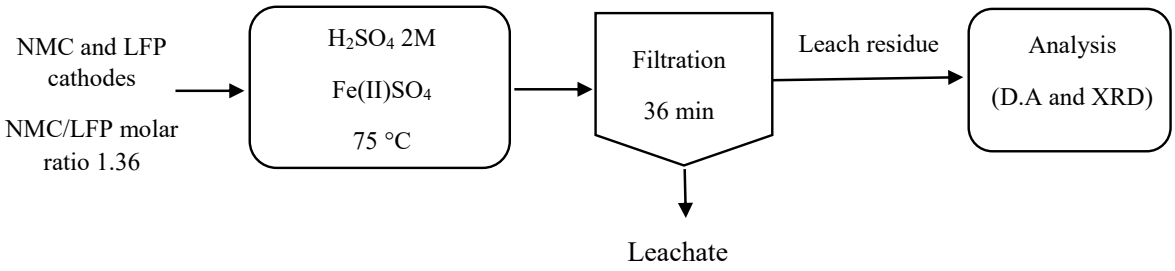

Figure 5.10. Simplified flow sheet for initial simultaneous addition of $Fe(II)SO_4$, NMC and LFP

Figure 5.11 shows leaching efficiencies for Mn, Ni, Co, Li, Fe and P at Fe^{2+}/NMC molar ratio 0.27 under the specified conditions. As the figure shows, the trend is the same for all metals. Leaching efficiencies for Mn, Ni, Co and Li increased quickly in the first minute to around 90% and then increased gradually, to 97.1%, 97.7%, 97.8% and 99.2%, respectively, at 35 minutes. Though initial leaching efficiencies for Fe and P were lower (44.4% and 51.9%, respectively), they also gradually increased as the reaction progressed, reaching 52.3% and 57%, respectively, by the end of the assay. Table 5.8 shows the ORP data from initial minutes to the end of reaction, in which all of Fe^{2+} oxidized to Fe^{3+} leading to the reduction of NMC.

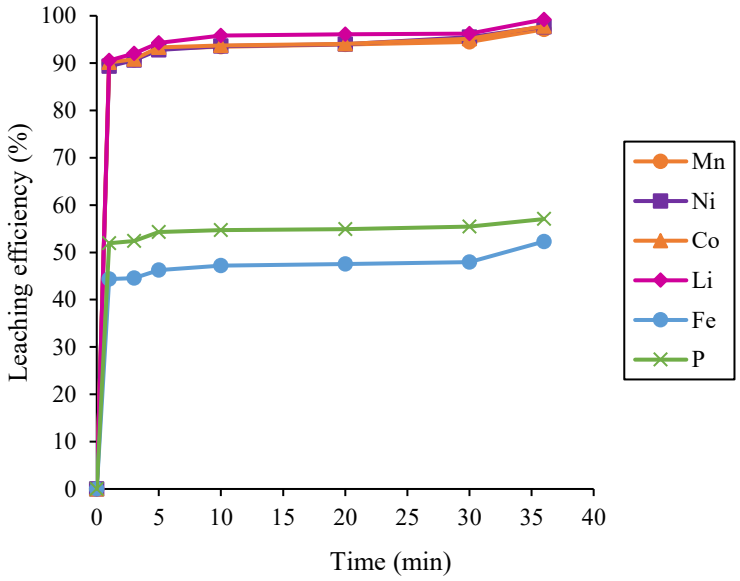

Figure 5.11. Leaching efficiencies for Mn, Ni, Co, Li, Fe and P (2 M H_2SO_4, NMC/LFP molar ratio 1.36, Fe^{2+}/NMC molar ratio 0.27, S/L ratio 0.15 g/mL, 75°C) with initial simultaneous addition of $FeSO_4$, NMC and LFP

To further analyze the combined reaction of NMC, LFP and $FeSO_4$, the molar ratio of Fe^{2+}/NMC was increased to 0.74 in the second assay. Figure 5.12 shows leaching efficiencies for Mn, Ni, Co, Li, Fe and P at Fe^{2+}/NMC molar ratio 0.74 as a function of time. A similar trend was observed for all metals over the reaction. However, initial leaching efficiencies for Mn, Ni and Co were higher than in the previous assay at 96.9%, 98.1% and 98.2%, respectively. Their leaching efficiency stabilized around 100% at the end of assay. Li leaching efficiency gradually increased over the course of the reaction, eventually reaching 98.6%. The graph shows the lower leaching efficiencies for Fe and P during the first minutes (34.9% and 39.9%, respectively) and the gradual increase to 40.5% and 45.9% by the end of the assay.

Increasing Fe^{2+}/NMC molar ratio from 0.27 to 0.74 clearly led to a significant improvement in leaching efficiencies for Mn, Ni and Co, while leaching of Fe and P decreased. Table 5.8 shows ORP values during the reaction for both assays. ORP at Fe^{2+}/NMC molar ratio 0.74 is lower than ORP at Fe^{2+}/NMC molar ratio 0.27, which means more Fe^{2+} released into the solution.

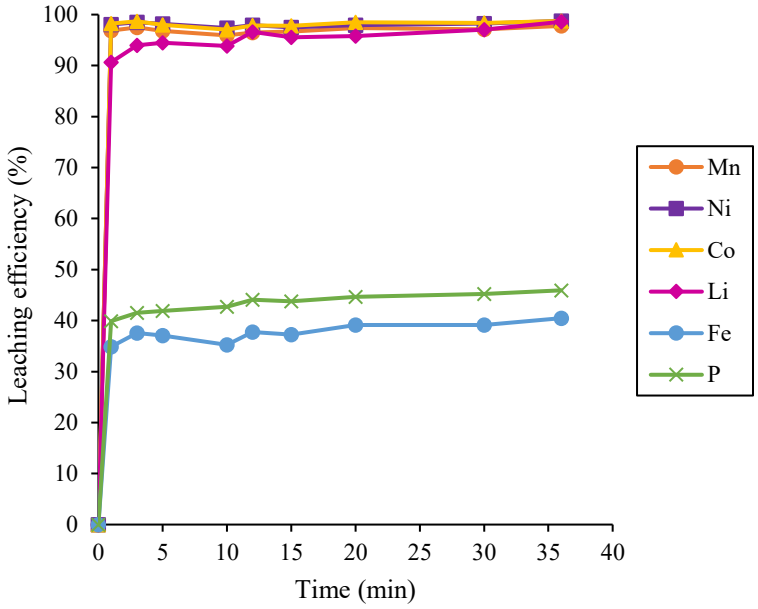

Figure 5.12. Leaching efficiencies for Mn, Ni, Co, Li, Fe and P (2 M H_2SO_4, NMC/LFP molar ratio 1.36, Fe^{2+}/NMC molar ratio 0.74, S/L ratio 0.15 g/mL, 75°C) with initial simultaneous addition of $FeSO_4$, NMC and LFP

Table 5.8. Effect of Fe^{2+}/NMC molar ratio on ORP (v) with Fe^{2+}/NMC molar ratios 0.27 and 0.74 (2 M H_2SO_4, NMC/LFP molar ratio 1.36, S/L ratio 0.15 g/mL, 75°C) and initial simultaneous addition of $FeSO_4$, NMC and LFP

Time	Fe^{2+}/NMC molar ratio 0.27 ORP (V)	Fe^{2+}/NMC molar ratio 0.74 ORP (V)
0	0.584	0.582
1	0.819	0.689
3	0.869	0.673
5	0.916	0.664
10	0.953	0.654
15	0.936	0.652
20	0.936	0.651
30	0.932	0.658

Table 5.9 shows the metal content (mmol/g) of the leach residues obtained at Fe^{2+}/NMC molar ratios 0.27 and 0.74. At Fe^{2+}/NMC molar ratio of 0.27, the leach residue contained relatively low amounts of transition metals with Mn (0.10 mmol/g), Ni (0.25 mmol/g), Co (0.08 mmol/g) and Li (0.24 mmol/g), suggesting that the NMC was not completely leached. However, at Fe^{2+}/NMC molar ratio of 0.74, the content of Mn, Ni, and Co in the residue decreased and became negligible, indicating that they were completely leached. The Fe and P content remained relatively similar under both conditions. Figures 5.13 and 5.14 show the XRD patterns of these two leach residues. The results show that as the molar ratio of Fe^{2+}/NMC increased from 0.27 to 0.74, the NMC phase was fully dissolved, leaving only $FePO_4$ in the leach residue.

Table 5.9. Effect of Fe^{2+}/NMC molar ratio on metal content (mmol/g) of leach residues with Fe^{2+}/NMC molar ratios 0.27 and 0.74 (2 M H_2SO_4, NMC/LFP molar ratio 1.36, S/L ratio 0.15 g/mL, 75°C) and initial simultaneous addition of $FeSO_4$, NMC and LFP

Fe^{2+}/NMC molar ratio	**Metal content (mmol/g)**					
	Mn	**Ni**	**Co**	**Li**	**Fe**	**P**
0.27	0.10	0.25	0.08	0.24	6.23	5.71
0.74	0.06	0.11	0.04	0.35	6.07	5.61

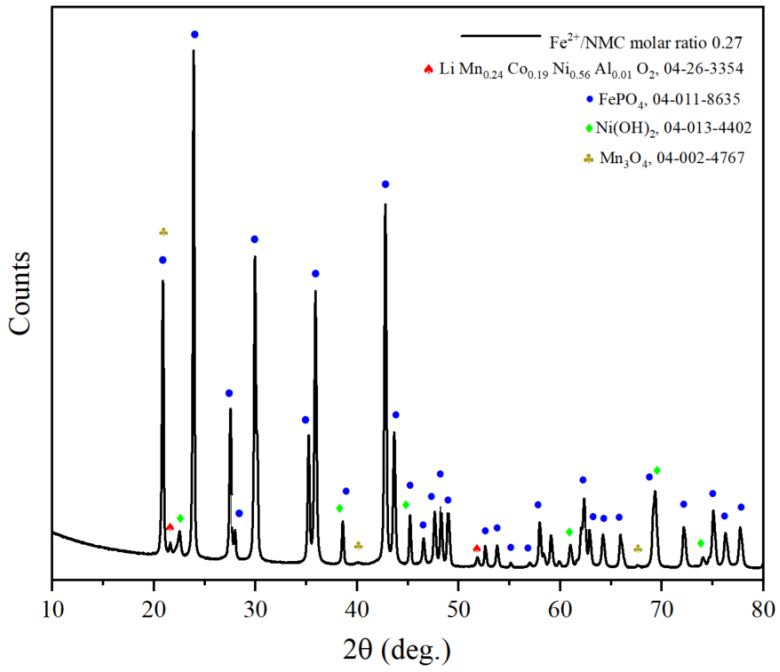

Figure 5.13. XRD pattern of leach residue (2 M H_2SO_4, NMC/LFP molar ratio 1.36, Fe^{2+}/NMC molar ratio 0.27, S/L ratio 0.15 g/mL, 75°C) with initial simultaneous addition of $FeSO_4$, NMC and LFP (XRD carried out with Co source)

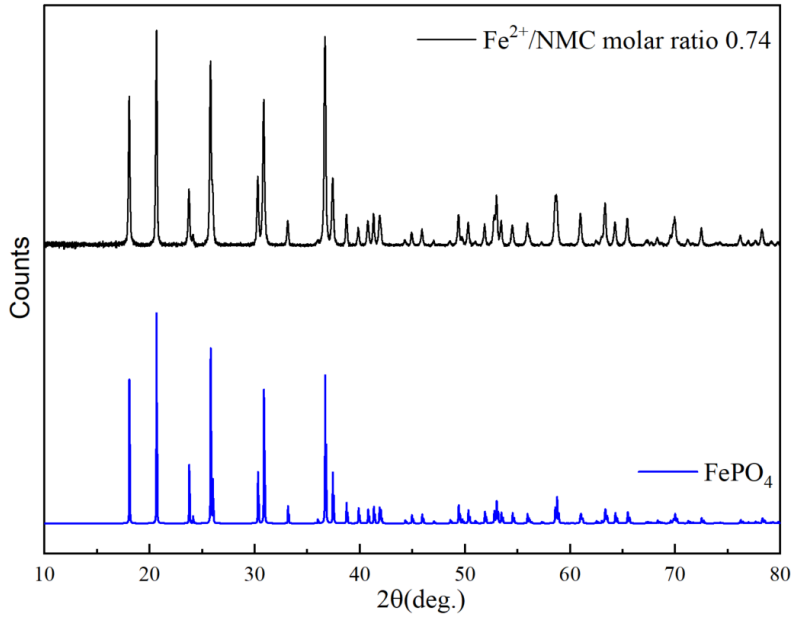

Figure 5.14. XRD pattern of leach residue (2 M H_2SO_4, NMC/LFP molar ratio 1.36, Fe^{2+}/NMC molar ratio 0.74, S/L ratio 0.15 g/mL, 75°C) with initial simultaneous addition of $FeSO_4$, NMC and LFP, and pattern of $FePO_4$ (COD ID: 1525576).

5.3.3. Addition of NMC to an initial mixture of $Fe(III)_2(SO_4)_3$ and LFP

An assay was designed to investigate the effect of adding NMC to an initial mixture of $Fe(III)_2(SO_4)_3$ and LFP, as well as the initial reaction of Fe^{3+} ions and LFP. In this assay, 0.0204 moles of $Fe(III)_2(SO_4)_3$ (the equivalent of 0.0408 moles of Fe^{3+} ions) were added to a sulphuric acid solution, and then LFP was added. After allowing the reaction to proceed for 10 minutes, NMC was then introduced into the mixture, as shown in Figure 5.15. Table 5.10 shows the experimental design.

Table 5.10. Experimental design for study of addition of NMC to initial mixture of $Fe_2(SO_4)_3$ and LFP

Assay	H_2SO_4 concentration (M)	$Fe(III)_2(SO_4)_3$ concentration (M)	Moles of Fe^{+3}	Fe^{3+}/LFP molar ratio	NMC/LFP molar ratio	Solid-liquid ratio (g/mL)	Temperature (°C)	Time (min)
1	2	0.095	0.0408	0.37	1.36	0.15	75	36

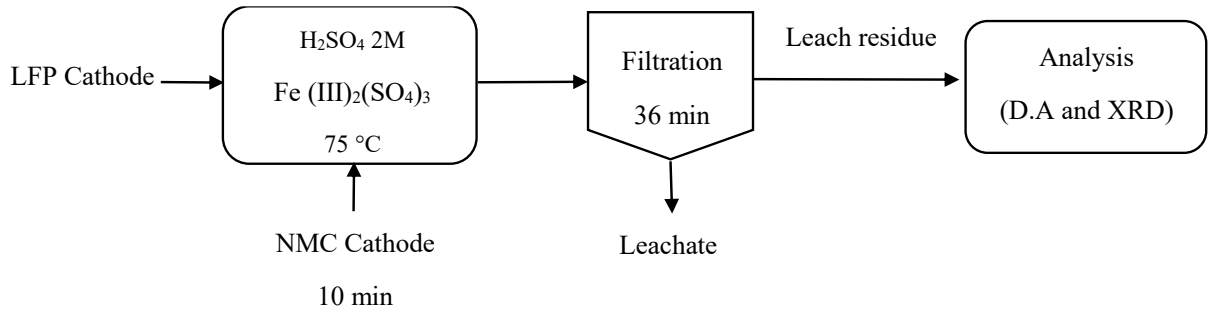

Figure 5.15. Simplified flow sheet of addition of NMC to an initial mixture of $Fe(III)_2(SO_4)_3$ and LFP

Figure 5.16 shows leaching efficiencies for Mn, Ni, Co, Li, Fe and P for this assay as a function of time. As the figure shows, leaching efficiencies for Li, Fe and P increased rapidly in the first minutes and then increased gradually, reaching 99.9%, 93.6% and 94.2%, respectively, by the end of 10 minutes. All of the Li from the LFP was dissolved during the reaction of LFP and Fe^{3+} in the sulphuric acid media. The addition of NMC at 10 minutes, did not affect leaching efficiencies for Fe and P, which increased very slowly over time to 96.7% and 97.3% by the end of the assay. The addition of NMC caused a high leaching efficiency

of Li from both LFP and NMC and it increased slowly to 96.8% at 36 minutes. By adding NMC to the leaching solution, the leaching efficiency of Mn, Ni and Co increased 80.8%, 81.1%, and 80.6%, respectively at 36 minutes.

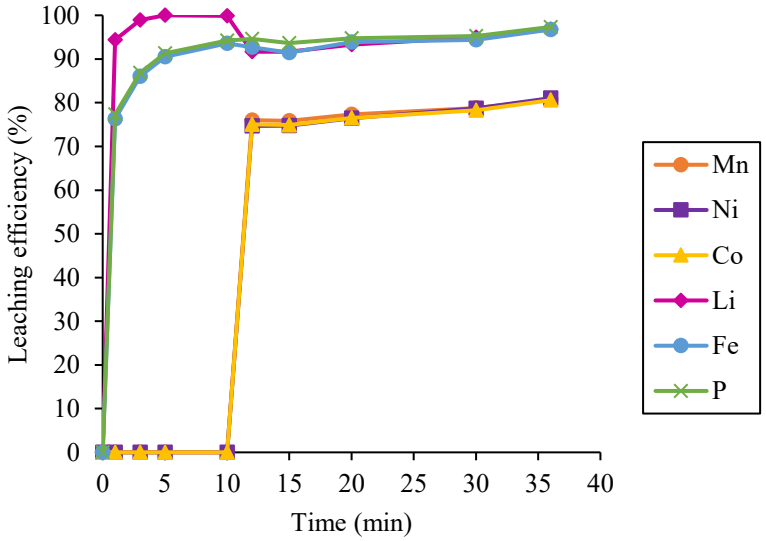

Figure 5.16. Leaching efficiencies for Mn, Ni, Co, Li, Fe and P (2 M H_2SO_4, NMC/LFP molar ratio 1.36, S/L ratio 0.15 g/mL, 75°C) with addition of NMC to initial mixture of $Fe_2(SO_4)_3$ and LFP at 10 minutes

Table 5.11 shows the ORP data during the assay. These data indicate presence of Fe^{2+} for the first 10 minutes, then its oxidization to Fe^{3+} from 10 to 30 min with the addition of NMC. Table 5.12 show the metal content (mmol/g) of leach residue. The residue contained significant amounts of Mn (1.55 mmol/g), Ni (4.56 mmol/g), Co (1.50 mmol/g), and Li (2.14 mmol/g), indicating that the NMC could not leached effectively under these conditions. In contrast, the Fe and P content in the leach residue was relatively low, at 0.94 mmol/g and 0.78 mmol/g, respectively, suggesting their high leaching efficiency. Figure 5.17 shows the XRD pattern of the leach residue obtained under this assay conditions. It shows that NMC remained in the leach residue a long with a small portion of $FePO_4$.

Table 5.11. Effect of Fe^{3+}/LFP molar ratio on ORP (V) (2 M H_2SO_4, NMC/LFP molar ratio 1.36, S/L ratio 0.15 g/mL, 75°C) with addition of NMC to initial mixture of $Fe_2(SO_4)_3$ and LFP at 10 minutes

Time	Fe^{3+}/LFP molar ratio 0.37
	ORP (V)
0	1.055
1	0.645
3	0.635
5	0.632
10	0.629
12	1.093
15	0.980
20	1.006
30	1.045

Table 5.12. Effect of Fe^{3+}/LFP molar ratio on metal content (mmol/g) in leach residue (2 M H_2SO_4, NMC/LFP molar ratio 1.36, S/L ratio 0.15 g/mL, 75°C) with addition of NMC to initial mixture of $Fe_2(SO_4)_3$ and LFP at 10 minutes

Fe^{3+}/LFP molar ratio	**Metal content (mmol/g)**					
	Mn	**Ni**	**Co**	**Li**	**Fe**	**P**
0.37	1.55	4.56	1.50	2.14	0.94	0.78

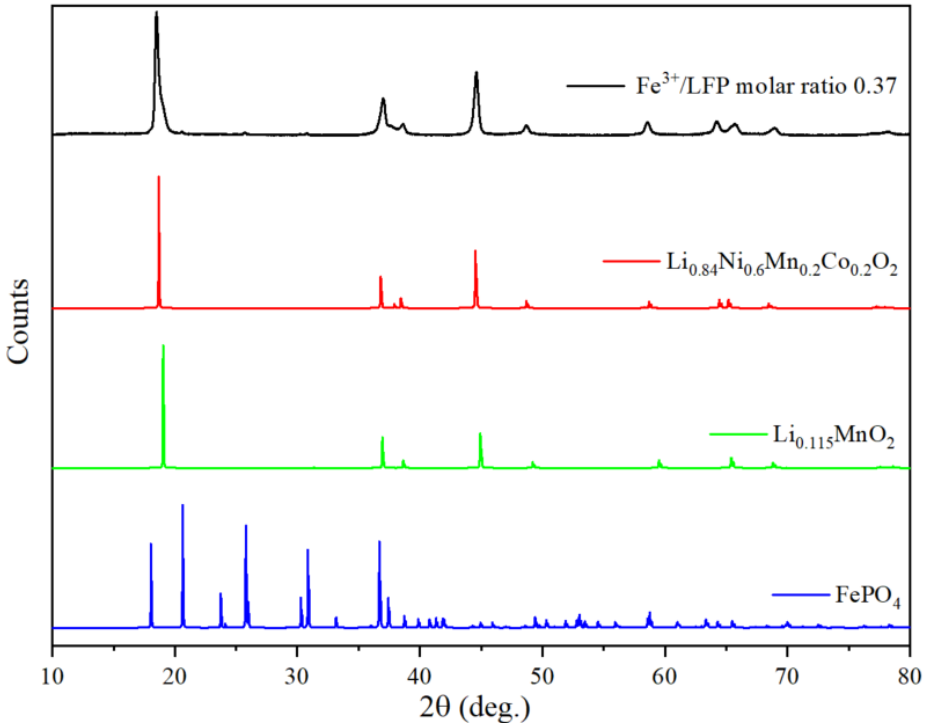

Figure 5.17. XRD pattern of leach residue (2 M H_2SO_4, NMC/LFP molar ratio 1.36, S/L ratio 0.15 g/mL, 75°C, addition of NMC to initial mixture of $Fe_2(SO_4)_3$ and LFP at 10 minutes) and of $Li_{0.84}Ni_{0.6}Mn_{0.2}Co_{0.2}O_2$ (COD ID: 4002444), $Li_{0.115}MnO_2$ (COD ID: 8103495) and $FePO_4$ (COD ID: 1525576)

5.4. Discussion

- Effect of Fe(II)SO_4 addition on metals leaching efficiencies

Prior results suggested that there were interactions between NMC and LFP in a H_2SO_4 solution. The Fe^{2+} ions present in LFP were able to reduce Mn, Ni, and Co to lower oxidation states that those presented in NMC, improving the leaching efficiency within the first 30 minutes. This was confirmed by the increase of ORP of leachate during the first 30 minutes (Table 5.2), this means that Fe^{2+} from LFP was oxidized to Fe^{3+} releasing electrons which were accepted by the transitional metals decreasing their oxidation state. As shown in Equation (4.1), 1 mole of LFP was required for reducing 1 mole of NMC (Ni^{3+}, Mn^{4+} and Co^{3+}). However, the amount of Fe^{2+} provided by LFP was not sufficient to reduce all atoms of metals of NMC in both assays, as shown in Table 5.13. The leaching efficiency of Mn, Ni and Co obtained approximately 80 % for both assays during this period. Therefore, an additional reducing agent was necessary for complete reducing of NMC and leach 100% of them.

Table 5.13. Calculation of $Fe(II)SO_4$, NMC and LFP moles based on the experimental design

Assay	$Fe(II)SO_4$ Concentration (M)	$Fe(II)SO_4$ (Fe^{2+}) moles	NMC moles	LFP (Fe^{2+}) moles
1	0.095	0.0204	0.149	0.110
2	0.285	0.0612	0.149	0.110

This study highlighted the significant role of $Fe(II)SO_4$ as a reducing agent in improving the leaching efficiency of Mn, Ni, and Co from mixed NMC/LFP in H_2SO_4 solution. The addition of $Fe(II)SO_4$ at 30 minutes led to a marked improvement in the leaching efficiency of Mn, Ni, and Co at both $Fe(II)SO_4$ concentration of 0.095 M and 0.285 M. However, as shown in Figure 5.2, the concentration of $Fe(II)SO_4$ 0.095 M, which provided 0.0204 moles of Fe^{2+} (source of electrons) was not enough to reduce all of metals from NMC. The residual metal content as shown in Table 5.3, and the XRD analysis in Figure 5.5 confirmed the presence of unreacted NMC in the leach residue.

When the $Fe(II)SO_4$ concentration was increased to 0.190 M (0.0408 moles of Fe^{2+}) in the second assay, the complete leaching of Mn, Ni, and Co was obtained just 5 minutes after the addition of $Fe(II)SO_4$ (Figure 5.3). This suggests that the increased release of Fe^{2+} supplied enough electrons to fully reduce the metals present in NMC. The ORP of leachate showed 0.717 V upon the addition of 0.190 M $Fe(II)SO_4$, indicating that the oxidation state of Fe^{2+} had changed to Fe^{3+}. As the $Fe(II)SO_4$ was further added, the ORP values gradually decreased, reflecting the increase of Fe^{2+} concentration in the solution. The XRD analysis in Figure 5.5 confirmed the disappearance of NMC crystalline peaks and the formation of $FePO_4$ in the leach residue.

The addition of $Fe(II)SO_4$ had a negligible effect on the dissolution of Fe and P in the first assay. However, a slight decrease was observed in the second assay. This could be due to the precipitation of Fe^{3+} because of acid consumption by the complete dissolution of NMC and changing pH as discussed in Equation 3.11. However, this precipitate was not stable, and the leaching efficiency of Fe and P was 67 % and 64 %, respectively, by the end of the reaction.

Studies by Yunhui et al. [89] and Zou et al. [85] also report improvement in Ni, Mn and Co leaching rates through the use of Fe^{2+} ions derived from LFP. Their study, however, did not analyze the effect of $Fe(II)SO_4$ on cooperative acid leaching of NMC and LFP, highlighting a novel aspect of the present study.

- Effect of LFP addition on NMC leaching in a ferrous sulfate solution

The results show that there were interactions between LFP and NMC components during leaching in a ferrous sulfate solution. The reaction between NMC and Fe^{2+} can be represented by Equation (5.1), which shows that one mole of Fe^{2+} is required to reduce one mole of NMC:

$$10\ LiNi_{0.6}Mn_{0.2}Co_{0.2}O_2\ (s) + 20\ H_2SO_4\ (aq) + 10\ FeSO_4\ (aq) = 6\ NiSO_4\ (aq) + 2\ CoSO_4\ (aq) + 2\ MnSO_4\ (aq) + 5\ Li_2SO_4\ (aq) + 5\ Fe_2(SO_4)_3\ (aq) + 20\ H_2O\ (l) \quad (5.1)$$

The results show that the Fe^{2+} ions from $Fe(II)SO_4$ were able to reduce Mn, Ni, and Co to low oxidation state, improving the leaching efficiency within the first 10 minutes. The increasing of the ORP of leachate during this period confirmed the oxidation of Fe^{2+} to Fe^{3+} (Table 5.5). However, the leaching efficiency was only 42.5% for Mn, 55.9% for Ni, and 56.0% for Co at a Fe^{2+}/NMC molar ratio of 0.27 (Figure 5.7). This was probably due to the insufficient amount of Fe^{2+} (0.0408 moles) to reduce 0.149 moles of NMC. The electrons released were not enough to fully reduce all the transition metals, as shown in Table 5.14. With the addition of LFP, the leaching efficiencies of Mn, Ni, and Co increased progressively to nearly 100% by the end of the assays. This means that the 0.110 moles of LFP (Fe^{2+}) provided enough electrons to fully reduce the remaining NMC. The oxidation of Fe^{2+} from LFP to Fe^{3+} was confirmed by ORP, which dropped from 1.412 V at 10 minutes to 0.832 V at 12 minutes, then slightly increased to 0.916 V by the end of assay. The leaching efficiency of Fe and P was 43.3% and 46.2% respectively at 12 minutes and remained constant until 36 minutes. Regarding Li dissolution, results showed that Li was completely leached from both NMC and LFP by the end of the assay. This confirms the delithiation of LFP, which was supported by the XRD analysis (Figure 5.9), showing the formation of $Fe(III)PO_4$ in the leach residue.

When the Fe^{2+}/NMC molar ratio was increased to 0.74, the leaching efficiency of Mn, Ni and Co significantly improved (all exceeding 80% within 10 minutes) due to high availability of Fe^{2+} (0.110 moles) from $Fe(II)SO_4$ as shown in Table 5.14. The ORP data confirmed the oxidation of Fe^{2+} to Fe^{3+} obtaining 1.363 V at 10 minutes. Li leaching remained stable, regardless of Fe^{2+} concentration. This confirmed that Li dissolution was not redox-limited at these levels of ORP and proceeds readily in H_2SO_4 solution as discussed in the previous chapters. Regarding the reaction of Fe^{2+} and NMC, Zou et al. [86] report asimilar effect of Fe^{2+} on the dissolution of NMC, in which high concentration of Fe^{2+} boosted the reduction of NMC111.

With the addition of LFP, the leaching efficiencies of Mn, Ni, and Co increased to nearly 100% by the end of the assay. As discussed earlier, this improvement was due to the sufficient availability of Fe^{2+} (0.110 moles) released from LFP, which provided electrons for reducing the remained NMC (approximately 20%).

However, the amount of Fe^{2+} from LFP was in excess, which was confirmed by ORP. In this assay, the dissolution of Fe and P was lower than at Fe^{2+}/NMC ratio of 0.27, due to the decreased acidity of the solution, as a great portion of the acid had been consumed during the initial leaching of NMC. Referring to Equation (3.11), the low acidity medium favors the formation of $Fe(III)PO_4$. As a result, the large amount of $Fe(III)PO_4$ was formed at the Fe^{2+}/NMC ratio of 0.74. This is confirmed by the metal content of the leach residues (Table 5.6) and the XRD analysis (Figure 5.9).

Table 5.14. Calculation of NMC, LFP and $Fe(II)SO_4$ moles based on the experimental design

Fe^{2+}/NMC molar ratio	$Fe(II)SO_4$ (Fe^{2+}) moles	NMC moles	LFP (Fe^{2+}) moles
0.27	0.0408	0.149	0.110
0.74	0.1101	0.149	0.110

In the second system, LFP was initially added to the mixture of $Fe(II)SO_4$ and NMC at same Fe^{2+}/NMC molar ratios of the first system. It was observed that the presence of LFP at the beginning of the assay improved the leaching efficiency of transition metals during the initial minutes, under both Fe^{2+}/NMC molar ratios of 0.27 and 0.74. The total availability of Fe^{2+} from both $Fe(II)SO_4$ and LFP improved Mn, Ni and Co dissolution for both assays as shown in Table 5.15. However, the NMC was not completely dissolved up to the end of assay at Fe^{2+}/NMC molar ratio of 0.27. This suggests that the reduction of NMC required more than the stoichiometric amount of Fe^{2+} to provide sufficient electrons. The ORP results confirmed (Table 5.8) that the total of Fe^{2+} was oxidized to Fe^{3+} during the leaching process at this molar ratio. In contrast, the lower ORP observed at molar ratio of 0.74 than 0.27, indicating that the amount of Fe^{2+} exceeded the stoichiometric requirement for the reduction of NMC. As observed, at Fe^{2+}/NMC molar ratio of 0.74, the leaching efficiency of Fe and P was lower than the efficiencies at 0.27, due to the complete reduction of NMC and the decreased acidity of the solution, as discussed in the first system. This decrease of Fe and P dissolution led to the formation of high mass of $Fe(III)PO_4$ in the leach residue at Fe^{2+}/NMC molar ratio of 0.74, as confirmed by XRD analysis (Figure 5.14). Li dissolution followed the same trend in both assays and was complete regardless of the Fe^{2+} concentration.

Table 5.15. Calculation of NMC, LFP and Fe(II)SO_4 moles based on the experimental design

Fe^{2+}/NMC molar ratio	Fe(II)SO_4 (Fe^{2+}) moles	NMC moles	LFP (Fe^{2+}) moles	Total moles of Fe^{2+}
0.27	0.0408	0.149	0.110	0.1508
0.74	0.1101	0.149	0.110	0.2201

To make a clear comparison between the two systems, Figure 5.18 shows the effect of addition LFP at different timing on leaching efficiency of Mn, Ni, Co, Li, Fe and P under the conditions of 2 M H_2SO_4 NMC/LFP molar ratio 1.36, Fe^{2+}/NMC molar ratio 0.27, S/L 0.15 g/mL and 75 °C. It was observed that with the initial addition of LFP to NMC and Fe(II)SO_4 solution, the extraction of Mn, Ni and Co increased quickly near 90 % for the three metals during the first minutes and then gradually to 97.1%, 97.7% and 97.8% respectively at 36 minutes. However, when LFP was added at 10 minutes, 100% extraction of these metals was obtained. This little improvement could be due to high availability of acid for NMC leaching during first 10 minutes and then reduction of the unreacted NMC after the addition of LFP. The timing of LFP addition had a negligible effect on the dissolution of Li, however, as its leaching efficiency remained consistently high in both conditions. Regarding Fe and P, their leaching efficiencies were affected by the timing of LFP addition. In the system where LFP was present from the beginning, Fe and P were leached more efficiently and rapidly than the other system. This can be due to the high initial acid available for LFP dissolution in this system. In contrast, when LFP was added at 10 minutes, the prior consumption of acid by the NMC leaching led to decreased Fe and P dissolution, leading to formation large mass of $FePO_4$ in the leach.

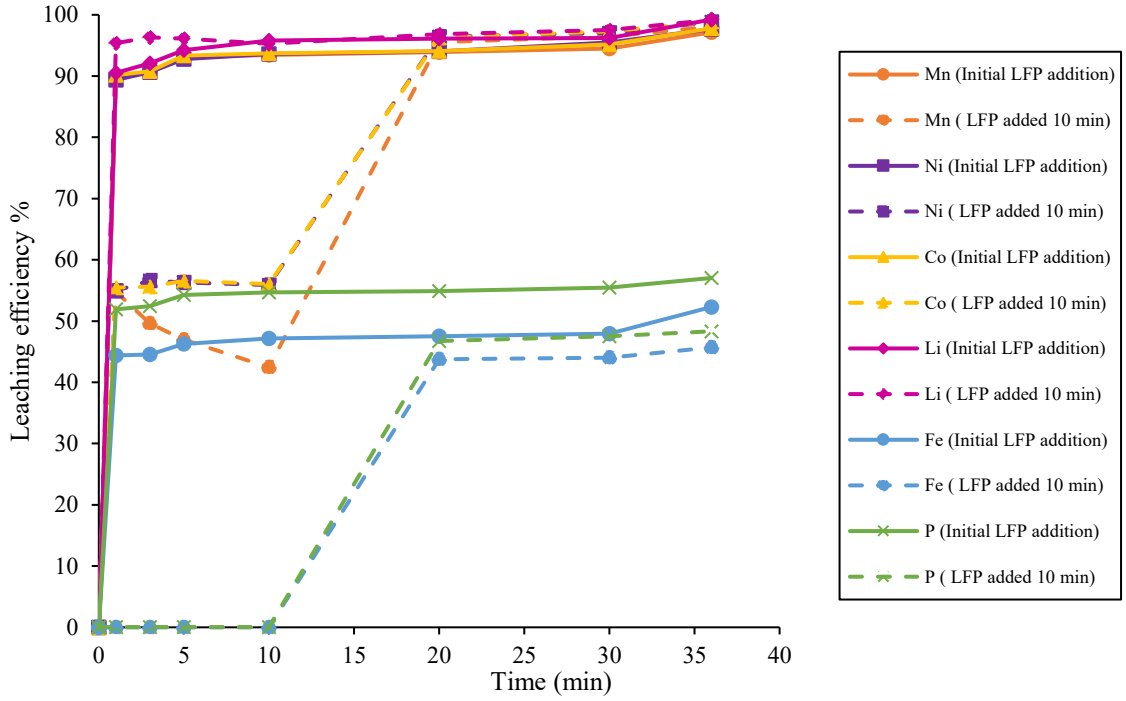

Figure 5.18. Effect of the timing of the addition of LFP on leaching efficiencies for Mn, Ni, Co, Li, Fe and P (2 M H_2SO_4, NMC/LFP molar ratio 1.36, Fe^{2+}/NMC molar ratio 0.27, S/L ratio 0.15 g/mL, 75°C)

In comparison with the literature, Zou et al. [86] investigated the effect of different LFP addition timings on the reduction of NMC 111. These research report higher final leaching efficiencies for Mn, Ni and Co when LFP was added immediately than when added after one hour of leaching under conditions of 2 M H_2SO_4, LFP/(sum of Ni+Mn+Co) molar ratio 0.6, 60°C and 3 hours. Our study, however, showed similar final leaching efficiencies for Mn, Ni and Co regardless of the timing of the LFP addition with both Fe^{2+}/NMC molar ratios tested. Moreover, Zou et al. report that all the LFP added fully dissolved in the solution and no $FePO_4$ was found in the leach residue. In our study, on the other hand, not only was complete dissolution of NMC achieved in a shorter time but the orthorhombic $FePO_4$ remained in the leach residue—a significant difference in residue formation between the two studies.

- Addition of NMC to an initial mixture of $Fe(III)_2(SO_4)_3$ and LFP

This study aimed to understand both the initial reaction between Fe^{3+} ions and LFP, and the subsequent effect of NMC addition on metal leaching efficiency. During the first 10 minutes of the reaction, before NMC was added, the leaching system primarily consisted of Fe^{3+} ions from $Fe(III)_2(SO_4)_3$ reacting with LFP in the H_2SO_4 medium. This reaction is described by Equation (5.2) [116].

$$2LiFe(II)PO_4\ (s) + Fe(III)_2(SO_4)_3\ (aq) = 2Fe(II)SO_4\ (aq) + Li_2SO_4\ (aq) + 2Fe(III)PO_4\ (s) \quad (5.2)$$

This redox reaction indicates that $Fe(III)_2(SO_4)_3$ acts as oxidizing agent and Fe^{2+} ions in LFP oxidize to Fe^{3+}, forming insoluble $Fe(III)PO_4$ in the leach residue**.** The theoretical molar ratio of Fe^{3+} in $Fe(III)_2(SO_4)_3$ to Fe^{2+} in LFP for complete oxidation is 1:1. In this essay, 94 % of Fe and P leached within the first 10 minutes, this indicates that the H_2SO_4 solution 2 M could dissolve LFP as discussed in chapter III. However, due to presence of Fe^{3+} (0.0408 moles) in the solution, small part of the Fe^{2+} in LFP oxidized to Fe^{3+}. This amount of Fe^{3+} from $Fe(III)_2(SO_4)_3$ was not sufficient to oxidize all the Fe^{2+} in LFP (0.110 moles), as shown in Table 5.16. The sharp drop in ORP (Table 5.11), from 1.055 V to 0.629 V during this period, confirmed the reduction of Fe^{3+} from $Fe(III)_2(SO_4)_3$ to Fe^{2+} and partial oxidation of LFP. The acidic nature of the solution affected the precipitation of $Fe(III)PO_4$ as leach residue [69, 114]. The complete dissolution of Li from LFP during this period was due to highly acidic solution.

With NMC addition, the leaching efficiency of Mn, Ni, and Co was around 76 % within the first minutes and gradually increased to 81% by the end of the assay. The ORP results confirmed the oxidation of Fe^{2+} to Fe^{3+} and providing the electrons for NMC reduction after 10 minutes. However, the total Fe^{2+}available was below the stoichiometric requirement for full NMC dissolution, as supported by the leach residual metal content (Table 5.12) and XRD analysis (Figure 5.17).

Table 5.16. Calculation of NMC, LFP and $Fe(III)_2(SO_4)_3$ moles based on the experimental design

Fe^{3+}/LFP molar ratio	$Fe(III)_2(SO_4)_3$ Concentration (M)	$Fe(III)_2(SO_4)_3$ moles	Fe^{+3} moles	NMC moles	LFP (Fe^{2+}) moles
0.37	0.095	0.0204	0.0408	0.149	0.110

This results also supported by the literature. Dai et al. [116], for example, studied the reaction of $Fe_2(SO_4)_3$ and LFP in an acid-free system, and showed that Fe(III) from $Fe_2(SO_4)_3$ replaced Fe^{2+} in $LiFePO_4$ by leveraging the similar olivine-type structure of $LiFePO_4$ and $FePO_4$.

5.5. Conclusion

In this chapter, the effects of adding $Fe(II)SO_4$ and $Fe(III)_2(SO_4)_3$ on the acid leaching of NMC and LFP cathode materials were analyzed. This study suggests the redox interaction between NMC, LFP, Fe^{2+} or Fe^{3+} in sulphuric acid, which can be interpreted as synergistic reaction that facilitates NMC leaching while leading to $Fe(III)PO_4$ formation. The results showed that Fe^{2+}, whether introduced through $Fe(II)SO_4$ or released from LFP, acted as reducing agent and enhanced the leaching efficiency of Mn, Ni and Co from mixed NMC and LFP. The presence of LFP further improved metal recovery, regardless of the addition sequence. The increase of Fe^{2+}/NMC molar ratio from 0.27 to 0.74 enhanced the solubilization of Mn, Ni and Co and led to 100% dissolution of NMC at the end of assay. This preserve a greater amount of orthorhombic $FePO_4(s)$ as a by-product during the leaching of an LFP and NMC mixture.

The results show that $Fe(III)_2(SO_4)_3$ acts as an oxidizing agent for LFP dissolution; however, the insufficient amount of Fe^{3+} present limited the extent of this oxidation. These findings highlight the importance of the $Fe(III)_2(SO_4)_3$/LFP molar ratio for the complete dissolution of NMC and the formation of a high mass of orthorhombic $FePO_4(s)$ as leach residue.

CHAPTER VI: CONCLUSION AND RECOMMENDATIONS

This comprehensive study of the synergistic recovery of metals from NMC and LFP cathode materials of Lithium-ion batteries (LIBs) through acid leaching addresses a significant gap in current knowledge of LIBs recycling. The acid leaching process studied proved very effective in extracting metals from both NMC and LFP cathode materials as well as mixtures of the two while producing high-value orthorhombic $FePO_4$ as a by-product.

The first contribution of this thesis is proposing the single cathode acid leaching. The effect of operating parameters on the individual acid leaching NMC and LFP was studied. The findings emphasized the effect of H_2SO_4 concentration, S/L ratio, and the presence of H_2O_2 were significant on the leaching efficiency and selectivity of metal recovery processes. The results indicated that the concentration of 2 M H_2SO_4 was identified as optimal for obtaining effective dissolution of both NMC and LFP materials. The S/L ratio was identified as a critical parameter, with low ratio (0.10 g/mL) obtaining best leaching efficiency for both NMC and LFP materials. Conversely, high S/L ratios decreased leaching efficiency, consistent with trends reported in existing literature. H_2O_2 addition showed distinct effects on the leaching of NMC and LFP. For NMC, H_2O_2 significantly enhanced metal dissolution and the complete dissolution was obtained under the conditions of H_2SO_4 2 M, H_2O_2 0.68 M, S/L 0.10 g/mL, 75 °C and 82 min. In contrast, for LFP, H_2O_2 acted as an oxidizing agent, leading to decreased leaching efficiency of Fe and P at high S/L ratio of 0.20 g/mL, due to the formation of hydrated $FePO_4$.

Secondly, in order to develop a flexible hydrometallurgical process which capable of efficiently recycling mixed stream of LIBs, this study proposed an innovative acid leaching approach of mixed NMC and LFP materials. It focused on reaction mechanisms and investigating the effects of various operating parameters on metal leaching efficiency. This study provided new insights into the synergistic reaction between NMC and LFP in H_2SO_4, which significantly enhances leaching efficiencies for Mn, Ni and Co from NMC and as well as formation of high value orthorhombic $FePO_4$. The findings indicated that S/L ratio of 0.15 g/mL yields the highest NMC recovery in the leachate and maximizes $FePO_4$ formation in the residue. The addition of H_2O_2 significantly enhanced transition metal dissolution; however, its concentration must be carefully controlled to balance leaching efficiency with economic and safety considerations. NMC/LFP molar ratio also influenced on metal dissolution, a ratio of 1.36 yielding best results. Additionally, H_2SO_4 concentration was as key factor, with 2 M H_2SO_4 found to be the most effective for maximizing the dissolution of Mn, Ni, Co, and Li. The best operating conditions for complete NMC dissolution and maximum $FePO_4$ formation were identified as: 2 M H_2SO_4, 0.68 M H_2O_2, S/L ratio 0.15 g/mL, NMC/LFP molar ratio 1.36, temperature 75°C and reaction time 51 minutes.

Furthermore, this work provided new insights into the cooperative leaching mechanisms of NMC and LFP in the presence of $Fe(II)SO_4$ or $Fe(III)_2(SO4)_3$ in the H_2SO_4 medium, and the redox reaction involved. $Fe(II)SO_4$ was identified as a key reducing agent, with 0.190 M being sufficient for complete NMC dissolution. Increasing the Fe^{2+}/NMC molar ratio significantly improved leaching efficiencies for Mn, Ni and Co and as well as $FePO_4$ formation. The study also revealed that the addition of LFP improved leaching efficiencies for Mn, Ni and Co regardless of its timing addition. The orthorhombic $FePO_4$ was recovered as solid by product, demonstrating the potential for sustainable recycling strategies for mixed cathode materials of LIBs.

In this study, a method using H_2SO_4 was developed for extracting metals from NMC and LFP cathode materials, separately and mixed. The findings demonstrated that LFP can significantly affect process efficiency and profitability. They also provide critical insights into the role of $Fe(II)SO_4$ as a reducing agent and the optimization of Fe^{2+} usage to improve selective leaching in mixed NMC and LFP systems. While this study successfully identified key parameters for optimizing the leaching of both NMC and LFP, further research is needed to optimize leaching conditions and evaluate their economic feasibility. Additionally, the impact of impurities in real-world battery waste streams, which could affect metal recovery efficiencies, was not addressed and remains a critical area for future investigation. Moreover, a deep understanding of the kinetics of $FePO_4$ formation and the implications for process efficiency is essential. Future studies could focus on optimizing the selective leaching of LFP in a mixed stream of LIBs to produce a higher yield of $FePO_4$.

REFERENCES

1.D. Gernaat, H. S. De Boer, V. Daioglou, S. Yalew, C. Müller,D. Vuuren. Climate change impacts on renewable energy supply. Nature Climate Change. 2021;11.

2.Y. Miao, L. Liu, Y. Zhang, Q. Tan,J. Li. An overview of global power lithium-ion batteries and associated critical metal recycling. Journal of Hazardous Materials. 2022;425:127900.

3.F. Maisel, C. Neef, F. Marscheider-Weidemann,N. F. Nissen. A forecast on future raw material demand and recycling potential of lithium-ion batteries in electric vehicles. Resources, Conservation and Recycling. 2023;192:106920.

4.E. Foreman, W. Zakri, M. Hossein Sanatimoghaddam, A. Modjtahedi, S. Pathak, A. G. Kashkooli et al. A Review of Inactive Materials and Components of Flexible Lithium-Ion Batteries. Advanced Sustainable Systems. 2017;1(11).

5.M. A. J.-M. Tarascon. Issues and challenges facing rechargeable lithium batteries. Nature. 2001;414.

6.H. Löbberding, S. Wessel, C. Offermanns, M. Kehrer, J. Rother, H. Heimes et al. From Cell to Battery System in BEVs: Analysis of System Packing Efficiency and Cell Types. World Electric Vehicle Journal. 2020;11(4):77.

7.M. Kaya. State-of-the-art lithium-ion battery recycling technologies. Circular Economy. 2022;1(2):100015.

8.R. Hausbrand, G. Cherkashinin, H. Ehrenberg, M. Gröting, K. Albe, C. Hess et al. Fundamental degradation mechanisms of layered oxide Li-ion battery cathode materials: Methodology, insights and novel approaches. Materials Science and Engineering: B. 2015;192:3-25.

9. J. Jyoti, B. P. Singh,S. K. Tripathi. Recent advancements in development of different cathode materials for rechargeable lithium ion batteries. Journal of Energy Storage. 2021;43.

10.F. Larouche, F. Tedjar, K. Amouzegar, G. Houlachi, P. Bouchard, G. P. Demopoulos et al. Progress and status of hydrometallurgical and direct recycling of Li-Ion batteries and beyond. Materials. 2020;13(3):801.

11.A. Manthiram. A reflection on lithium-ion battery cathode chemistry. Nature Communications. 2020;11.

12.S. Theivaprakasam, G. Girard, P. Howlett, M. Forsyth, S. Mitra,D. MacFarlane. Passivation behaviour of aluminium current collector in ionic liquid alkyl carbonate (hybrid) electrolytes. npj Materials Degradation. 2018;2.

13.P. Zhu, D. Gastol, J. Marshall, R. Sommerville, V. Goodship,E. Kendrick. A review of current collectors for lithium-ion batteries. Journal of Power Sources. 2021;485:229321.

14.H. Cheng, J. Shapter, Y. Li,G. Gao. Recent progress of advanced anode materials of lithium-ion batteries. Journal of Energy Chemistry. 2020;57.

15.B. L. Ellis, K. T. Lee,L. F. Nazar. Positive Electrode Materials for Li-Ion and Li-Batteries. Chemistry of Materials. 2010;22(3):691-714.

16.F. Cheng, J. Liang, Z. Tao,J. Chen. Functional Materials for Rechargeable Batteries. Advanced materials (Deerfield Beach, Fla). 2011;23:1695-715.

17.Y. Chen,Y. Liu. Development of lithium nickel cobalt manganese oxide as cathode material for commercial lithium-Ion batteries. Nanostructured Materials for Next-Generation Energy Storage and Conversion2019. p. 331-46.

18.S. B. Chikkannanavar, D. M. Bernardi,L. Liu. A review of blended cathode materials for use in Li-ion batteries. Journal of Power Sources. 2014;248:91-100.

19.Y. Yang, F. Liu, S. Song, H. Tang, S. Ding, W. Sun et al. Recovering valuable metals from the leaching liquor of blended cathode material of spent lithium-ion battery. Journal of Environmental Chemical Engineering. 2020;8(5):104358.

20. Z. Gong. Recent advances in the research of polyanion-type cathode materials for Li-ion batteries. Energy & Environmental Science. 2011;4:3223-42.
21. A. Chakraborty, S. Kunnikuruvan, S. Kumar, B. Markovsky, D. Aurbach, M. Dixit et al. Layered cathode materials for lithium-Ion batteries: Review of computational studies on LiNi1-x-y Cox Mny O2 and LiNi1-x-y Cox Aly O2. Chemistry of Materials. 2020.
22. A. Rajkamal, A. Sharma, B. K. Pullagura, R. Thapa,H. Kim. Engineering lithium nickel cobalt manganese oxides cathodes: A computational and experimental approach to bridging gaps. Chemical Engineering Journal. 2024;481:148223.
23. K. M. Winslow, S. J. Laux,T. G. Townsend. A review on the growing concern and potential management strategies of waste lithium-ion batteries. Resources, Conservation and Recycling. 2018;129:263-77.
24. A. M. Bernardes, D. C. R. Espinosa,J. A. S. Tenório. Recycling of batteries: a review of current processes and technologies. Journal of Power Sources. 2004;130(1):291-8.
25. A. D. Zand,M. A. Abduli. Current situation of used household batteries in Iran and appropriate management policies. Waste Management. 2008;28(11):2085-90.
26. P. Coonen,G. Allard, editors. Sorting, a profession in its own. Proceedings of the 22nd ICBR-International Congress on Battery Recycling, Lisbon, Portugal; 2017: ICBR.
27. A. M. Anne-Antoine Otron, L.-H. Tran,J.-F. Blais. Sustainable extraction and purification of REE and other metals from unsorted battery waste. Minerals Engineering. 2025;228:109322.
28. J. Li, X. Li, Q. Hu, Z. Wang, J. Zheng, L. Wu et al. Study of extraction and purification of Ni, Co and Mn from spent battery material. Hydrometallurgy. 2009;99:7-12.
29. X. Zhang, Y. Xie, X. Lin, H. Li,H. Cao. An overview on the processes and technologies for recycling cathodic active materials from spent lithium-ion batteries. Journal of Material Cycles and Waste Management. 2013;15(4):420-30.
30. J. Xu, H. R. Thomas, R. W. Francis, K. R. Lum, J. Wang,B. Liang. A review of processes and technologies for the recycling of lithium-ion secondary batteries. Journal of Power Sources. 2008;177(2):512-27.
31. F. Larouche, G. P. Demopoulos, K. Amouzegar, P. Bouchard,K. Zaghib, editors. Recycling of Li-Ion and Li-Solid State Batteries: The Role of Hydrometallurgy2018; Cham: Springer International Publishing.
32. S. Sloop, L. Crandon, M. Allen, K. Koetje, L. Reed, L. Gaines et al. A direct recycling case study from a lithium-ion battery recall. Sustainable Materials and Technologies. 2020;25:e00152.
33. X. Zheng, Z. Zhu, X. Lin, Y. Zhang, Y. He, H. Cao et al. A mini-review on metal recycling from spent lithium ion batteries. Engineering. 2018;4(3):361-70.
34. A. Chitre, D. Freake, L. Lander, J. Edge,M.-M. Titirici. Towards a more sustainable lithium-ion battery future: recycling LIBs from electric vehicles. Batteries & Supercaps. 2020;3(11):1126-36.
35. L.-F. Zhou, D. Yang, T. Du, H. Gong,W.-B. Luo. The current process for the recycling of spent lithium ion batteries. Frontiers in Chemistry. 2020;8(1027).
36. Z. Takacova, T. Havlik, F. Kukurugya,D. Orac. Cobalt and lithium recovery from active mass of spent Li-ion batteries: Theoretical and experimental approach. Hydrometallurgy. 2016;163.
37. N. J. Boxall, N. Adamek, K. Y. Cheng, N. Haque, W. Bruckard,A. H. Kaksonen. Multistage leaching of metals from spent lithium ion battery waste using electrochemically generated acidic lixiviant. Waste Management. 2018;74:435-45.
38. J. Guan, Y. Li, Y. Guo, R. Su, G. Gao, H. Song et al. Mechanochemical process enhanced cobalt and lithium recycling from wasted lithium-ion batteries. ACS Sustainable Chemistry & Engineering. 2016;5.
39. X. Chen, H. Ma, C. Luo,T. Zhou. Recovery of valuable metals from waste cathode materials of spent lithium-ion batteries using mild phosphoric acid. Journal of Hazardous Materials. 2017;326:77-86.

40. L. Yao, Y. Feng,G. Xi. A new method for the synthesis of LiNi1/3Co1/3Mn1/3O2 from waste lithium ion batteries. RSC Advances. 2015;5(55):44107-14.
41. L. Li, J. Lu, L. Zhai, X. Zhang, L. Curtiss, Y. Jin et al. A facile recovery process for cathodes from spent lithium iron phosphate batteries by using oxalic acid. CSEE Journal of Power and Energy Systems. 2018;4:219-25.
42. Y. Zheng, W. Song, W. T. Mo, L. Zhou,J. W. Liu. Lithium fluoride recovery from cathode material of spent lithium-ion battery. RSC Advances. 2018;8(16):8990-8.
43. W. Gao, X. Zhang, X. Zheng, X. Lin, H. Cao, Y. Zhang et al. Lithium carbonate recovery from cathode scrap of spent lithium-ion battery: A closed-loop process. Environmental Science and Technology. 2017;51(3):1662-9.
44. J. Kang, G. Senanayake, J. Sohn,S. M. Shin. Recovery of cobalt sulfate from spent lithium ion batteries by reductive leaching and solvent extraction with Cyanex 272. Hydrometallurgy. 2010;100(3):168-71.
45. L. Chen, X. Tang, Y. Zhang, L. Li, Z. Zeng,Y. Zhang. Process for the recovery of cobalt oxalate from spent lithium-ion batteries. Hydrometallurgy. 2011;108(1):80-6.
46. A. Chernyaev, Y. Zou, B. P. Wilson,M. Lundström. The interference of copper, iron and aluminum with hydrogen peroxide and its effects on reductive leaching of LiNi1/3Mn1/3Co1/3O2. Separation and Purification Technology. 2022;281:119903.
47. P. Meshram, B. D. Pandey,T. R. Mankhand. Hydrometallurgical processing of spent lithium ion batteries (LIBs) in the presence of a reducing agent with emphasis on kinetics of leaching. Chemical Engineering Journal. 2015;281:418-27.
48. S. Ghassa, A. Farzanegan, M. Gharabaghi,H. Abdollahi. The reductive leaching of waste lithium ion batteries in presence of iron ions: Process optimization and kinetics modelling. Journal of Cleaner Production. 2020;262.
49. S. Ghassa, A. Farzanegan, M. Gharabaghi,H. Abdollahi. Iron scrap, a sustainable reducing agent for waste lithium ions batteries leaching: An environmentally friendly method to treating waste with waste. Resources, Conservation and Recycling. 2021;166:105348.
50. P. Meshram, D. Abhilash, B. Pandey, T. Mankhand,H. Deveci. Acid baking of spent lithium ion batteries for selective recovery of major metals: A two-step process. Journal of Industrial and Engineering Chemistry. 2016;43.
51. N. Vieceli, C. Nogueira, C. Guimarães, M. Pereira, F. Durão,F. Margarido. Hydrometallurgical recycling of lithium-ion batteries by reductive leaching with sodium metabisulphite. Waste Management. 2017;71.
52. P. Zhang, T. Yokoyama, O. Itabashi, T. M. Suzuki,K. Inoue. Hydrometallurgical process for recovery of metal values from spent lithium-ion secondary batteries. Hydrometallurgy. 1998;47(2):259-71.
53. D. Ferreira, L. Prados, D. Majuste,M. Mansur. Hydrometallurgical separation of aluminium, cobalt, copper and lithium from spent Li-ion batteries. Journal of Power Sources - J POWER SOURCES. 2009;187:238-46.
54. W. Gao, J. Song, H. Cao, X. Lin, X. Zhang, X. Zheng et al. Selective recovery of valuable metals from spent lithium-ion batteries – Process development and kinetics evaluation. Journal of Cleaner Production. 2018;178:833-45.
55. S. Kim, D. Yang, K. Rhee,J. Sohn. Recycling process of spent battery modules in used hybrid electric vehicles using physical/chemical treatments. Research on Chemical Intermediates. 2014;40(7):2447-56.
56. L.-P. He, S.-Y. Sun, X.-F. Song,J.-G. Yu. Leaching process for recovering valuable metals from the LiNi1/3Co1/3Mn1/3O2 cathode of lithium-ion batteries. Waste Management. 2017;64:171-81.

57. L. Li, Y. Bian, X. Zhang, Q. Xue, E. Fan, F. Wu et al. Economical recycling process for spent lithium-ion batteries and macro- and micro-scale mechanistic study. Journal of Power Sources. 2018;377:70-9.
58. L. Li, Y. Bian, X. Zhang, Y. Guan, E. Fan, F. Wu et al. Process for recycling mixed-cathode materials from spent lithium-ion batteries and kinetics of leaching. Waste Management. 2018;71:362-71.
59. L. Li, E. Fan, Y. Guan, X. Zhang, Q. Xue, L. Wei et al. Sustainable recovery of cathode materials from spent lithium-ion batteries using lactic acid leaching system. ACS Sustainable Chemistry & Engineering. 2017;5(6):5224-33.
60. R.-C. Wang, Y.-C. Lin,S.-H. Wu. A novel recovery process of metal values from the cathode active materials of the lithium-ion secondary batteries. Hydrometallurgy. 2009;99(3):194-201.
61. H. Chen, S. Gu, Y. Guo, X. Dai, L. Zeng, K. Wang et al. Leaching of cathode materials from spent lithium-ion batteries by using a mixture of ascorbic acid and HNO3. Hydrometallurgy. 2021;205:105746.
62. X. Yang, P. Dong, T. Hao, Y. Zhang, Q. Meng, Q. Li et al. A combined method of leaching and Co-precipitation for recycling spent Lini0.6Co0.2Mn0.2O2 cathode materials: Process optimization and performance aspects. The Journal of The Minerals, Metals & Materials Society. 2020;72:3843–52.
63. J. Yang, L.-x. Jiang, F.-y. Liu, M. Jia,Y.-q. Lai. Reductive acid leaching of valuable metals from spent lithium-ion batteries using hydrazine sulfate as reductant. Transactions of Nonferrous Metals Society of China. 2020;30(8):2256-64.
64. W. Lv, Z. Wang, H. Cao, X. Zheng, W. Jin, Y. Zhang et al. A sustainable process for metal recycling from spent lithium-ion batteries using ammonium chloride. Waste Management. 2018;79:545-53.
65. Y. Yang, X. Meng, H. Cao, X. Lin, C. Liu, Y. Sun et al. Selective recovery of lithium from spent lithium iron phosphate batteries: a sustainable process. Green Chemistry. 2018;20(13):3121-33.
66. E. Fan, L. Li, X. Zhang, Y. Bian, Q. Xue, J. Wu et al. Selective recovery of Li and Fe from spent lithium-ion batteries by an environmentally friendly mechanochemical approach. ACS Sustainable Chemistry & Engineering. 2018;6(8):11029-35.
67. J. Kumar, X. Shen, B. Li, H. Liu,J. Zhao. Selective recovery of Li and FePO(4) from spent LiFePO(4) cathode scraps by organic acids and the properties of the regenerated LiFePO(4). Waste Management. 2020;113:32-40.
68. H. Mahandra,A. Ghahreman. A sustainable process for selective recovery of lithium as lithium phosphate from spent LiFePO4 batteries. Resources, Conservation and Recycling. 2021;175:105883.
69. F. Larouche, K. Amouzegar, G. Houlachi, P. Bouchard,G. Demopoulos. Conversion of LiFePO4 to FePO4 via selective lithium bicarbonation: A direct pathway towards battery recycling. Journal of The Electrochemical Society. 2022;169.
70. H. Li, S. Xing, Y. Liu, F. Li, H. Guo,G. Kuang. Recovery of lithium, iron, and phosphorus from spent LiFePO4 batteries using stoichiometric sulfuric acid leaching system. ACS Sustainable Chemistry & Engineering. 2017;5(9):8017-24.
71. R. Zheng, L. Zhao, W. Wang, Y. Liu, Q. Ma, D. Mu et al. Optimized Li and Fe recovery from spent lithium-ion batteries via a solution-precipitation method. RSC Advances. 2016;6(49):43613-25.
72. D. Bian, Y. Sun, S. Li, Y. Tian, Z. Yang, X. Fan et al. A novel process to recycle spent LiFePO4 for synthesizing LiFePO4/C hierarchical microflowers. Electrochimica Acta. 2015;190.
73. W.-b. Lou, Y. Zhang, Y. Zhang, S.-l. Zheng, P. Sun, X.-j. Wang et al. Leaching performance of Al-bearing spent LiFePO4 cathode powder in H2SO4 aqueous solution. Transactions of Nonferrous Metals Society of China. 2021;31(3):817-31.

74. J. I. G. Dawkins, Y. Pan, M. Z. Ghavidel, J. Geissler, B. Krueger, D. Chhin et al. Exploring the synergistic effects of dual-layer electrodes for high power Li-Ion batteries. ChemElectroChem. 2023;10(21):e202300279.
75. K. Zaghib,C. M. Julien. Structure and electrochemistry of FePO4·2H2O hydrate. Journal of Power Sources. 2005;142(1):279-84.
76. F. Pagnanelli, P. Altimari, M. Colasanti, J. Coletta, L. D'Annibale, A. Mancini et al. Recycling Li-Ion batteries via the re-synthesis route: Improving the process sustainability by using lithium iron phosphate (LFP) scraps as reducing agents in the leaching operation. Metals. 2024;14:1275.
77. X. Chen, J. Li, D. Kang, T. Zhou,H. Ma. Novel closed-loop process for simultaneous recovery of valuable metals and iron from mixed type of spent lithium-ion batteries. Green Chemistry. 2019;21.
78. Z. Xu, Y. Dai, D. Hua, H. Gu,N. Wang. Creative method for efficiently leaching Ni, Co, Mn, and Li in a mixture of LiFePO4 and LiMO2 using only Fe(III). ACS Sustainable Chemistry & Engineering. 2021;9(11):3979-84.
79. R. Zheng, W. Wang, Y. Dai, Q. Ma, Y. Liu, D. Mu et al. A closed-loop process for recycling LiNixCoyMn(1−x−y)O2 from mixed cathode materials of lithium-ion batteries. Green Energy and Environment. 2017;2(1):42-50.
80. H. Zou, E. Gratz, D. Apelian,Y. Wang. A novel method to recycle mixed cathode materials for lithium ion batteries. Green Chemistry. 2013;15(5):1183-91.
81. W. Chu, Y. Zhang, X. Chen, Y. Huang, H. Cui, M. Wang et al. Synthesis of LiNi0.6Co0.2Mn0.2O2 from mixed cathode materials of spent lithium-ion batteries. Journal of Power Sources. 2019;449:227567.
82. Y. Jiang, X. Chen, S. Yan, S. Li,T. Zhou. Pursuing green and efficient process towards recycling of different metals from spent lithium-ion batteries through Ferro-chemistry. Chemical Engineering Journal. 2021;426:131637.
83. H. Tang, F. Tan, X. Dai, Y. Qiao,X. Zheng. Comprehensive recovery of mixed spent of LiNixCoyMn(1−x−y)O2 and LiFePO4. Journal of Material Cycles and Waste Management. 2020;22(6):1734-43.
84. S.-L. Song, R.-Q. Liu, M.-M. Sun, A.-G. Zhen, F.-Z. Kong,Y. Yang. Hydrometallurgical recovery of lithium carbonate and iron phosphate from blended cathode materials of spent lithium-ion battery. Rare Metals. 2023.
85. J. Zou, D. Peng, W. Hu, S. Su, X. Wang, Z. Zhao et al. All-element recovery and regeneration of mixed LiNixCoyMn1−x−yO2/LiFePO4 cathode materials by synergistic redox processes. Chemical Communications. 2024;60(13):1778-81.
86. Y. Zou, A. Chernyaev, M. Ossama, S. Seisko,M. Lundström. Leaching of NMC industrial black mass in the presence of LFP. Scientific Reports. 2024;14(1):10818.
87. I. Balázs Illés,T. Kékesi. Extraction of pure Co, Ni, Mn, and Fe compounds from spent Li-ion batteries by reductive leaching and combined oxidative precipitation in chloride media. Minerals Engineering. 2023;201:108169.
88. X. Zhou, W. Yang, X. Liu, J. Tang, F. Su, Z. Li et al. One-step selective separation and efficient recovery of valuable metals from mixed spent lithium batteries in the phosphoric acid system. Waste Management. 2023;155:53-64.
89. Y. Hua, Z. Xu, B. Zhao,Z. Zhang. Electric potential-determined redox intermediates for effective recycling of spent lithium-ion batteries. Green Chemistry. 2022;24(9):3723-35.

90. S. Gu, L. Zhang, B. Fu, J.-W. Ahn,X. Wang. Recycling of mixed lithium-ion battery cathode materials with spent lead-acid battery electrolyte with the assistance of thermodynamic simulations. Journal of Cleaner Production. 2020;266:121827.
91. N. E. Darrell Henry, John Goodge, David Mogk. X-ray reflection in accordance with Bragg's Law [Available from: https://serc.carleton.edu/research_education/geochemsheets/BraggsLaw.html.
92. C.M.C. Barbara L Dutrow. X-ray Powder Diffraction (XRD) [Available from: https://serc.carleton.edu/research_education/geochemsheets/techniques/XRD.html.
93. Scanning Electron Microscopy [Available from: https://www.nanoscience.com/techniques/scanning-electron-microscopy/.
94. W. Jensen. Interpreting Images from Scanning Electron Microscopy 2022 [Available from: https://deringerney.com/interpreting-images-from-scanning-electron-microscopy/.
95. F. M. Dunnivant,J. W. Ginsbach. Flame atomic absorbance and emission spectroscopy and inductively coupled spectrometry - mass spectrometry. Whitman College2009. Available from: http://people.whitman.edu/~dunnivfm/FAASICPMS_Ebook/Prelim/index.html.
96. S. J. Hill. Inductively coupled plasma spectrometry and its applications. United Kingdom: Blackwell publishing; 2006.
97. T. J. Manning,W. R. Grow. Inductively coupled plasma - atomic emission spectrometry. The Chemical Educator. 1997;2(1):1-19.
98. L. Azhari, X. Zhou, B. Sousa, Z. Yang, G. Gao,Y. Wang. Effects of extended aqueous processing on structure, chemistry, and performance of polycrystalline LiNixMnyCozO2 cathode powders. ACS Applied Materials & Interfaces. 2020;12(52):57963-74.
99. R. Sattar, S. Ilyas, H. N. Bhatti,A. Ghaffar. Resource recovery of critically-rare metals by hydrometallurgical recycling of spent lithium ion batteries. Separation and Purification Technology. 2019;209:725-33.
100. Y. Song, P. Y. Zavalij, M. Suzuki,M. S. Whittingham. New iron(III) phosphate phases: Crystal structure and electrochemical and magnetic properties. Inorganic Chemistry. 2002;41(22):5778-86.
101. C. Peschel, S. van Wickeren, Y. Preibisch, V. Naber, D. Werner, L. Frankenstein et al. Comprehensive characterization of shredded lithium-ion battery recycling material. Chemistry – A European Journal. 2022;28(22):e202200485.
102. N. Zhang, J. Li, H. Li, A. Liu, Q. Huang, L. Ma et al. Structural, electrochemical, and thermal properties of nickel-rich LiNixMnyCozO2 materials. Chemistry of Materials. 2018;30(24):8852-60.
103. H. Mahandra,A. Ghahreman. A sustainable process for selective recovery of lithium as lithium phosphate from spent LiFePO4 batteries. Resources, Conservation and Recycling. 2021;175.
104. M. E. Boiko, M. D. Sharko, A. M. Boiko, A. V. Bobyl,V. I. Nikolaev. Studying LiFePO4 powder samples Via X-ray diffraction techniques using artificial neural networks. Technical Physics Letters. 2023;49(12):228-31.
105. G. Liang, K. Park, J. Li, R. E. Benson, D. Vaknin, J. T. Markert et al. Anisotropy in magnetic properties and electronic structure of single-crystal LiFePO4. Physical Review B. 2008;77(6):064414.
106. A. B. Botelho Junior, S. Stopic, B. Friedrich, J. A. S. Tenório,D. C. R. Espinosa. Cobalt recovery from Li-ion battery recycling: A critical review. Metals. 2021;11(12):1999.
107. CRC Handbook of Chemistry and Physics: A Ready-Reference of Chemical and Physical Data, 85th ed Edited by David R. Lide (National Institute of Standards and Technology). CRC Press LLC: Boca Raton, FL. 2004. 2712. ISBN 0-8493-0485-7. Journal of the American Chemical Society. 2005;127(12):4542-.

108.J. Partinen, P. Halli, B. P. Wilson,M. Lundström. The impact of chlorides on NMC leaching in hydrometallurgical battery recycling. Minerals Engineering. 2023;202:108244.
109.K. Davis,G. P. Demopoulos. Hydrometallurgical recycling technologies for NMC Li-ion battery cathodes: current industrial practice and new R&D trends. RSC Sustainability. 2023;1(8):1932-51.
110. M.Wang, K. Liu, S. Dutta, D. S. Alessi, J. Rinklebe, Y. S. Ok et al. Recycling of lithium iron phosphate batteries: Status, technologies, challenges, and prospects. Renewable and Sustainable Energy Reviews. 2022;163:112515.
111.P. M. Kobylin, H. Sippola,P. A. Taskinen. Thermodynamic model for acidic Fe(II) sulphate from solubility data. Calphad. 2012;38:185-93.
112.J. Hu, H. Guo, Y. Li, H. Wang, Z. Wang, W. Huang et al. Understanding Li-ion thermodynamic and kinetic behaviors in concentrated electrolyte for the development of aqueous lithium-ion batteries. Nano Energy. 2021;89:106413.
113.S.-g. Zhu, W.-z. He, G.-m. Li, X. Zhou, Z. Xiaojun,J.-w. Huang. Recovery of Co and Li from spent lithium-ion batteries by combination method of acid leaching and chemical precipitation. Transactions of Nonferrous Metals Society of China. 2012;22:2274–81.
114.X.-j. Wang, S.-l. Zheng, Y. Zhang, Y. Zhang, S. Qiao, Z.-q. Long et al. Sulfuric acid leaching of ball-milling activated FePO4 residue after lithium extraction from spent lithium iron phosphate cathode powder. Waste Management. 2022;153:31-40.
115.Y. Dai, N. Wang, Z. Xu, H. Gu, M. Chen,D. Hua. Acid-free leaching nickel, cobalt, manganese, and lithium from spent lithium-ion batteries using Fe(II) and Fe(III) solution. Journal of Sustainable Metallurgy. 2022;8(2):863-71.
116.Y. Dai, Z. Xu, D. Hua, H. Gu,N. Wang. Theoretical-molar Fe3+ recovering lithium from spent LiFePO4 batteries: an acid-free, efficient, and selective process. Journal of Hazardous Materials. 2020;396:122707.

APPENDICES

APPENDIX A: STATISTICAL ANALYSIS

For the statistical study, a one-way ANOVA (p-value < 0.05) followed by Tukey's Honestly Significant Difference (HSD) post-hoc test was performed using R software (R Core Team, version 4.4.1, 2024). The purpose was to investigate the effect of solid-liquid (S/L) ratio on leaching efficiencies for Mn, Ni, Co, Li, Fe and P from a mixture of NMC and LFP under conditions of 2 M H_2SO_4, 0.68 M H_2O_2, 75°C, reaction time 82 minutes. The independent variable was the S/L ratio (0.05, 0.10, 0.15 and 0.20 g/mL), while the dependent variable was metal leaching efficiency. Table 1 presents the leaching efficiencies for these metals at each S/L ratio, with duplicate tests.

ANOVA was used to identify statistically significant differences (p-value < 0.05) in leaching efficiencies for Mn, Ni, Co, Li, Fe and P across the four S/L ratios. Tukey's HSD was then applied to determine which specific S/L ratios showed significant differences. The results for each metal are summarized in the ANOVA tables below, which include pairwise comparisons pinpointing differences in leaching efficiency.

Table 1: The effect of solid-liquid (S/L) ratio on leaching efficiencies for Mn, Ni, Co, Li, Fe and P (with duplicate) (2 M H_2SO_4, 0.68M H_2O_2, 75°C, 82 minutes)

S/L (g/mL)	**Leaching efficiency %**											
	Mn-1	**Mn-2**	**Ni-1**	**Ni-2**	**Co-1**	**Co-2**	**Li-1**	**Li-2**	**Fe-1**	**Fe-2**	**P-1**	**P-2**
0.05	100.0	100.0	100.0	100.0	100.0	100.0	100.0	100.0	100.0	100.0	100.0	100.0
0.10	99.9	96.1	100.0	96.0	100.0	95.9	100.0	99.8	93.4	85.3	93.8	85.7
0.15	99.2	99.2	99.5	99.7	99.6	99.6	99.6	99.7	34.6	37.6	37.9	44.2
0.20	77.7	73.9	78.6	75.3	78.7	74.9	96.1	95.1	21.7	20.7	22.1	18.7

Table 2 shows a one-way ANOVA investigating the impact of S/L ratio on Mn leaching efficiency under conditions of 2 M H_2SO_4, 0.68 M H_2O_2, 75°C and 82 minutes. The results indicate a statistically significant impact of S/L ratio on Mn leaching efficiency ($p = 0.00056$). Tukey's HSD test revealed that S/L ratio 0.20 results in a significantly lower leaching efficiency compared to the other S/L ratios. Specifically:

- S/L ratio 0.20 vs 0.05: difference in leaching efficiency is -24.2 ($p = 0.00076$), a substantial decrease
- S/L ratio 0.20 vs 0.10: difference is -22.2 ($p = 0.00107$), a significant reduction
- S/L ratio 0.20 vs 0.15: difference is -23.4 ($p = 0.00087$), also significant

Differences between S/L ratios 0.05, 0.10 and 0.15 g/mL, however, were not statistically significant ($p > 0.05$), suggesting that Mn leaching efficiency remains relatively consistent across these lower ratios.

Table 2. One-way ANOVA of effect of S/L ratio on Mn leaching efficiency
(2 M H_2SO_4, 0.68M H_2O_2, 75°C, 82 minutes)

Source of variation	**Degrees of freedom (df)**	**Sum of squares (SS)**	**Mean square (MS)**	**F-statistic**	***p*-value**
Between groups	3	816.06	272.02	75.35	0.00056
Residuals	4	14.44	3.61		
Comparison	**Diff**	**Lwr**	**Upr**	**Adjusted *p*-value**	
S/L ratio 0.10 vs 0.05	-2	-9.73463	5.734625	0.7324	
S/L ratio 0.15 vs 0.05	-0.8	-8.53463	6.934625	0.9719	
S/L ratio 0.20 vs 0.05	-24.2	-31.9346	-16.4654	0.00076	
S/L ratio 0.15 vs 0.10	1.2	-6.53463	8.934625	0.9167	
S/L ratio 0.20 vs 0.10	-22.2	-29.9346	-14.4654	0.00107	
S/L ratio 0.20 vs 0.15	-23.4	-31.1346	-15.6654	0.00087	

*Diff: difference between means of the two groups; Lwr, Upr: lower and upper endpoint of confidence interval at 95% default; and adjusted *p*-value: *p*-value after adjustment for the multiple comparisons.

The same analyses were carried out for the other metals. As shown in Table 3, ANOVA analysis under the same conditions demonstrated that S/L ratio had a significant effect on Ni leaching efficiency ($p = 0.000584$). Tukey's HSD test confirmed that Ni leaching efficiency is significantly lower at S/L ratio 0.20 than at S/L ratios 0.05, 0.10 and 0.15 g/mL. No significant differences were found among the lower ratios.

For Co (Table 4), ANOVA results also indicate that S/L ratio has a statistically significant effect (p= 0.000763), and Tukey's HSD again confirms a significantly lower leaching efficiency at S/L ratio 0.20 than at S/L ratios 0.05, 0.10 and 0.15, as was the case with Mn and Ni. No significant differences were observed among the lower ratios.

Table 3. One-way ANOVA of effect of S/L ratio on Ni leaching efficiency (2 M H_2SO_4, 0.68 M H_2O_2, 75°C, 82 minutes)

Source of variation	**Degrees of freedom (df)**	**Sum of squares (SS)**	**Mean square (MS)**	**F-statistic**	***p*-value**
Between groups	3	747.1	249.02	73.98	0.000584
Residuals	4	13.5	3.37		
Comparison	**Diff**	**Lwr**	**Upr**	**adjusted *p*-value**	
S/L ratio 0.10 vs 0.05	-2	-9.46894	5.468937	0.713606	
S/L ratio 0.15 vs 0.05	-0.4	-7.86894	7.068937	0.99576	
S/L ratio 0.20 vs 0.05	-23.05	-30.5189	-15.5811	0.000807	
S/L ratio 0.15 vs 0.10	1.6	-5.86894	9.068937	0.819723	
S/L ratio 0.20 vs 0.10	-21.05	-28.5189	-13.5811	0.001152	
S/L ratio 0.20 vs 0.15	-22.65	-30.1189	-15.1811	0.000864	

Table 4. One-way ANOVA of effect of S/L ratio on Co leaching efficiency (2 M H_2SO_4 0.68 M H_2O_2, 75°C, 82 minutes)

Source of variation	**Degrees of freedom (df)**	**Sum of squares (SS)**	**Mean square (MS)**	**F-statistic**	***p*-value**
Between groups	3	756.2	252.08	64.53	0.000763
Residuals	4	15.6	3.91		
Comparison	**Diff**	**Lwr**	**Upr**	**adjusted *p*-value**	
S/L ratio 0.10 vs 0.05	-2.05	-10.095734	5.995734	0.740109	
S/L ratio 0.15 vs 0.05	-0.4	-8.445734	7.645734	0.996594	
S/L ratio 0.20 vs 0.05	-23.2	-31.245734	-15.154266	0.001053	
S/L ratio 0.15 vs 0.10	1.65	-6.395734	9.695734	0.836552	
S/L ratio 0.20 vs 0.10	-21.15	-29.195734	-13.104266	0.00151	
S/L ratio 0.20 vs 0.15	-22.8	-30.845734	-14.754266	0.001127	

A shown in Table 5, ANOVA results show that S/L ratio had a significant effect on Li leaching efficiency (p = 0.000667). Tukey's HSD test again confirmed that Li leaching efficiency was significantly lower at

S/L ratio 0.20 than at the other ratios, with p-values all below 0.05. In contrast, no significant differences were found among the lower S/L ratios (0.05, 0.10 and 0.15), suggesting efficiency remains stable until the ratio reaches 0.20.

Table 5. One-way ANOVA of effect of S/L ratio on Li leaching efficiency (2 M H_2SO_4, 0.68 M H_2O_2, 75°C, 82 minutes)

Source of variation	**Degrees of freedom (df)**	**Sum of squares (SS)**	**Mean square (MS)**	**F-statistic**	***p*-value**
Between groups	3	27.224	9.075	69.14	0.000667
Residuals	4	0.525	0.131		
Comparison	**Diff**	**Lwr**	**Upr**	**adjusted *p*-value**	
S/L ratio 0.10 vs 0.05	-0.1	-1.574807	1.374807	0.9915516	
S/L ratio 0.15 vs 0.05	-0.35	-1.824807	1.124807	0.7751798	
S/L ratio 0.20 vs 0.05	-4.4	-5.874807	-2.925193	0.0009215	
S/L ratio 0.15 vs 0.10	-0.25	-1.724807	1.224807	0.8960137	
S/L ratio 0.20 vs 0.10	-4.3	-5.774807	-2.825193	0.0010085	
S/L ratio 0.20 vs 0.15	-4.05	-5.524807	-2.575193	0.0012743	

For Fe, ANOVA results indicate S/L ratio had a significant impact on Fe leaching efficiency (p = 3.24e-05), as shown in Table 6. Tukey's HSD confirmed significantly lower efficiencies at S/L ratios of 0.15 and 0.20 than at S/L ratios 0.05 and 0.10 (all p-values < 0.05). Notably, the biggest decline in efficiency was at S/L ratio 0.20, while differences between 0.05 and 0.10 were not statistically significant.

ANOVA results show that S/L ratio also had a significant influence on P leaching efficiency (p = 8.21e-05), as shown in Table 7. Tukey's HSD test confirmed significantly lower leaching efficiencies at S/L ratios 0.15 and 0.20 that at S/L ratios 0.05 and 0.10 (p < 0.05). S/L ratio 0.20 had the most considerable impact, while no significant difference was found between 0.05 and 0.10.

Table 6. One-way ANOVA of effect of S/L ratio on Fe leaching efficiency
(2 M H_2SO_4, 0.68M H_2O_2, 75°C, 82 minutes)

Source of variation	**Degrees of freedom (df)**	**Sum of squares (SS)**	**Mean square (MS)**	**F-statistic**	***p*-value**
Between groups	3	9054	3018.0	319.3	3.24e-05
Residuals	4	38	9.5		
Comparison	**Diff**	**Lwr**	**Upr**	**adjusted *p*-value**	
S/L ratio 0.10 vs 0.05	-10.65	-23.16498	1.864983	0.0824335	
S/L ratio 0.15 vs 0.05	-63.9	-76.41498	-51.385017	0.0001322	
S/L ratio 0.20 vs 0.05	-78.8	-91.31498	-66.285017	6.95E-05	
S/L ratio 0.15 vs 0.10	-53.25	-65.76498	-40.735017	0.0002349	
S/L ratio 0.20 vs 0.10	-68.15	-80.66498	-55.635017	0.0001098	
S/L ratio 0.20 vs 0.15	-14.9	-27.41498	-2.385017	0.0280482	

Table 7: One-way ANOVA of effect of S/L ratio on P leaching efficiency
(2 M H_2SO_4, 0.68 M H_2O_2, 75°C, 82 minutes)

Source of variation	**Degrees of freedom (df)**	**Sum of squares (SS)**	**Mean square (MS)**	**F-statistic**	***p*-value**
Between groups	3	8762	2920.6	199.9	8.21e-05
Residuals	4	58	14.6		
Comparison	**Diff**	**Lwr**	**Upr**	**adjusted *p*-value**	
S/L ratio 0.10 vs 0.05	-10.25	-25.80871	5.30871	0.1672219	
S/L ratio 0.15 vs 0.05	-58.95	-74.50871	-43.39129	0.0003603	
S/L ratio 0.20 vs 0.05	-79.6	-95.15871	-64.04129	0.0001314	
S/L ratio 0.15 vs 0.10	-48.7	-64.25871	-33.14129	0.000763	
S/L ratio 0.20 vs 0.10	-69.35	-84.90871	-53.79129	0.0002006	
S/L ratio 0.20 vs 0.15	-20.65	-36.20871	-5.09129	0.0192521	

Leaching efficiencies for all metals decreased under the specified conditions when S/L ratio was increased. However, differences among the lower ratios (0.05, 0.10 and 0.15) were generally not significant, suggesting that leaching efficiency remains relatively stable when S/L ratio is kept below 0.20. S/L ratio 0.20 g/mL consistently resulted in significantly lower leaching efficiencies. These findings are compatible with our experimental results (4.2.2) and highlight the importance of optimizing S/L ratio to maximize leaching efficiency (upper limit around 0.15 under the conditions used in this study).

APPENDIX B: DETAILED PIPETTE ERROR CALCULATION

Table 1 shows detailed pipette error calculations for different dilutions.

Table 1. Pipette errors at different dilutions

Parameter	DF10 (*)	DF100	DF1000
General error of each pipette	0.8%	0.8%	0.8%
Volume of nitric acid added	9 mL	9.9 mL	9 mL
Volume of sample added	1 mL	0.1 mL	0
Volume of DF100	0	0	1 mL
$\sigma_{9.9}$mL (error for 9.9 mL pipette)	0.0792 mL	0.0792 mL	N/A
$\sigma_{0.1}$mL (error for 0.1 mL pipette)	0.0008 mL	0.0008 mL	N/A
σ_{9}mL (error for 9 mL pipette)	N/A	N/A	0.072 mL
σ_{1}mL (error for 1 mL pipette)	N/A	N/A	0.008 mL
V_{total} (total volume)	10.0 mL	10.0 mL	10.0 mL
σ_{total} (combined error)	$\sqrt{(0.072^2 + 0.008^2)}$ = 0.0724 mL	$\sqrt{(0.0792^2 + 0.0008^2)}$ = 0.0792 mL	$\sqrt{(0.072^2 + 0.008^2)}$ = 0.0724 mL
Relative error	(0.0724 / 10.0) × 100% = 0.724%	(0.0792 / 10.0) × 100% = 0.792% ≈ 0.8%	(0.0724 / 10.0) × 100% = 0.724%

* DF: dilution factor

Calculating errors for DF10:

- General error of each pipette: 0.8%
- Volume of nitric acid added: 9 mL
- Volume of sample added: 1 mL

Error calculation:

1. For 9 mL pipette:

σ_{9mL}: $9 \times \frac{0.8}{100} = 0.072$ mL

2. For 1 mL pipette:

σ_{1mL}: $1 \times \frac{0.8}{100} = 0.008$ mL

3. Combine the errors

V_{total}= 9.0 mL+ 1.0 mL= 10.0 mL

$$\sigma_{total} = \sqrt{\sigma_{9mL}{}^2 + \sigma_{1mL}{}^2}$$

$$\sigma_{total} = \sqrt{(0.072)^2 + (0.008)^2} = 0.0724\text{mL}$$

To express the error as a percentage of the total volume:

Relative error = $\frac{\sigma_{total}}{V_{total}} \times 100\%$

Relative error: $\frac{0.0724}{10.0} \times 100\% = 0.724\%$

Calculate errors for DF100:

1. For 9.9 mL pipette:

$\sigma_{9.9mL}$: $9.9 \times \frac{0.8}{100} = 0.0792$ mL

2. For 0.1 mL pipette:

$\sigma_{0.1mL}$: $0.1 \times \frac{0.8}{100} = 0.0008$ mL

3. Combine the errors

V_{total}= 9.9 mL+ 0.1 mL= 10.0 mL

$$\sigma_{total} = \sqrt{\sigma_{9.9mL}{}^2 + \sigma_{0.1mL}{}^2}$$

$$\sigma_{total} = \sqrt{(0.0792)^2 + (0.0008)^2} = 0.0792 \text{ mL}$$

Relative error: $\frac{0.0792}{10.0} \times 100\% = 0.792\% \approx 0.8\%$

Calculate errors for DF1000:

- General error of each pipette: 0.8%
- Volume of nitric acid added: 9 mL

- Volume of FD100 added: 1 mL

Error calculation:

4. For 9 mL pipette:

σ_{9mL}: $9 \times \frac{0.8}{100} = 0.072$ mL

5. For 1 mL pipette:

σ_{1mL}: $1 \times \frac{0.8}{100} = 0.008$ mL

6. Combine the errors

V_{total}= 9.0 mL+ 1.0 mL= 10.0 mL

$$\sigma_{total} = \sqrt{{\sigma_{9mL}}^2 + {\sigma_{1mL}}^2}$$

$$\sigma_{total} = \sqrt{(0.072)^2 + (0.008)^2} = 0.0724 \text{ mL}$$

Relative error: $\frac{0.0724}{10.0} \times 100\% = 0.724\%$